Summer 2011

A numerical method for studying thermal deformation in 3D double-layered thin films with imperfect interfacial thermal contact exposed to ultrashort-pulsed lasers

Runzhou Liu

A NUMERICAL METHOD FOR STUDYING THERMAL DEFORMATION IN 3D DOUBLE-LAYERED THIN FILMS WITH IMPERFECT INTERFACIAL THERMAL CONTACT EXPOSED TO ULTRASHORT-PULSED LASERS

by

Runzhou Liu, B.S., M.S.

A Dissertation Presented in Partial Fulfillment
Of the Requirements for the Degree
Doctor of Philosophy

COLLEGE OF ENGINEERING AND SCIENCE
LOUISIANA TECH UNIVERSITY

August 2011

LOUISIANA TECH UNIVERSITY

THE GRADUATE SCHOOL

April 28, 2011

Date

We hereby recommend that the dissertation prepared under our supervision by Runzhou Liu

entitled

A NUMERICAL METHOD FOR STUDYING THERMAL DEFORMATION IN 3D DOUBLE-LAYERED THIN FILMS WITH IMPERFECT INTERFACIAL THERMAL CONTACT EXPOSED TO ULTRASHORT-PULSED LASERS

be accepted in partial fulfillment of the requirements for the Degree of Doctor of Philosophy

Supervisor of Dissertation Research

Head of Department

Department

Recommendation concurred in:

Advisory Committee

Approved:

Director of Graduate Studies

Approved:

Dean of the Graduate School

Dean of the College

GS Form 13a
(6/07)

ABSTRACT

Micro heat transfer induced by Ultrashort-pulsed lasers is an important research topic in mechanical engineering and material science. In order to apply ultrashort-pulsed lasers successfully, studying the thermal deformation in double-layered thin films with imperfect thermal interfacial contact induced by ultrashort-pulsed lasers is important for preventing thermal damage. For the ultrashort-pulsed laser, the thermal damage is different from that caused by the long-pulsed lasers, and ultrafast cracks occur after heating.

This dissertation presents a new finite difference method for investigating the thermal deformation in a 3D gold-chromium thin film with imperfect interfacial thermal contact exposed to ultrashort-pulsed lasers. The method is obtained based on the parabolic two-step model and implicit finite difference schemes on a staggered grid. The method accounts for the coupling effect between lattice temperature and strain rate, as well as for the hot electron-blast effect in momentum transfer. In the calculations, a fourth-order compact scheme is employed for evaluating the stress derivatives in the dynamic equations of motion. The method allows us to avoid non-physical oscillation in the solution. In particular, the temperature change across an imperfect thermal interfacial contact can be expressed by the fourth-power law for radiation, which gives nonlinear temperature distribution around the interface, and we obtain successfully the stress

change across the interface based on the fourth-power law for radiation by an iterative numerical method.

Numerical results show that when the center part of a top surface was irradiated by ultrashort-pulsed lasers, there are no non-physical oscillations in the solution, and the solution is grid independent; hence, the scheme is considered to be stable. The results also show that the temperature distribution from the top surface discontinuously across the imperfect thermal interface to the bottom, and the displacement and stress alterates from a negative value to a positive value at the center along the z direction, and along x and y directions, indicating that the central part of the upper layer of the thin film expands during heating. The obtained model and numerical scheme in this dissertation will provide a theoretical tool for studying thermal deformation in multi-layered metal thin film exposed to ultrashort-pulsed lasers which have been used in laser process.

APPROVAL FOR SCHOLARLY DISSEMINATION

The author grants to the Prescott Memorial Library of Louisiana Tech University the right to reproduce, by appropriate methods, upon request, any or all portions of this Dissertation. It is understood that "proper request" consists of the agreement, on the part of the requesting party, that said reproduction is for his personal use and that subsequent reproduction will not occur without written approval of the author of this Dissertation. Further, any portions of the Dissertation used in books, papers, and other works must be appropriately referenced to this Dissertation.

Finally, the author of this Dissertation reserves the right to publish freely, in the literature, at any time, any or all portions of this Dissertation.

Author Runzhou Liu

Date 04/28/2011

DEDICATION

I dedicate this dissertation to my parents, who trusted, respected, and supported me and have done their best to provide me comfortable conditions for living and studying.

TABLE OF CONTENTS

LIST OF TABLES

LIST OF FIGURES

ACKNOWLEDGEMENTS

I am grateful to the people who have helped me to fulfill this dissertation. I wish to express my sincere gratitude and appreciation to my advisor, Dr. Weizhong Dai, for his generous advice and guidance with great patience. It is my honor to be his student. Without his guidance and advice, this dissertation could not have been completed. I would like to thank Dr. Songming Hou for his support and for his linear algebra class. I would also thank to Dr. Christian Duncan for his computer graphics in computer science course. Sincere acknowledgement is also extended to Dr. Dexter Cahoy for his patience to teach me about statistics and the time series. The special appreciation to Dr. Katie Evans is for her kind help and support. I thank the professors above for their kindness of serving as advisory committee members.

I owe a lot to my parents, my father Ruifeng Liu and my mother Xiufang Li, for their endless supporting of me and having done their best to provide me comfortable conditions for living and studying. Finally, I want to express my appreciation to all my friends. This dissertation is dedicated to all the above named.

CHAPTER ONE

INTRODUCTION

1.1 General Overview

Ultrashort-pulsed lasers have the pulse duration within the order of sub-picoseconds to femtoseconds. Such a unique character will make the ultrashort-pulsed lasers have a great advantage in limiting the undesirable spread of the thermal process zone in the heated sample [1], [16], and being an ideal candidate for precise thermal processing of functional nanophase materials [1], [16].

Since ultrashort-pulsed lasers have been widely used in structure monitoring of thin metal films [2], [3]; laser micromachining [4]; patterning [5]; structural tailoring of microfilms [6]; and laser synthesis and processing in thin-film deposition [7]; we need to pay attention to three key factors in order to apply high-energy ultrashort-pulsed lasers successfully. There are three key factors indicate (1) well characterized pulse width, intensity, and experimental techniques are required; (2) we need to have reliable and accurate microscale heat transfer models; and (3) it is very important to prevent thermal damage.

To date, researchers have developed many models that focus on heat transfer in the context of ultrashort-pulsed lasers. However, there are only a few mathematical models for studying thermal deformation induced by ultrashort-pulsed lasers [1], [8], [9],

[10], [11], [12], [13], [14], [15], [16], [17], [18]. In particularly, Tzou et al. [1] developed a 1D model in a double-layered metal thin film. The model was obtained using a differential-difference approach. Chen et al. [11] considered a 2D axis-symmetric cylindrical metal thin film and presented an explicit finite difference scheme by adding an artificial viscosity term to eliminate numerical oscillations. Dai et al. [8], [12], [13], [14], [15], [16] developed a kind of finite difference scheme for studying thermal deformation in 2D and 3D metal thin films exposed to ultrashort-pulsed lasers. In their schemes, they employed the parabolic or hyperbolic two-step heat transport equations coupled with implicit finite difference schemes on a staggered grid. Also these schemes considered the coupling effect between lattice temperature and strain rate, as well as for the hot-electron blast effect in momentum transfer. In particular, Dai et al. [11], [15], [16] used a fourth-order compact finite difference scheme for solving derivatives of stresses in the dynamic equations of motion so that the non-physical oscillations in 3D cases can be prevented. Recently, Qi and Suh [17], [18] have presented a 2D model for studying thermal damage in a cylindrical semiconductor thin film subject to ultrafast laser heating.

In this dissertation, we consider a 3D double-layered metal thin film with imperfect thermal contact between layers and study thermal deformation in the 3D thin film exposed to ultrashort-pulsed lasers. The perfect thermal contact means the interface is smooth, and two metal films are fully attached to each other so that the temperature and heat flux are continuous across the interface. Conversely, the imperfect thermal contact will result in the discontinued temperature and heat flux conducting nonlinear behavior across the interface. It should be pointed out that layered metal thin films are

considered because they are widely used in engineering applications due to the fact that a single metal layer often cannot satisfy all mechanical, thermal and electronic requirements. Because of multilayers, the imperfect thermal contact between layers may occur sometimes and, hence, the stress and displacement caused by the hot-electron-blast effect across the interface between layers may be changed sharply or discontinuely, resulting in possible thermal damage. As we know, the temperature change across an imperfect thermal contact interface can be expressed by the fourth-power law for radiation [19], [20], [21], which gives a nonlinear temperature distribution around the interface. However, finding a mathematical model governing stress and displacement changes across such an interface can be challenging. Most existing models for stress change [22], [23], [24], [25], [26], [27], [28] across the interface are complicated when applied to the 3D metal thin film exposed to ultrashort-pulsed lasers. Dai and his colleagues [14] considered a 2D double-layered metal thin film case and presented a formula for stress change across the interface, which was obtained based on the theory of elasticity [29], [30]. However, when applied to the present 3D case, the formula becomes very complex.

The motivation of my dissertation is to extend previous research on 3D double-layered thin film with perfect thermal interfacial contact case to the imperfect thermal interfacial contact case. In this case, we avoid seeking a mathematical model for stress change across the interface, and obtain the stress change across the interface based on only the fourth-power law for radiation and using an iterative numerical method.

1.2 Research Objective

The objective of my dissertation was to develop a numerical method for studying thermal deformation in 3D double-layered thin films with imperfect interfacial thermal contact exposed to ultrashort-pulsed lasers. This method was based on the dynamic equations of motion coupled with two-step parabolic heat transport equations.

To achieve this objective, the steps below were followed:

Step 1. Considered a 3D double-layered thin film structure in Cartesian coordinates and define its geometry. Propose the energy equations and dynamic equations of motion and initial and boundary conditions as the governing equations for describing thermal deformation in the double-layered thin film induced by ultrashort-pulsed lasers, where the interface between layers have imperfect thermal contact.

Step 2. Introduced three velocity components in x, y, z directions into the model, and rewrite the dynamic equations of motion to simplify the calculation and avoid numerical oscillations.

Step 3. Constructed a 3D staggered grid and design a finite difference scheme based on the staggered grid.

Step 4. Employed a fourth-order compact finite difference scheme for evaluating stress derivatives and substitute obtained values of these stress derivatives into the dynamic equations of motion. Hence the third-order derivatives of stresses and shear stresses raised by the numerical method are eliminated to prevent non-physical oscillations in the solutions.

Step 5. Applied the fourth-power law for radiation and use an iterative numerical method to obtain the stress change across the interface which has an imperfectly thermal interfacial contact induced by the ultrashort-pulsed lasers.

Step 6. Employed the developed numerical method to obtain the values of electron and lattice temperature, normal and shear stresses, normal strains and shear strains, displacements and velocities in x, y and z directions, respectively.

Step 7. Tested the numerical method, check the grid independence of the finite difference scheme by using different meshes and analyze the solutions.

1.3 Organization

Chapter One gives a general description of the research objectives in this dissertation.

Chapter Two introduces the main literature regarding the heat transfer in thin films, particular models that represent the thermal deformation, the process of microscale heat transfer of phonon-electron interaction model and the parabolic two-step model for micro thin films, as well as previous works on heat transfer in thin films.

Chapter Three sets up the heat transfer model for a 3D double-layered thin film with imperfect interfacial thermal contact exposed to ultrashort-pulsed lasers. Dynamic equations of motion and parabolic two-step heat conduction equations are considered to be the governing equations for describing thermal deformation in the 3D thin films induced by ultrashort-pulsed lasers heating on the center of the surface.

Chapter Four gives the numerical method used in this research for solving the governing equations set up in Chapter Three.

Chapter Five tests the mathematical model and numerical method in a 3D double-layered thin film with imperfect interfacial thermal contact exposed to ultrashort-pulsed lasers. Based on the obtained temperature distributions, stresses, strains and displacements will be calculated.

Finally, Chapter Six summarizes the dissertation research and suggests possible future research works.

CHAPTER TWO

BACKGROUND AND PREVIOUS WORK

Chapter Two introduces the main literature regarding the heat transfer in thin films, particular models that represent the thermal deformation, which is the process of microscale heat transfer of phonon-electron interaction model and the parabolic two-step model for micro thin films, as well as previous works on heat transfer in thin films.

2.1 Microscale Heat Transfer Model

2.1.1 Macroscopic Heat Transfer

This section cites results from some previous literatures [31], [32], [33]. In thermodynamics, heat is defined as energy transfer due to temperature gradients or differences. Heat transfer is the process of energy transition from carriers with high temperature to carriers with low temperature. A microscopic view in metals, electrons and phonons are the main energy carriers. There are three modes of heat transfer: conduction, convection and radiation. In this dissertation, we will consider heat transfer on 3D double-layered thin films with imperfect thermal interfacial contact between layers exposed to ultrashort-pulsed lasers described as radiation mode; whereas, heat transfer across the double-layered metal thin films is called conduction mode.

The difference between conduction, convection and radiation is important to understand the heat transfer. Conduction is by molecules that travel a very short distance

before colliding with another molecule and exchanging energy and these energy carriers have a shorter mean free path. However, radiation is by photons, which travel almost unimpeded through the air from one surface to another, such that energy carriers have a long, mean free path. Convection is defined as the transport of energy by bulk motion of a medium. Our research will focus on heat transfer by phonon-electron interaction in double-layered metallic films.

Macro heat conduction describes macroscopic behavior of conduction of thermal energy. In the classical theory of heat transfer, the main phenomenological law that governs heat conduction is Fourier's law. It is a constitutive equation that depicts the way in which cause varies with effect.

Fourier's law of heat conduction,

$$\vec{q} = -k\nabla T\,, \tag{2.1}$$

where k is the thermal conductivity of the material, dictates that the heat flux vector ($\vec{q}$) and the temperature gradient (∇T) across a material volume must occur at the same time .

The energy equation derived from the first law of thermodynamics is

$$-\nabla\cdot\vec{q} = C_p\frac{\partial T}{\partial t} - Q\,, \tag{2.2}$$

where C_p is the volumetric heat capacity and Q is the heat source. Substituting Equation (2.1) into Equation (2.2), we can obtain the traditional heat diffusion equation:

$$C_p\frac{\partial T}{\partial t} = \nabla\cdot(k\nabla T) + Q\,. \tag{2.3}$$

Equation (2.3) is often referred to as a parabolic equation, and as a result, any temperature disturbance will propagate at an infinite speed.

Fourier's law breaks down at temperatures near absolute zero and breaks down further when the pulsed duration becomes extremely small, even on the order of picoseconds or femtoseconds. A typical case occurs in the ultrashort-pulsed laser heating in the thermal processing of materials [34], [35]. For very short laser-pulsed heating, the physical dimension in microscale heat transfer is of the same order of magnitude as the electron free path, the response time is of this same magnitude. This fact indicates that the temperature gradient is not descriptive for a thin film of the same thickness as the mean free path [36]. Specific to microscale heat transfer, Fourier's law does not accurately predict the transient temperature during microscale ($<10^{-12}s$) laser heating of thin metal films ($<10^{-16}m$) [37], [38], [39].

2.1.2 Two-Step Heat Transfer Model

In microscale, the phonon-electron interaction model was proposed to describe a two-step process for energy transport. For considering the phonon-electron interaction, the conventional model should be revised to fit the heat transfer theories in microscale. For those electrons with much smaller heat capacity than metal lattice, the heating system involves excitation of the electrons and heating of the metal lattice through phonon-electron interaction in short times [36]. The phonon-electron interaction model was expected to exactly describe this two primary phases for energy transport. The first phase describes the deposition of energy on electrons, and the second describes the transfer of the energy from the electrons to the lattice.

Parabolic two-step model for heat transfer can be expressed as follows:

$$C_e(T_e)\frac{\partial T_e}{\partial t} = \nabla\cdot(k\nabla T_e) - G(T_e - T_l) + Q, \tag{2.4}$$

$$C_l(T_l)\frac{\partial T_l}{\partial t} = G(T_e - T_l)\,. \tag{2.5}$$

Here, $C_e(T_e)$ is the electron heat capacity, k is the thermal conductivity, G is the electron-lattice coupling factor, $C_l(T_l)$ is the lattice heat capacity, and subscripts e and l represent the electron and metal lattice, respectively.

Equation (2.4) represents the first step, which describes the deposition of energy heating on electrons, and Equation (2.5) represents the second step, which involves the transfer of the energy from electrons to the lattice. Here, the effect of heat conduction through the metal lattice is not considered at this time. In this dissertation, Equation (2.4) is used for calculating the unknown electron-gas temperature (T_e), and Equation (2.5) is used for calculating the unknown metal-lattice temperature (T_l).

Tzou et al. pointed out for an electron gas temperature lower than the Fermi temperature, of the order of 10^4 K, the electron heat capacity (C_e) is proportional to the electron temperature [36]. This argument makes the equation give nonlinear solutions. Therefore, the electron heat capacity C_e can be obtained from Barron's research [40]:

$$C_e = \gamma_e T_e, \tag{2.6}$$

where γ_e is known as the electron specific heat coefficient and can be obtained it from experiments.

The phonon-electron coupling factor describes the energy exchange between phonons and electrons [41]:

$$G = \frac{\pi^2}{6}\frac{m_e n_e v_s^2}{\tau_e T_e} \quad \text{For} T_e >> T_l, \tag{2.7}$$

where m_e is the electron mass, n_e is the number density of electrons per unit volume, and v_s is the speed of sound. It is obtained as

$$v_s = \frac{\sigma}{2\pi h}(6\pi^2 n_a)^{\frac{1}{3}} T_D, \tag{2.8}$$

where the quantity h is Planck's constant, k is the Boltzmann constant, n_a is the atomic number density per unit volume, and T_D represents the Debye temperature. The electron temperature (T_e) is much higher than the lattice temperature (T_l) in the early time response. Then the lattice temperature (T_l) increases, and as a result, the electron temperature (T_e) discreases due to the electron-lattice effect. The condition $T_e >> T_l$ in Equation (2.6) for the applicability of G is thus valid in the fast-transient process of electron-phonon dynamics. Within the limits of Wiedemann-Frenz's law, which states that for metals at moderate temperatures ($T_l > 0.48T_D$), the ratio of the thermal conductivity to the electrical conductivity is proportional to the temperature, and the constant of proportionality is independent of particular metal, the electron thermal conductivity can be expressed as [41]

$$k_e = \frac{\pi^2 n_e k^2 \tau_e T_e}{3m_e}, \tag{2.9}$$

or just set simply m_e,

$$m_e = \frac{\pi^2 n_e k^2 \tau_e T_e}{3k_e}. \tag{2.10}$$

We substitute Equation (2.10) into Equation (2.7) for the electron mass, and then we can calculate G as

$$G=\frac{\pi^4(n_e v k_s)^2}{18\sigma}. \tag{2.11}$$

This electron-lattice coupling factor is decided by the thermal conductivity (k) and the number density (n_e) of the electron gas. From Tzou's research, the electron-lattice coupling factor does not show a strong dependence upon temperature and is not affected by relaxation time [36].

In order to calculate the value of G, the number density (n_e) of the electron gas is a key quantity. Qiu and Tien assumed one free electron per atom for noble metals and employed the s-band approximation for the valence electrons in transition metals [42]. Therefore, the value for the number density of the electron gas is chosen as a fraction of the valence electrons. The phonon-electron coupling factor is calculated, and these experimentally obtained values are listed in Table 2.1 [44] for comparison.

Table 2.1 Phonon-electron coupling factor G for some noble and transition metals

Metal	Calculated, $\times 10^{16}$ W/m^{3}K	Measured, $\times 10^{16}$ W/m^{3}K
Cu	14	4.8 ± 0.7 [Brorson 1990] 10 [Elsayed-Ali 1987]
Ag	3.1	2.8 [Groeneveld 1990]
Au	2.6	2.8 ± 0.5 [Brorson 1990]
Cr	45 (n_e/n_a = 0.5)	42 ± 5 [Brorson 1990]
W	27 (n_e/n_a = 1.0)	26 ± 3 [Brorson 1990]
V	648 (n_e/n_a = 2.0)	523 ± 37 [Brorson 1990]
Nb	138 (n_e/n_a = 2.0)	387 ± 36 [Brorson 1990]
Pb	62	12.4 ± 1.4 [Brorson 1990]
Ti	202 (n_e/n_a = 1.0)	185 ± 16 [Brorson 1990]

Equation (2.4) is governed by diffusion in the electron gas and heat is transferred to the lattice in a lumped capacity sense through the coupling factor, G. In other words, the rate of energy increase in the metal lattice is proportional to the temperature difference between the metal lattice and the electrons. By eliminating the electron gas temperature, T_e, from Equation (2.4) and Equation (2.5) for constant thermal properties, one can show that:

$$\frac{1}{\alpha_T}\frac{\partial T_l}{\partial t}+\frac{1}{C_T^2}\frac{\partial^2 T_l}{\partial t^2}=\nabla^2 T_l+\frac{\alpha_e}{C_T^2}\frac{\partial}{\partial t}\left(\nabla^2 T_l\right), \tag{2.12}$$

where α_e is the thermal diffusivity of the electron gas and α_T is the equivalent thermal diffusivity represented by:

$$\alpha_T=\frac{k}{C_e+C_l}, \tag{2.13}$$

where C_T is the thermal wave speed and is represented by:

$$C_T=\sqrt{\frac{kG}{C_eC_l}}. \tag{2.14}$$

However, the author tried to simplify the discussion and ease the numerical analysis, this single equation form is seldom utilized. In this work, Equation (2.4) and Equation (2.5) are used.

Researchers determined the parabolic two-step model to be a good estimate [42]. To compare experimental results with a numerical model, the normalized temperature change in the electron gas is identical to the normalized reflectivity change on the film surface:

$$\frac{\Delta R}{(\Delta R)_{\max}}=\frac{\Delta T_e}{(\Delta T_e)_{\max}}, \tag{2.15}$$

where R denotes the reflectivity. The left side of Equation (2.15) can be measured by the front-surface-pump and back-surface-probe technique [36]. The right hand side of Equation (2.15) represents the solution to the numerical model for estimating heat propagation.

Figure 2.1 shows the resulting applicability of the parabolic two step model. The predicted temperature change at the surface of a thin gold film is compared with the experimental data collected [36].

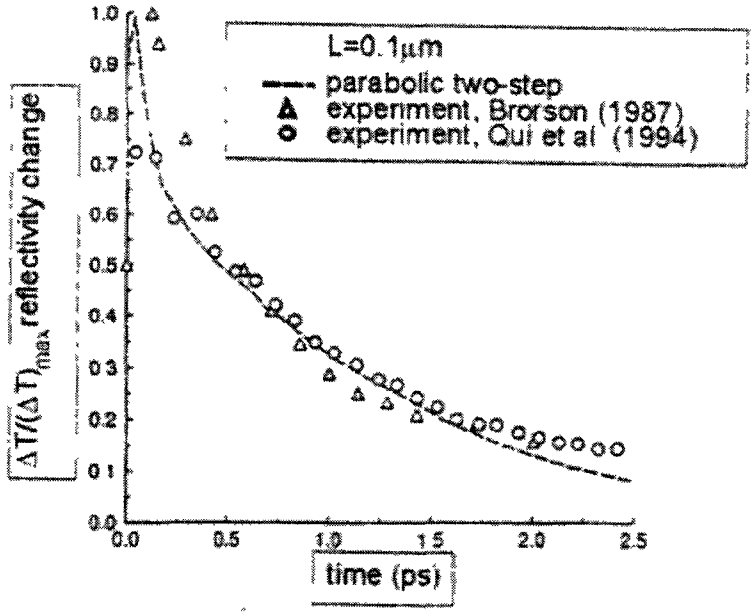

Figure 2.1 Normalized temperature change (reflectivity change) in gold film predicted by dual-phase-lag model.

2.2 Previous Models on Thermal Deformation in Thin Film

2.2.1 Two-Dimensional Parabolic Single Layered Heat Transfer Model

Dai et al. in 2006 developed a mathematical model for studying thermal deformation in a 2D single-layered thin film exposed to ultrashort-pulsed lasers based on parabolic two-step heat transfer equations [13], [14]. The 2D single-layered metal thin film structure is shown in Figure 2.2.

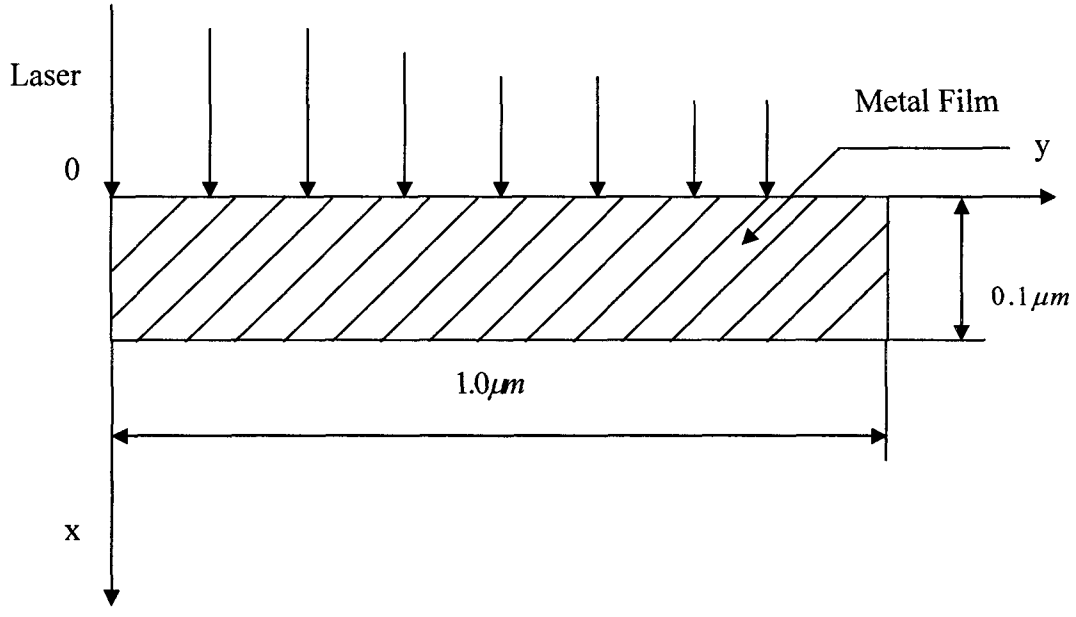

Figure 2.2 Configuration of a metal thin film exposed to ultrashort-pulsed lasers.

The governing equations for studying thermal deformation can be expressed as:

(1) Dynamic Equations of Motion [12], [43], [44], [45]

$$\rho\frac{\partial^2 u}{\partial t^2}=\frac{\partial\sigma_x}{\partial x}+\frac{\partial\sigma_{xy}}{\partial y}+2\Lambda T_e\frac{\partial T_e}{\partial x}, \tag{2.16}$$

$$\rho\frac{\partial^2 v}{\partial t^2}=\frac{\partial\sigma_{xy}}{\partial x}+\frac{\partial\sigma_y}{\partial y}+2\Lambda T_e\frac{\partial T_e}{\partial y}, \tag{2.17}$$

where

$$\sigma_x=\lambda(\varepsilon_x+\varepsilon_y)+2\mu\varepsilon_x-(3\lambda+2\mu)\alpha_T(T_l-T_0), \tag{2.18}$$

$$\sigma_y=\lambda(\varepsilon_x+\varepsilon_y)+2\mu\varepsilon_y-(3\lambda+2\mu)\alpha_T(T_l-T_0), \tag{2.19}$$

$$\sigma_{xy}=\mu\varepsilon_{xy}, \tag{2.20}$$

$$\varepsilon_x=\frac{\partial u}{\partial x},\varepsilon_y=\frac{\partial u}{\partial y},\varepsilon_{xy}=\frac{\partial u}{\partial y}+\frac{\partial v}{\partial x}, \tag{2.21}$$

$$\lambda=K-\frac{2}{3}\mu. \tag{2.22}$$

(2) Energy Equations [42], [45], [46]

$$C_e(T_e)\frac{\partial T_e}{\partial t}=\frac{\partial}{\partial x}\left[k_e(T_e,T_l)\frac{\partial T_e}{\partial x}\right]+\frac{\partial}{\partial y}\left[k_e(T_e,T_l)\frac{\partial T_e}{\partial y}\right]$$

$$-G(T_e-T_l)+Q, \tag{2.23}$$

$$C_l\frac{\partial T_l}{\partial t}=G(T_e-T_l)-(3\lambda+2\mu)\alpha_T T_0\frac{\partial}{\partial t}(\varepsilon_x+\varepsilon_y), \tag{2.24}$$

where the heat source is given by

$$Q=0.94J\frac{1-R}{t_p x_s}\exp\left[-\frac{x}{x_s}-\left(\frac{y}{y_s}\right)^2-2.77\left(\frac{t-2t_p}{t_p}\right)^2\right], \tag{2.25}$$

where, $C_e(T_e) = C_{e0}\left(\frac{T_e}{T_0}\right)$, and $k_e(T_e, T_l) = k_0\left(\frac{T_e}{T_l}\right)$. Equation (2.23) and Equation (2.24) are often referred to as parabolic two-step heat transport equations.

The boundary conditions are assumed to be stress free and thermally insulated:

$$\sigma_x = 0, \sigma_{xy} = 0, \text{ at } x = 0, L_x, \tag{2.26}$$

$$\sigma_y = 0, \sigma_{xy} = 0, \text{ at } y = 0, L_y, \tag{2.27}$$

$$\frac{\partial T_e}{\partial \vec{n}} = 0, \frac{\partial T_l}{\partial \vec{n}} = 0. \tag{2.28}$$

The initial conditions are assumed to be

$$T_e = T_l = T_0, u = v = 0,$$

$$\text{and } u_t = v_t = 0, \text{ at } t = 0. \tag{2.29}$$

Figures and discussions for the 2D single layer model are given in [14].

Figure 2.3 shows the change in electron temperature $\left[\frac{\Delta T_e}{(\Delta T_e)_{\max}}\right]$ at $x = 0$ μm and $y = 0$ μm. The maximum temperature rise of T_e (i.e. $(\Delta T_e)_{\max}$) is about 3791 K.

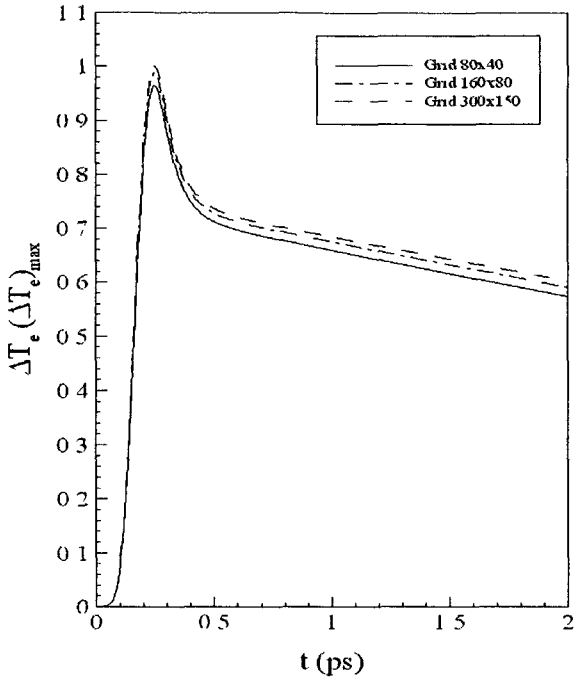

Figure 2.3 Change in electron temperature at $x = 0$ and $y = 0$ versus time for various meshes (80×40, 160×80, and 300×150).

Figure 2.4 shows the displacement (u) at $x = \frac{1}{2}\Delta x$, and $y = \Delta y$ versus time. It can be seen from both figures that the solutions are convergent as the mesh is getting finer.

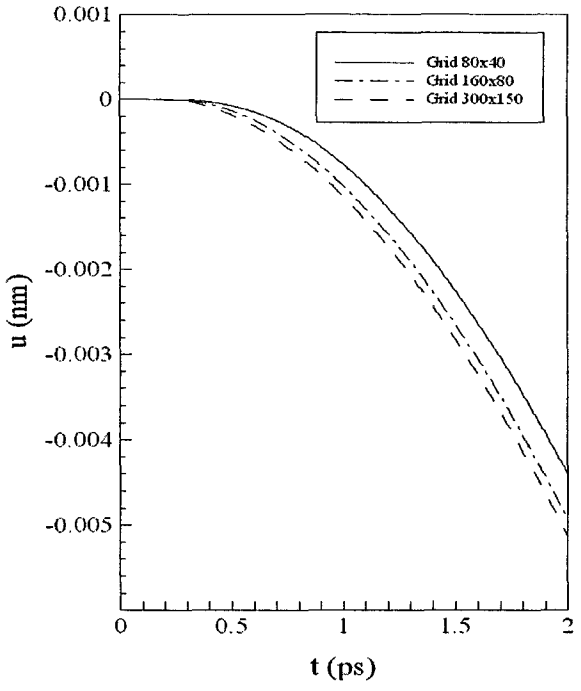

Figure 2.4 Displacement (u) at $x = \frac{1}{2}\Delta x$ and $y = \Delta y$ versus time for various meshes (80×40, 160×80, and 300×150).

Figure 2.5 shows comparison of the present method with Chen et al.'s method in [11] with regard to the normal stress (σ_x) at $y = \Delta y$ at t = 10 ps. There is no non-physical oscillation in present method, but it still exists in Chen et al.'s method.

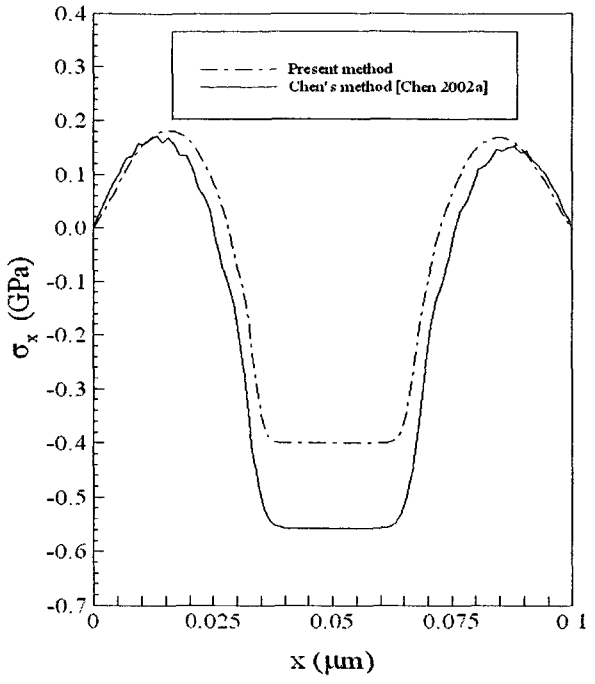

Figure 2.5 Comparison of the present method with Chen et al.'s method in [3] with regard to the normal stress (σ_x) at $y = \Delta y$ at t = 10 ps.

2.2.2 Two-Dimensional Parabolic Double Layered Heat Transfer Model

In 2008, Dai et al. extended their previous research and developed a mathematical model for studying thermal deformation in a 2D double-layered thin film exposed to ultrashort-pulsed lasers [13]. The 2D double-layered metal thin film structure is shown in Figure 2.6.

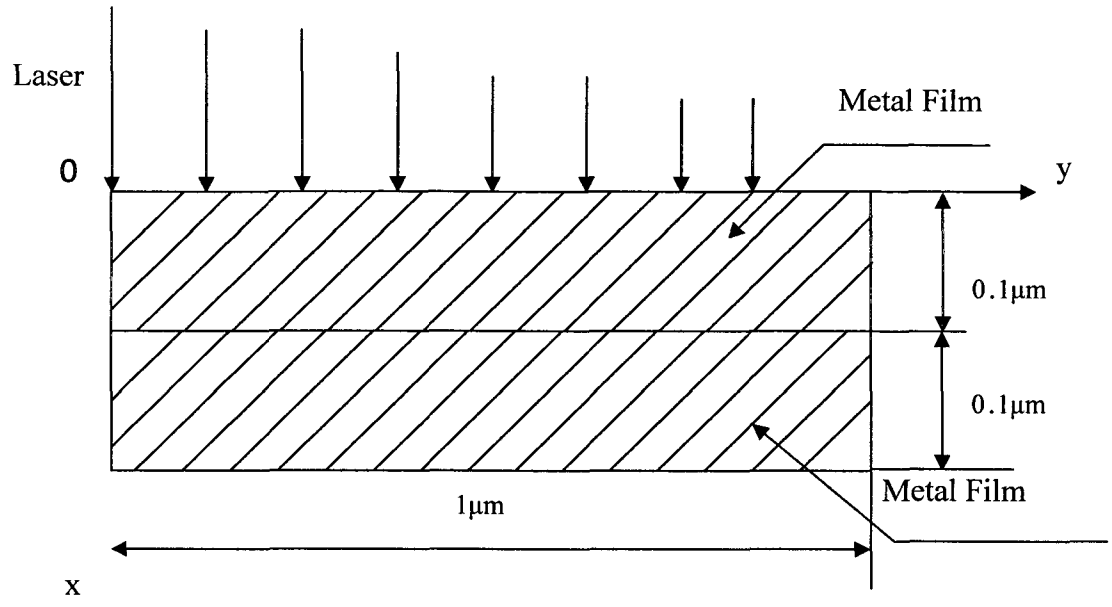

Figure 2.6 Configuration of a double-layered thin metal film exposed to ultrashort-pulsed lasers.

The governing equations for studying thermal deformation in a thin film are expressed as follows:

(1) Dynamic equations of motion [1], [9], [13], [43], [47]:

$$\rho^{(m)}\frac{\partial^2 u^{(m)}}{\partial t^2}=\frac{\partial \sigma_x^{(m)}}{\partial x}+\frac{\partial \sigma_{xy}^{(m)}}{\partial y}+2\Lambda^{(m)}T_e^{(m)}\frac{\partial T_e^{(m)}}{\partial x}, \tag{2.30}$$

$$\rho^{(m)}\frac{\partial^2 v^{(m)}}{\partial t^2}=\frac{\partial \sigma_{xy}^{(m)}}{\partial x}+\frac{\partial \sigma_y^{(m)}}{\partial y}+2\Lambda^{(m)}T_e^{(m)}\frac{\partial T_e^{(m)}}{\partial y}, \tag{2.31}$$

where

$$\sigma_x^{(m)}=\lambda^{(m)}\left(\varepsilon_x^{(m)}+\varepsilon_y^{(m)}\right)+2\mu^{(m)}\varepsilon_x^{(m)}-\left(3\lambda^{(m)}+2\mu^{m)}\right)\alpha_T^{(m)}\left(T_l^{(m)}-T_0\right), \tag{2.32}$$

$$\sigma_y^{(m)}=\lambda^{(m)}\left(\varepsilon_x^{(m)}+\varepsilon_y^{(m)}\right)+2\mu^{(m)}\varepsilon_y^{(m)}-\left(3\lambda^{(m)}+2\mu^{(m)}\right)\alpha_T^{(m)}\left(T_l^{(m)}-T_0\right), \tag{2.33}$$

$$\sigma_{xy}^{(m)}=\mu^{(m)}\gamma_{xy}^{(m)}, \tag{2.34}$$

$$\varepsilon_x^{(m)} = \frac{\partial u^{(m)}}{\partial x}, \quad \varepsilon_y^{(m)} = \frac{\partial v^{(m)}}{\partial y},$$

$$\gamma_{xy}^{(m)} = \frac{\partial u^{(m)}}{\partial y} + \frac{\partial v^{(m)}}{\partial x}. \tag{2.35}$$

Here, m = 1, 2, denotes layer 1 and layer 2, respectively; $u^{(m)}$ is the displacement in the thickness direction (x - direction) and $v^{(m)}$ is the displacement in the length direction (y-direction); $\varepsilon_x^{(m)}$ and $\varepsilon_y^{(m)}$ are the normal strains in x and y directions, respectively; $\gamma_{xy}^{(m)}$ is the shear strain; $\sigma_x^{(m)}$ and $\sigma_y^{(m)}$ are the normal stresses in x and y directions, respectively; $\sigma_{xy}^{(m)}$ is the shear stress; $T_e^{(m)}$ and $T_l^{(m)}$ are electron and lattice temperatures, respectively; T_0 is initial temperature; $\lambda^{(m)} = K^{(m)} - \frac{2}{3}\mu^{(m)}$ [48] where $\lambda^{(m)}$ is Lame constant, $K^{(m)}$ is bulk modulus, and $\mu^{(m)}$ is shear modulus; $\alpha_T^{(m)}$ is thermal expansion coefficient.

(2) Energy equations [1], [9], [13], [43], [47]:

$$\begin{aligned}(C_e(T_e))^{(m)} \frac{\partial T_e^{(m)}}{\partial t} &= \frac{\partial}{\partial x}\left[(k_e(T_e,T_l))^{(m)} \frac{\partial T_e^{(m)}}{\partial x}\right] \\ &+ \frac{\partial}{\partial y}\left[(k_e(T_e,T_l))^{(m)} \frac{\partial T_e^{(m)}}{\partial y}\right] - G^{(m)}\left(T_e^{(m)} - T_l^{(m)}\right) + Q,\end{aligned} \tag{2.36}$$

$$C_l^{(m)} \frac{\partial T_l^{(m)}}{\partial t} = G^{(m)}\left(T_e^{(m)} - T_l^{(m)}\right) - \left(3\lambda^{(m)} + 2\mu^{(m)}\right)\alpha_T^{(m)} \frac{\partial}{\partial t}\left(\varepsilon_x + \varepsilon_y\right), \tag{2.37}$$

where the heat source is given by

$$Q = 0.94J \frac{1-R}{t_p x_s} \exp\left[-\frac{x}{x_s} - \left(\frac{y}{y_s}\right)^2 - 2.77\left(\frac{t-2t_p}{t_p}\right)^2\right]. \tag{2.38}$$

Here, $(C_e(T_e))^{(m)} = C_{e0}^{(m)} \cdot \frac{T_e^{(m)}}{T_0}$ is the electron heat capacity; $(k_e(T_e, T_l))^{(m)}$ is the electron thermal conductivity; $G^{(m)}$ is the electron-lattice coupling factor; $C_l^{(m)}$ is the lattice heat capacities; Q is the energy absorption rate; J is the laser fluence; R is the surface reflectivity; t_p is the laser pulse duration; x_s is the optical penetration depth, and y_s is the spatial profile parameter.

(3) Initial and Boundary Conditions:

The boundary conditions are assumed to be

$$\sigma_x^{(1)} = 0, \quad \sigma_{xy}^{(1)} = 0, \quad \text{at } x = 0, \text{ and}$$

$$\sigma_x^{(2)} = 0, \quad \sigma_{xy}^{(2)} = 0, \quad \text{at } x = L_x, \tag{2.39}$$

$$\sigma_y^{(1)} = 0, \quad \sigma_{xy}^{(1)} = 0, \quad \text{at } y = 0, \text{ and}$$

$$\sigma_y^{(2)} = 0, \quad \sigma_{xy}^{(2)} = 0, \quad \text{at } y = L_y, \tag{2.40}$$

$$\frac{\partial T_e^{(m)}}{\partial \vec{n}} = 0, \quad \frac{\partial T_l^{(m)}}{\partial \vec{n}} = 0, \tag{2.41}$$

where $\vec{n}$ is the unit outward normal vector on the boundary. Here, insulated boundaries are imposed due to the assumption that there are no heat losses from the film surfaces in the short time response.

The initial conditions are assumed to be

$$T_e^{(m)} = T_l^{(m)} = T_0, \tag{2.42}$$

$$u^{(m)} = v^{(m)} = 0, \tag{2.43}$$

$$u_t^{(m)} = v_t^{(m)} = 0, \tag{2.44}$$

at $t = 0$, where $m = 1, 2$.

(4) Interfacial conditions:

There are two cases at the interface of the double-layered thin film. One is perfect thermal contact at interface, which is a simple one. The other is imperfect thermal contact at interface. Nonlinear interfacial condition for temperature is considered. The interfacial conditions for stress, strain, and displacement are derived.

Case 1: Perfectly thermal contact at interface

The perfect contact interfacial conditions are assumed to be, at $x = L_x / 2$,

$$u^{(1)} = u^{(2)}, \qquad v^{(1)} = v^{(2)}, \tag{2.45}$$

$$\sigma_x^{(1)} = \sigma_x^{(2)}, \quad \sigma_{xy}^{(1)} = \sigma_{xy}^{(2)}, \tag{2.46}$$

$$T_e^{(1)} = T_e^{(2)}, \quad k_e^{(1)} \frac{\partial T_e^{(1)}}{\partial x} = k_e^{(2)} \frac{\partial T_e^{(2)}}{\partial x}. \tag{2.47}$$

Case 2: Imperfectly thermal contact at interface

The nonlinear interfacial condition for T_e can be written as follows [49], [50], [51]:

$$-k_e^{(1)} \frac{\partial T_e^{(1)}}{\partial x} = -k_e^{(2)} \frac{\partial T_e^{(2)}}{\partial x} = \sigma\left[\left(T_e^{(1)}\right)^4 - \left(T_e^{(2)}\right)^4\right], \qquad T_e^{(1)} \neq T_e^{(2)}, \tag{2.48}$$

where $\sigma = 5.669 \times 10^{-8}\ \mathrm{W/m^2K^4}$ is Stefan-Boltzmann constant. Once T_e is obtained, T_l at interface can be obtained based on Equation (2.37).

To obtain the interfacial conditions for stress and displacement, Wang first assumed that shear stresses are equal at interface,

$$\sigma_{xy}^{(1)} = \sigma_{xy}^{(2)}. \tag{2.49}$$

From Equations (2.34) and (2.35), we obtain that $\mu^{(1)}\gamma_{xy}^{(1)} = \mu^{(2)}\gamma_{xy}^{(2)}$ and hence $\mu^{(1)}\left(\frac{\partial u^{(1)}}{\partial y} + \frac{\partial v^{(1)}}{\partial x}\right) = \mu^{(2)}\left(\frac{\partial u^{(2)}}{\partial y} + \frac{\partial v^{(2)}}{\partial x}\right)$. It is noted that if $\mu^{(1)}\frac{\partial u^{(1)}}{\partial y} = \mu^{(2)}\frac{\partial u^{(2)}}{\partial y}$ and $\mu^{(1)}\frac{\partial v^{(1)}}{\partial x} = \mu^{(2)}\frac{\partial v^{(2)}}{\partial x}$, then $\mu^{(1)}\left(\frac{\partial u^{(1)}}{\partial y} + \frac{\partial v^{(1)}}{\partial x}\right) = \mu^{(2)}\left(\frac{\partial u^{(2)}}{\partial y} + \frac{\partial v^{(2)}}{\partial x}\right)$ is satisfied. For the purpose of simple computation later on, we assume that $\mu^{(1)}\frac{\partial u^{(1)}}{\partial y} = \mu^{(2)}\frac{\partial u^{(2)}}{\partial y}$ and $\mu^{(1)}\frac{\partial v^{(1)}}{\partial x} = \mu^{(2)}\frac{\partial v^{(2)}}{\partial x}$. These equations lead to assume the interfacial condition for displacements to be, for simplicity,

$$\mu^{(1)}u^{(1)} = \mu^{(2)}u^{(2)} \quad \text{and} \quad \mu^{(1)}v^{(1)} = \mu^{(2)}v^{(2)}. \tag{2.50}$$

Based on this assumption, Wang et al. obtained that $\mu^{(1)}\frac{\partial u^{(1)}}{\partial x} = \mu^{(2)}\frac{\partial u^{(2)}}{\partial x}$ and hence $\mu^{(1)}\varepsilon_x^{(1)} = \mu^{(2)}\varepsilon_x^{(2)}$ from Eq. (2.39).

Since $\varepsilon_x^{(m)} = \frac{1}{E^{(m)}}\left[\left(1-\gamma^2\right)\sigma_x^{(m)} - \gamma\left(1+\gamma\right)\sigma_y^{(m)}\right] + \alpha_T^{(m)}\left(T_l^{(m)} - T_0\right)$ [23], [50], where E is Young's modulus and γ is Poisson ratio, Wang et al. substituted it into $\mu^{(1)}\frac{\partial u^{(1)}}{\partial x} = \mu^{(2)}\frac{\partial u^{(2)}}{\partial x}$ and obtained

$$\begin{aligned}&\frac{\mu^{(1)}}{E^{(1)}}\left[\left(1-\gamma^2\right)\sigma_x^{(1)} - \gamma\left(1+\gamma\right)\sigma_y^{(1)}\right] + \mu^{(1)}\alpha_T^{(1)}\left(T_l^{(1)} - T_0\right)\\ &= \frac{\mu^{(2)}}{E^{(2)}}\left[\left(1-\gamma^2\right)\sigma_x^{(2)} - \gamma\left(1+\gamma\right)\sigma_y^{(2)}\right] + \mu^{(2)}\alpha_T^{(2)}\left(T_l^{(2)} - T_0\right).\end{aligned} \tag{2.51}$$

Again, for simplicity, it was assumed that $\mu^{(1)}\left(\frac{(1-\gamma^2)\sigma_x^{(1)}}{E^{(1)}}\right)=\mu^{(2)}\left(\frac{(1-\gamma^2)\sigma_x^{(2)}}{E^{(2)}}\right)$

and $\frac{\mu^{(1)}}{E^{(1)}}\left(-\gamma(1+\gamma)\sigma_y^{(1)}\right)+\mu^{(1)}\alpha_T^{(1)}\left(T_l^{(1)}-T_0\right)=\frac{\mu^{(2)}}{E^{(2)}}\left(-\gamma(1+\gamma)\sigma_y^{(2)}\right)+\mu^{(2)}\alpha_T^{(2)}\left(T_l^{(2)}-T_0\right)$.

Since the interest was only in $\mu^{(1)}\left(\frac{(1-\gamma^2)\sigma_x^{(1)}}{E^{(1)}}\right)=\mu^{(2)}\left(\frac{(1-\gamma^2)\sigma_x^{(2)}}{E^{(2)}}\right)$, hence Wang et al. have interfacial condition to be

$$\mu^{(1)}\left(\frac{\sigma_x^{(1)}}{E^{(1)}}\right)=\mu^{(2)}\left(\frac{\sigma_x^{(2)}}{E^{(2)}}\right). \tag{2.52}$$

From above, we can see Wang et al. considered a 2D double-layered metal thin film case and presented a formula for stress change across the interface, which was obtained based on the theory of elasticity [30], [48]. However, when applied to the present 3D case, the formula becomes very complex. We do not have enough equations to find out the stress across the interface. In this study, we avoid seeking a mathematical model for stress change across the interface and obtain successfully the stress change across the interface based on only the fourth-power law for radiation and iterative numerical method.

Figures and discussions for the 2D double layer model are given in [14]:

Case 1: Perfectly thermal contact at interface

Figure 2.7 shows the change in electron temperature $\left[\frac{\Delta T_e}{(\Delta T_e)_{\max}}\right]$ at $x=0$ μm and $y=0$ μm with laser fluence J=500J/m^2. The maximum temperature rise of T_e (i.e. $(\Delta T_e)_{\max}$) is about 3790 K.

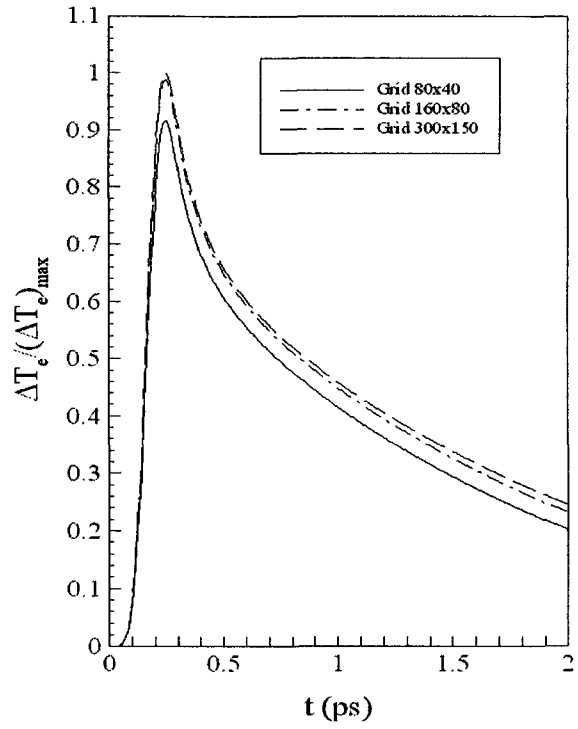

Figure 2.7 Change in electron temperature at $x = 0\,\mu m$ and $y = 0\,\mu m$ versus time for various meshes (80×40, 160×80, 300×150) with laser fluence J=500J/m^2.

Figure 2.8 shows the displacement (u) at $x = \frac{1}{2}\Delta x$, and $y = \Delta y$ versus time. It can be seen from both figures that the solution is grid independence and hence the scheme is considered to be stable.

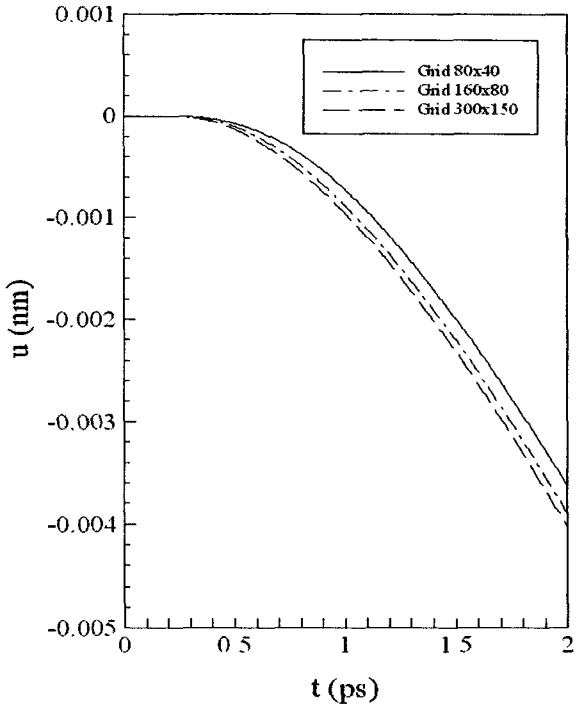

Figure 2.8 Displacement (u) at $x = \frac{1}{2}\Delta x$ and $y = \Delta y$ with laser fluuence of J=500J/m^2 versus time for various meshes ($80\times 40, 160\times 80, 300\times 150$).

Case 2: Imperfectly thermal contact at interface

Figure 2.9 shows the temperature change in electron temperature $\left[\frac{\Delta T_e}{(\Delta T_e)_{\max}}\right]$ at $x = 0$ μm and $y = 0$ μm with laser J=500J/m^2. The maximum temperature rise of T_e (i.e., $(\Delta T_e)_{\max}$) is about 5823 K.

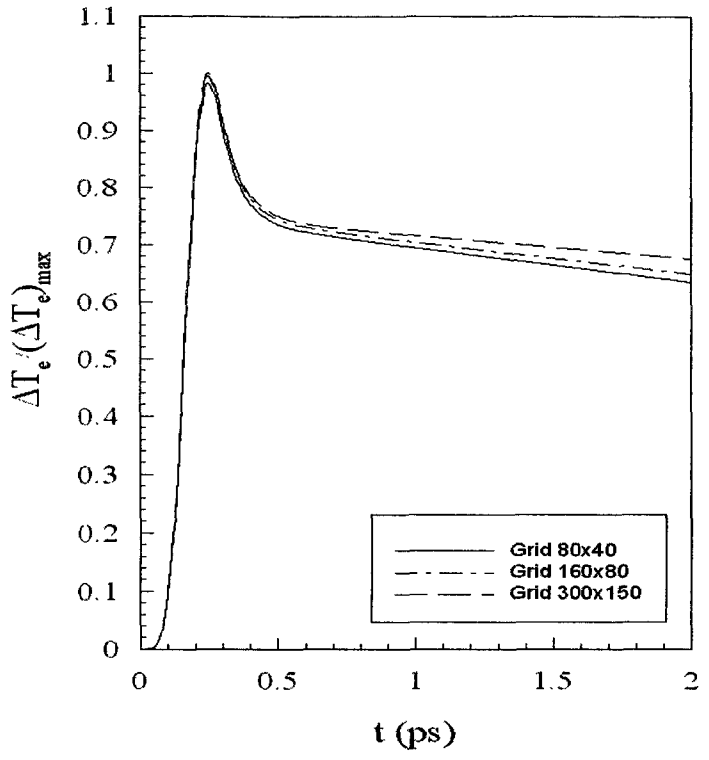

Figure 2.9 Change in electron temperature at $x = 0$ μm and $y = 0$ μm versus time for various meshes ($80\times40, 160\times80, 300\times150$).

Figure 2.10 shows the displacement (u) at $x = \frac{1}{2}\Delta x$, and $y = \Delta y$ versus time. It can be seen from both figures that the solution is grid independence and, hence, the scheme is considered to be stable.

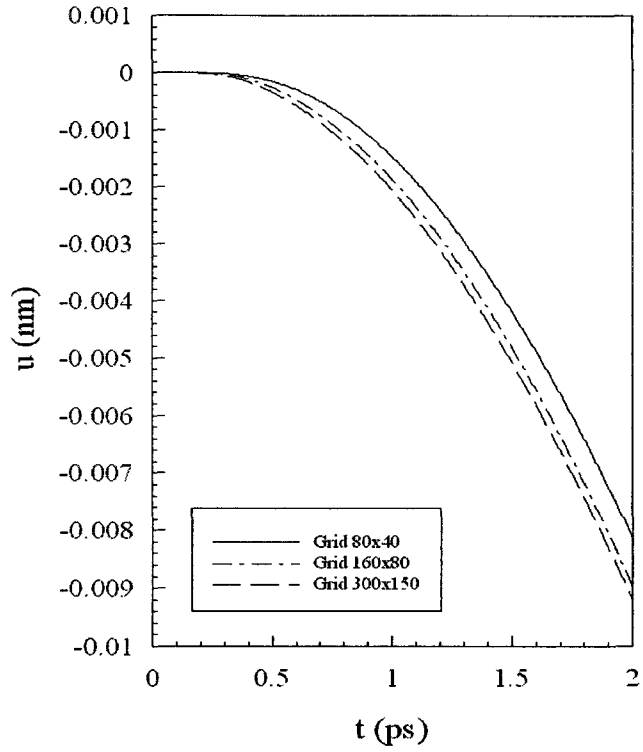

Figure 2.10 Displacement (u) at $x = \frac{1}{2}\Delta x$ and $y = \Delta y$ with laser J=500J/m^2 versus time for various meshes ($80\times40, 160\times80, 300\times150$).

Figures 2.11 and 2.12 show comparisons of electron temperature and lattice temperature, respectively, along x at $y = 0\,\mu$m between the perfect thermal contact and the imperfect thermal contact at interface with three different laser fluences (J=500J/m^2, 1000J/m^2 and 2000J/m^2) at different times (a) t = 0.25 ps, (b) t = 0.5 ps, (c) t = 1 ps, (d) t = 10 ps and (e) t = 20 ps. It can be seen that the electron temperature rises to its maximum at the beginning and then decreases while the lattice temperature rises gradually with time. Figure 2.11 shows clearly that there is a sharp discontinuity of electron temperature at the interface when imperfectly thermal contact exists between two bonded thin layers. Similar temperature discontinuity is observed at the interface for lattice temperature in Figure 2.12. These results indicate that imperfect thermal contact

at the interface provides a barrier to thermal energy diffusion across the interface. These two figures also show that electron temperature and lattice temperature are uniform throughout the chromium layer and uniform throughout the gold layer after a long period. The uniform electron and lattice temperatures are probably due to increased rate of collision between electrons and phonons in the gold layer as electron energy diffusion is inhibited at the interface.

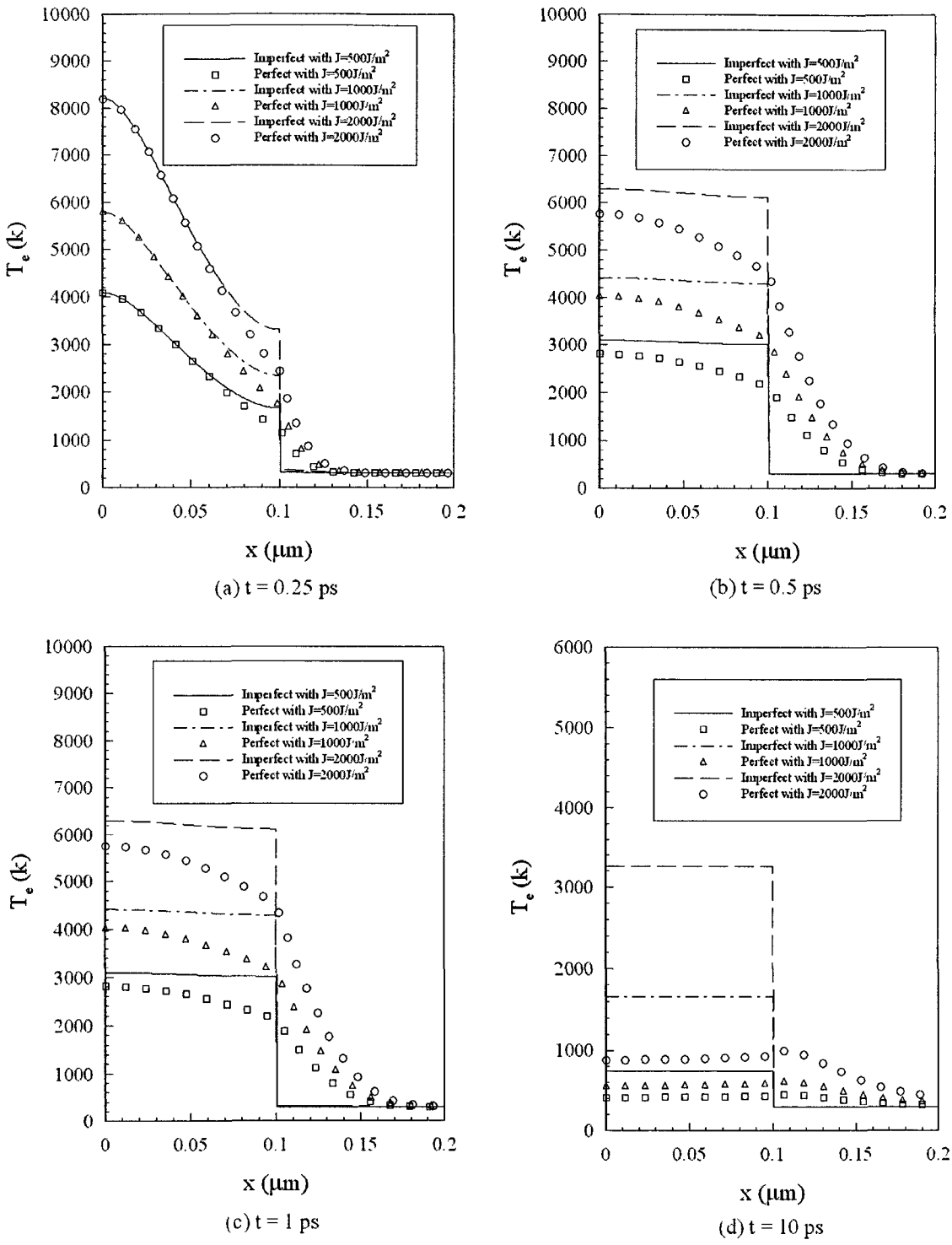

Figure 2.11 Comparison of electron temperature at $y = 0\,\mu m$ at different times between perfect and imperfect contact at interface with three different laser fluences.

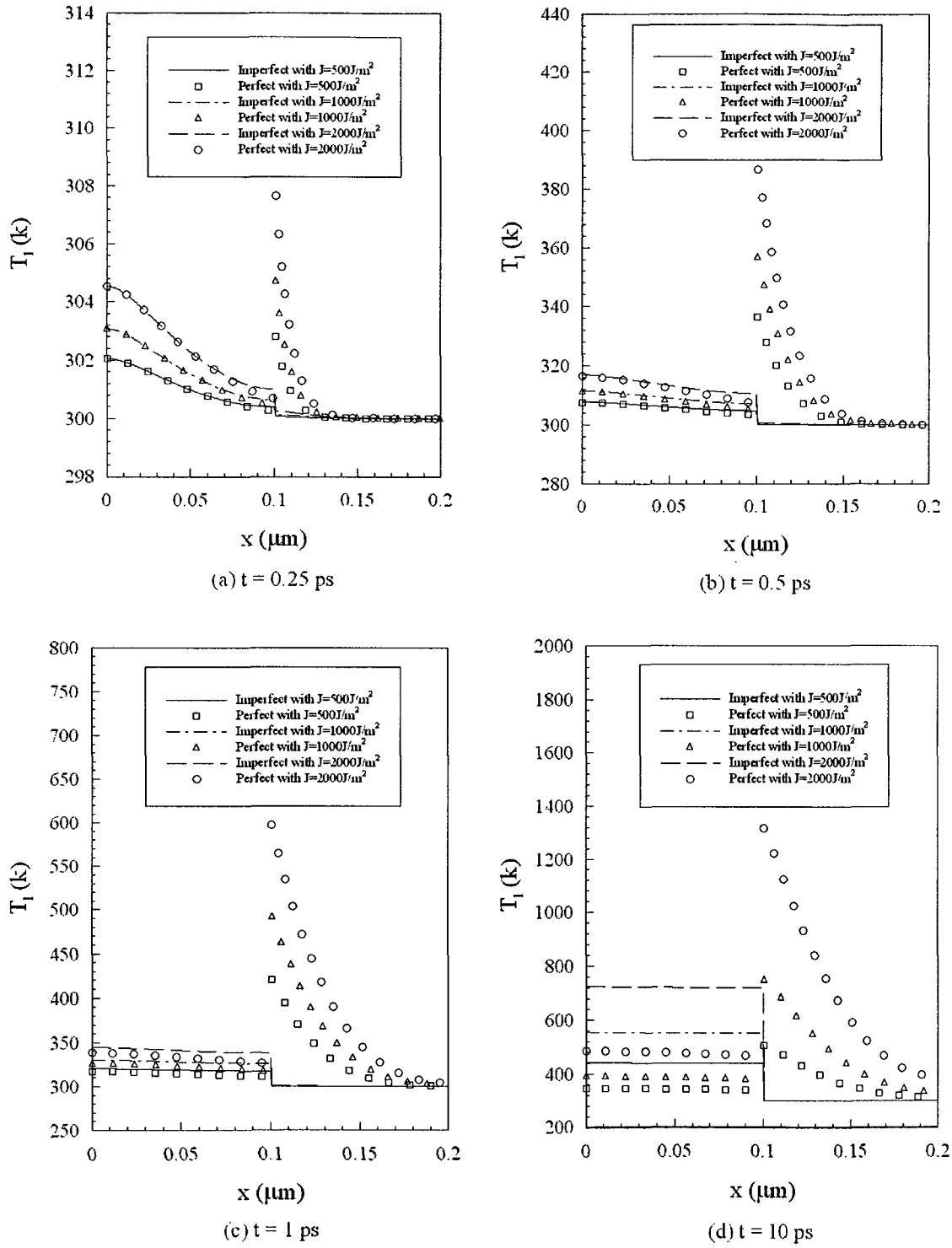

Figure 2.12 Comparison of lattice temperature at $y = 0$ μm at different times between perfect and imperfect contact at interface with three different laser fluences.

2.2.3 Three-Dimensional Parabolic Single Layered Heat Transfer Model

In 2008, Dai et al. developed a mathematical model for studying thermal deformation in a 3D single-layered thin film exposed to ultrashort-pulsed lasers based on parabolic two-step heat transfer equations [8], [16]. The 3D single-layered methal thin film structure is shown in Figure 2.13.

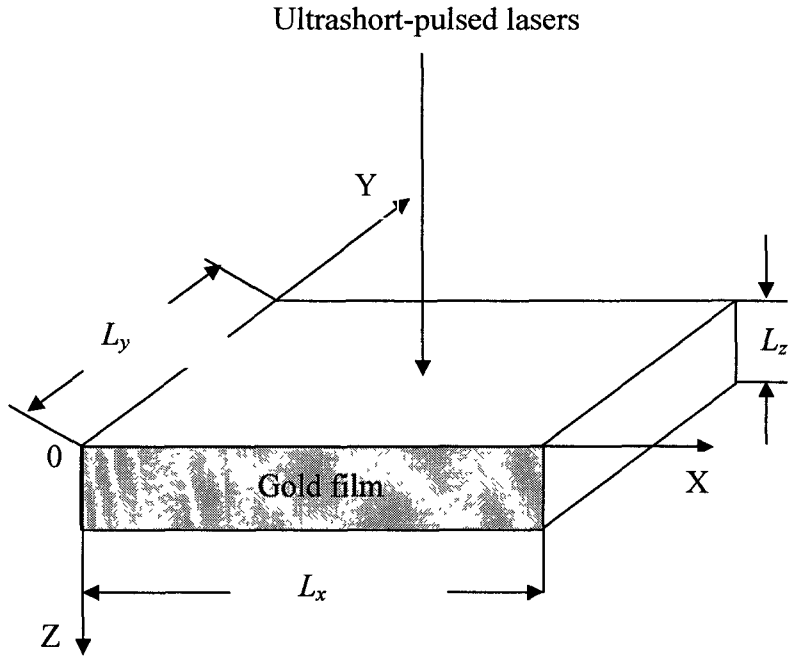

Figure 2.13 A 3D thin film with the dimension of 100μm × 100μm × 0.1μm, irradiated by ultrashort-pulsed lasers.

(1) Dynamic Equations of Motion [9], [12], [45], [46]

$$\rho \frac{\partial^2 u}{\partial t^2} = \frac{\partial \sigma_x}{\partial x} + \frac{\partial \sigma_{xy}}{\partial y} + \frac{\partial \sigma_{xz}}{\partial z} + 2\Lambda T_e \frac{\partial T_e}{\partial x}, \tag{2.53}$$

$$\rho \frac{\partial^2 v}{\partial t^2} = \frac{\partial \sigma_{xy}}{\partial x} + \frac{\partial \sigma_y}{\partial y} + \frac{\partial \sigma_{yz}}{\partial z} + 2\Lambda T_e \frac{\partial T_e}{\partial y}, \tag{2.54}$$

$$\rho\frac{\partial^2 w}{\partial t^2}=\frac{\partial\sigma_{xz}}{\partial x}+\frac{\partial\sigma_{yz}}{\partial y}+\frac{\partial\sigma_{z}}{\partial z}+2\Lambda T_e\frac{\partial T_e}{\partial z}, \tag{2.55}$$

where

$$\sigma_x=\lambda(\varepsilon_x+\varepsilon_y+\varepsilon_z)+2\mu\varepsilon_x-(3\lambda+2\mu)\alpha_T(T_l-T_0), \tag{2.56}$$

$$\sigma_y=\lambda(\varepsilon_x+\varepsilon_y+\varepsilon_z)+2\mu\varepsilon_y-(3\lambda+2\mu)\alpha_T(T_l-T_0), \tag{2.57}$$

$$\sigma_z=\lambda(\varepsilon_x+\varepsilon_y+\varepsilon_z)+2\mu\varepsilon_z-(3\lambda+2\mu)\alpha_T(T_l-T_0), \tag{2.58}$$

and

$$\sigma_{xy}=\mu\gamma_{xy},\sigma_{xz}=\mu\gamma_{xz},\sigma_{yz}=\mu\gamma_{yz}, \tag{2.59}$$

$$\varepsilon_x=\frac{\partial u}{\partial x},\varepsilon_y=\frac{\partial v}{\partial y},\varepsilon_z=\frac{\partial w}{\partial z}, \tag{2.60}$$

$$\gamma_{xy}=\frac{\partial u}{\partial y}+\frac{\partial v}{\partial x},\gamma_{xz}=\frac{\partial u}{\partial z}+\frac{\partial w}{\partial x},\gamma_{yz}=\frac{\partial v}{\partial z}+\frac{\partial w}{\partial y}. \tag{2.61}$$

(2) Energy Equations [9], [12], [46], [52]

$$\begin{aligned}C_e(T_e)\frac{\partial T_e}{\partial t}=&\frac{\partial}{\partial x}\left[k_e(T_e,T_l)\frac{\partial T_e}{\partial x}\right]+\frac{\partial}{\partial y}\left[k_e(T_e,T_l)\frac{\partial T_e}{\partial y}\right]+\frac{\partial}{\partial z}\left[k_e(T_e,T_l)\frac{\partial T_e}{\partial z}\right]\\&-G(T_e-T_l)+Q,\end{aligned} \tag{2.62}$$

$$C_l\frac{\partial T_l}{\partial t}=G(T_e-T_l)+(3\lambda+2\mu)\alpha_T T_0\frac{\partial}{\partial t}(\varepsilon_x+\varepsilon_y+\varepsilon_z), \tag{2.63}$$

where the heat source is considered to be a Gaussian distribution and is given by [36]:

$$Q(x,y,z,t)=0.94J\frac{1-R}{t_p\delta}\exp[-\frac{z}{\delta}-\frac{(x-x_0)^2+(y-y_0)^2}{r_s^2}-2.77(\frac{t-2t_p}{t_p})^2], \tag{2.64}$$

here, $C_e(T_e)=C_{e0}\left(\frac{T_e}{T_0}\right)$ is the electron heat capacity, $k_e(T_e,T_l)=k_0\left(\frac{T_e}{T_l}\right)$ is the thermal conductivity.

The boundary conditions are assumed to be stress free and thermally insulated [9], [53], [54]:

$$\sigma_x = 0, \quad \sigma_{xy} = 0, \ \sigma_{xz} = 0, \text{ at } x = 0, L_x, \tag{2.65}$$

$$\sigma_y = 0, \quad \sigma_{xy} = 0, \ \sigma_{yz} = 0, \text{at } y = 0, L_y, \tag{2.66}$$

$$\sigma_z = 0, \quad \sigma_{xz} = 0, \ \sigma_{yz} = 0, \text{at } z = 0, L_z, \tag{2.67}$$

$$\frac{\partial T_e}{\partial \vec{n}} = 0, \quad \frac{\partial T_l}{\partial \vec{n}} = 0, \tag{2.68}$$

The initial conditions are assumed to be:

$$T_e = T_l = T_0, \quad u = v = w = 0, \quad u_t = v_t = w_t = 0, \text{ at } t = 0. \tag{2.69}$$

Figures and discussions for the 3D single layer model:

Figure 2.14a shows the change in electron temperature ($\Delta T_e / (\Delta T_e)_{\max}$) at the center ($x_{center} = 50$ μm , $y_{center} = 50$ μm and $z = 0$ μm) with laser fluences J = 500 J/m^2. The maximum temperature rise of T_e (i.e., $(\Delta T_e)_{\max}$) is about 3755.7 K, which is close to around 3800 K obtained in [55]. Figure 2.14b shows the displacement (w) at the center (x_{center}, y_{center}, 0) versus time. It can be seen from both figures that the solution is grid independence and hence the scheme is considered to be stable.

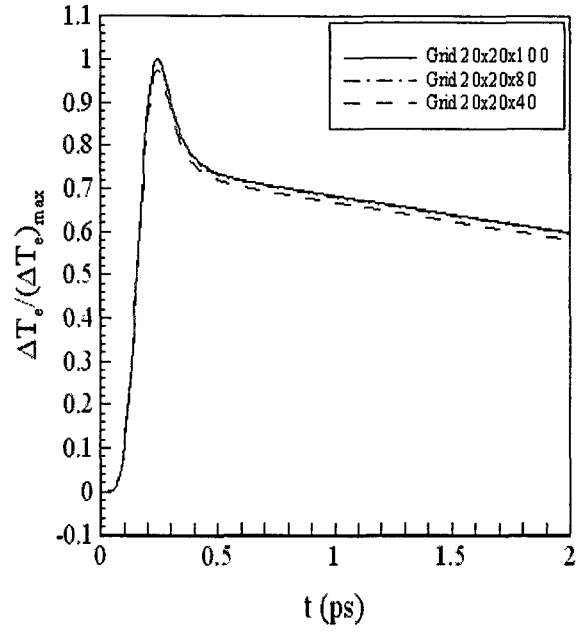

(a)

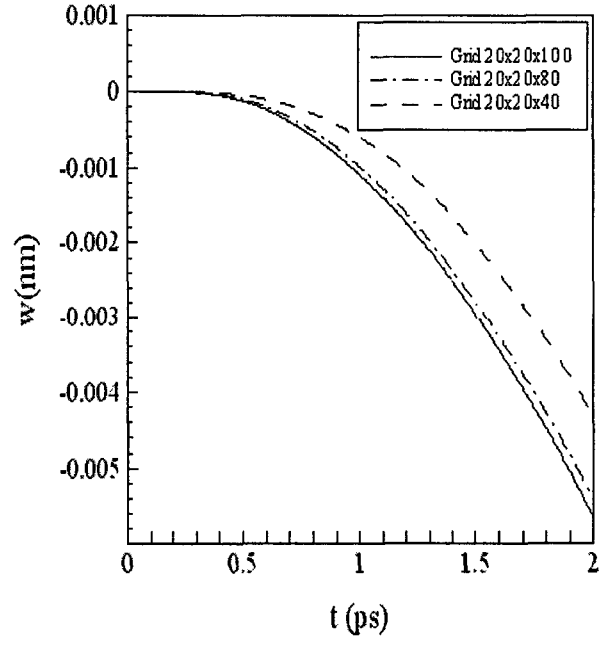

(b)

Figure 2.14 Change in electron temperature and displacements (w) at the center of top surface versus time for various grids ($20\times20\times40$, $20\times20\times80$, $20\times20\times100$) and laser fluence J of 500J/m^2.

2.2.4 Three-Dimensional Parabolic Double Layered Heat Transfer Model

In 2008, Dai et al. future developed a mathematical model for studying thermal deformation in a 3D double-layered thin film exposed to ultrashort-pulsed lasers based on parabolic two-step heat transfer equations [8], [16], as shown in Figure 2.15.

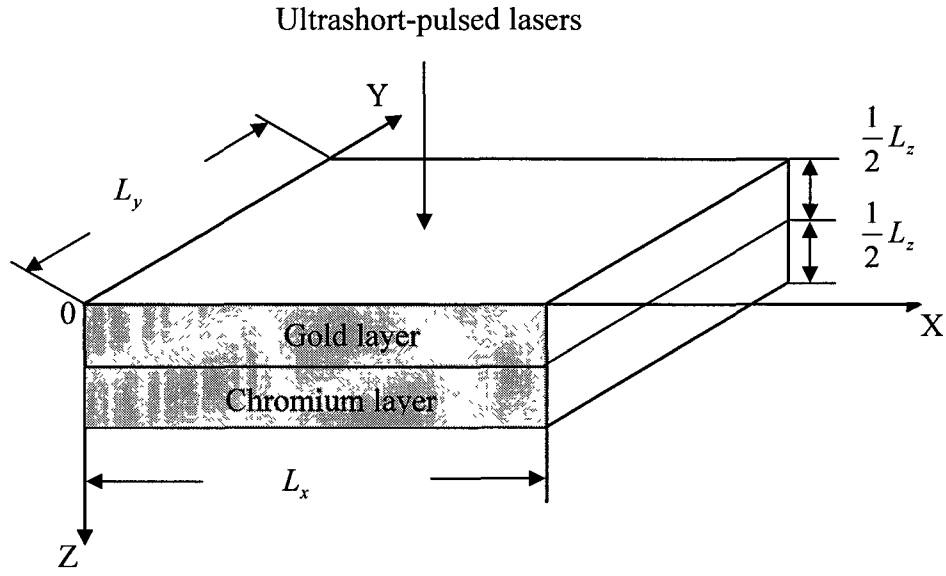

Figure 2.15 A 3D double-layered thin film irradiated by ultrashort-pulsed lasers.

The governing equations for studying thermal deformation in the thin film induced by ultrashort-pulsed lasers can be expressed as follows:

(1) Dynamic Equations of Motion [9], [12], [45], [46]

$$\rho\frac{\partial^2 u}{\partial t^2}=\frac{\partial \sigma_x}{\partial x}+\frac{\partial \sigma_{xy}}{\partial y}+\frac{\partial \sigma_{xz}}{\partial z}+2\Lambda T_e\frac{\partial T_e}{\partial x}, \tag{2.70}$$

$$\rho\frac{\partial^2 v}{\partial t^2}=\frac{\partial \sigma_{xy}}{\partial x}+\frac{\partial \sigma_y}{\partial y}+\frac{\partial \sigma_{yz}}{\partial z}+2\Lambda T_e\frac{\partial T_e}{\partial y}, \tag{2.71}$$

$$\rho\frac{\partial^2 w}{\partial t^2}=\frac{\partial \sigma_{xz}}{\partial x}+\frac{\partial \sigma_{yz}}{\partial y}+\frac{\partial \sigma_z}{\partial z}+2\Lambda T_e\frac{\partial T_e}{\partial z}, \tag{2.72}$$

where

$$\sigma_x = \lambda(\varepsilon_x + \varepsilon_y + \varepsilon_z) + 2\mu\varepsilon_x - (3\lambda + 2\mu)\alpha_T(T_l - T_0), \tag{2.73}$$

$$\sigma_y = \lambda(\varepsilon_x + \varepsilon_y + \varepsilon_z) + 2\mu\varepsilon_y - (3\lambda + 2\mu)\alpha_T(T_l - T_0), \tag{2.74}$$

$$\sigma_z = \lambda(\varepsilon_x + \varepsilon_y + \varepsilon_z) + 2\mu\varepsilon_z - (3\lambda + 2\mu)\alpha_T(T_l - T_0), \tag{2.75}$$

and

$$\sigma_{xy} = \mu\gamma_{xy}, \sigma_{xz} = \mu\gamma_{xz}, \sigma_{yz} = \mu\gamma_{yz}, \tag{2.76}$$

$$\varepsilon_x = \frac{\partial u}{\partial x}, \varepsilon_y = \frac{\partial v}{\partial y}, \varepsilon_z = \frac{\partial w}{\partial z}, \tag{2.77}$$

$$\gamma_{xy} = \frac{\partial u}{\partial y} + \frac{\partial v}{\partial x}, \gamma_{xz} = \frac{\partial u}{\partial z} + \frac{\partial w}{\partial x}, \gamma_{yz} = \frac{\partial v}{\partial z} + \frac{\partial w}{\partial y}. \tag{2.78}$$

(2) Energy Equations [9], [12], [46], [52]

$$C_e(T_e)\frac{\partial T_e}{\partial t} = \frac{\partial}{\partial x}\left[k_e(T_e, T_l)\frac{\partial T_e}{\partial x}\right] + \frac{\partial}{\partial y}\left[k_e(T_e, T_l)\frac{\partial T_e}{\partial y}\right] + \frac{\partial}{\partial z}\left[k_e(T_e, T_l)\frac{\partial T_e}{\partial z}\right] - G(T_e - T_l) + Q, \tag{2.79}$$

$$C_l\frac{\partial T_l}{\partial t} = G(T_e - T_l) + (3\lambda + 2\mu)\alpha_T T_0\frac{\partial}{\partial t}(\varepsilon_x + \varepsilon_y + \varepsilon_z), \tag{2.80}$$

where the heat source is considered to be a Gaussian distribution and is given by [36]:

$$Q(x, y, z, t) = 0.94J\frac{1 - R}{t_p\delta}\exp[-\frac{z}{\delta} - \frac{(x - x_0)^2 + (y - y_0)^2}{r_s^2} - 2.77\left(\frac{t - 2t_p}{t_p}\right)^2], \tag{2.81}$$

here, $C_e(T_e) = C_{e0}\left(\frac{T_e}{T_0}\right)$ is the electron heat capacity, $k_e(T_e, T_l) = k_0\left(\frac{T_e}{T_l}\right)$ is the thermal conductivity,

The boundary conditions are assumed to be stress free and thermally insulated [9], [53], [54]:

$$\sigma_x = 0, \quad \sigma_{xy} = 0, \ \sigma_{xz} = 0, \text{ at } x = 0, L_x, \tag{2.82}$$

$$\sigma_y = 0, \quad \sigma_{xy} = 0, \ \sigma_{yz} = 0, \text{at } y = 0, L_y, \tag{2.83}$$

$$\sigma_z = 0, \quad \sigma_{xz} = 0, \ \sigma_{yz} = 0, \text{at } z = 0, L_z, \tag{2.84}$$

$$\frac{\partial T_e}{\partial \vec{n}} = 0, \quad \frac{\partial T_l}{\partial \vec{n}} = 0 . \tag{2.85}$$

The interfacial conditions are assumed to be perfect thermal contact at $z = \frac{L_z}{2}$ (the continuity of temperature and heat flux across the interface),

$$u^{(1)} = u^{(2)}, v^{(1)} = v^{(2)}, w^{(1)} = w^{(2)}, \tag{2.86a}$$

$$\sigma_z^{(1)} = \sigma_z^{(2)}, \sigma_{xz}^{(1)} = \sigma_{xz}^{(2)}, \sigma_{yz}^{(1)} = \sigma_{yz}^{(2)}, \tag{2.86b}$$

$$T_e^{(1)} = T_e^{(2)}, k_e^{(1)} \frac{\partial T_e^{(1)}}{\partial z} = k_e^{(2)} \frac{\partial T_e^{(2)}}{\partial z}. \tag{2.86c}$$

The initial conditions are assumed to be:

$$T_e = T_l = T_0, \quad u = v = w = 0, \quad u_t = v_t = w_t = 0, \text{ at } t = 0. \tag{2.87}$$

Figures and discussions for the 3D single layer model:

Figure 2.16a shows the changes in electron temperature ($\Delta T_e / (\Delta T_e)_{\max}$) at the center ($x_{center} = 50$ μm , $y_{center} = 50$ μm, and $z = 0$ μm) of the thin film with a laser fluence of $J = 500$ J/m^2. The maximum temperature rise of T_e (i.e., $(\Delta T_e)_{\max}$) is about 3765 K, which is close to the 3727 K obtained in [55]. From Figure 2.16b, the negative value of displacement (w) indicates that the thin film at the center (x_{center}, y_{center}, 0) is expanding along the negative z direction. It can be seen from both figures that the solutions are convergent as the mesh is getting finer.

Figures 2.17 shows electron temperature of the double-layered thin film along z direction at (x_{center}, y_{center}) with three different laser fluences (J=500 J/m^2, 1000 J/m^2 and 2000 J/m^2) at different times (a) t = 0.25 ps, (b) t = 0.5 ps, (c) t = 10 ps, and (d) t = 20 ps, respectively. It can be seen that the electron temperature is in maximum at t = 0.25 ps, then it is decays with time and it is almost uniform at t = 20 ps along z direction.

Figures 2.18 shows lattice temperature of the double-layered thin film along z direction at (x_{center}, y_{center}) with three different laser fluences (J=500 J/m^2, 1000 J/m^2 and 2000 J/m^2) at different times (a) t = 0.25 ps, (b) t = 0.5 ps, (c) t = 10 ps, and (d) t = 20 ps, respectively. The lattice temperature increases gradually with time in both gold and chromium layers. Since the conductivity of chromium is bigger than that of gold, the lattice temperature increases drastically across the interface.

Figure 2.19 shows the displacement (w) of the thin film along z at (x_{center}, y_{center}) at different times (a) t = 5 ps, (b) t = 10 ps, (c) t = 15 ps, and (d) t = 20 ps with a mesh of $20\times20\times80$ and three different laser fluences (J =500 J/m^2, 1000 J/m^2 and 2000 J/m^2). From this figure, one may see the film is expanding. At t = 10 ps and t = 20 ps, the displacement shows a clear alteration across the interface, implying that both layers push each other.

Figure 2.20 shows the normal stress σ_z along z at (x_{center}, y_{center}) at different times (a) t = 5 ps, (b) t = 10 ps, (c) t = 15 ps, and (d) t = 20 ps with a mesh of $20\times20\times80$ and three different laser fluences (J=500 J/m^2, 1000 J/m^2 and 2000 J/m^2). It can be seen that σ_z is smooth and does not appear to have local oscillations.

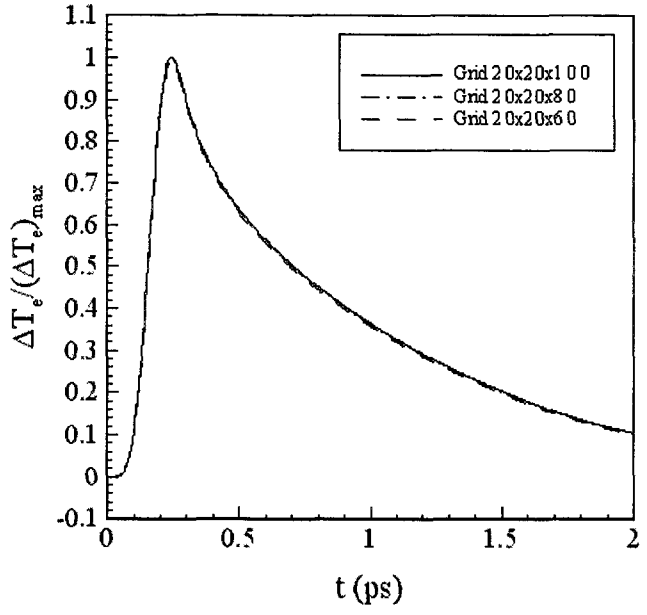

(a)

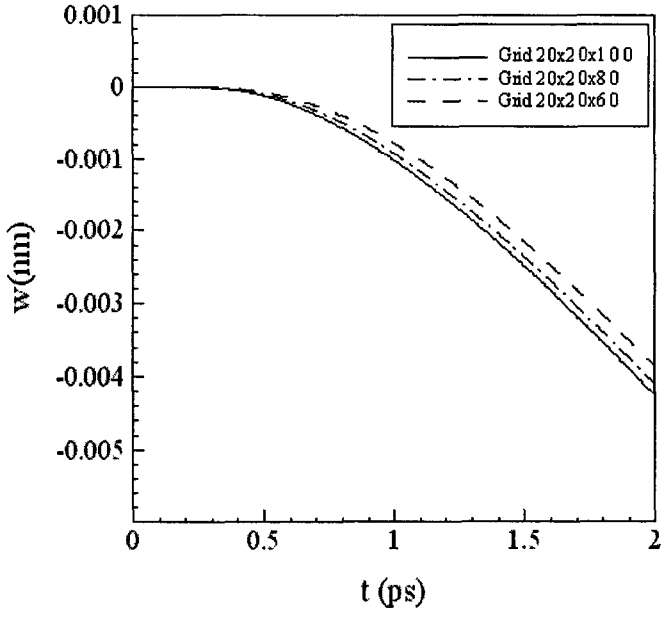

(b)

Figure 2.16 (a) Change in electron temperature and (b) displacements at the center of top surface of thin film versus time with laser fluence (J) of 500J/m^2. The w is the displacement at (x_{center}, y_{center}, 0) of thin film.

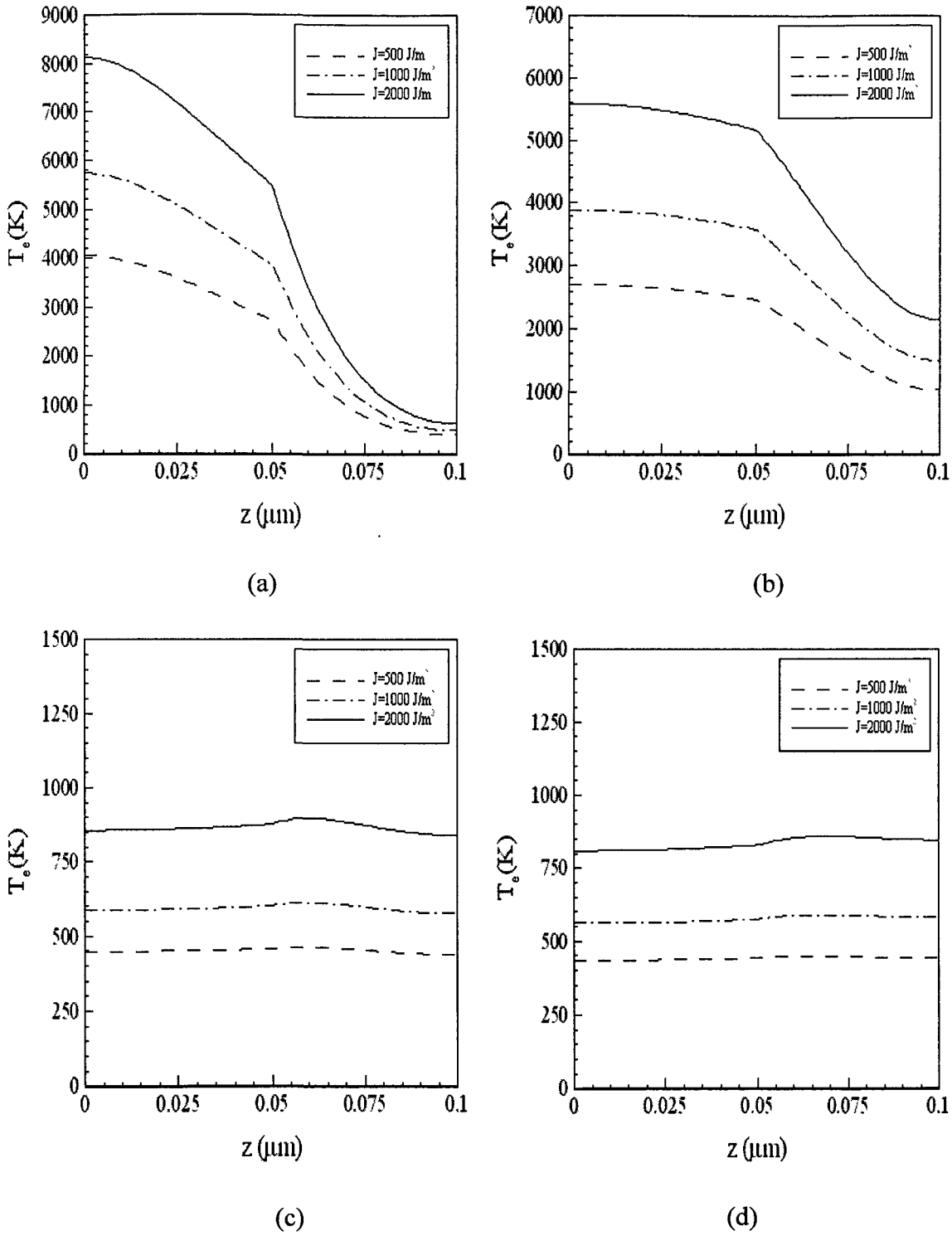

Figure 2.17 Electron temperature profiles along z at (x_{center}, y_{center}) at different times (a) t = 0.25 ps, (b) t = 0.5 ps, (c) t = 10 ps, and (d) t = 20 ps with a mesh of 20 × 20 × 80 and three different laser fluences (J) of 500J/m^2, 1000J/m^2 and 2000J/m^2.

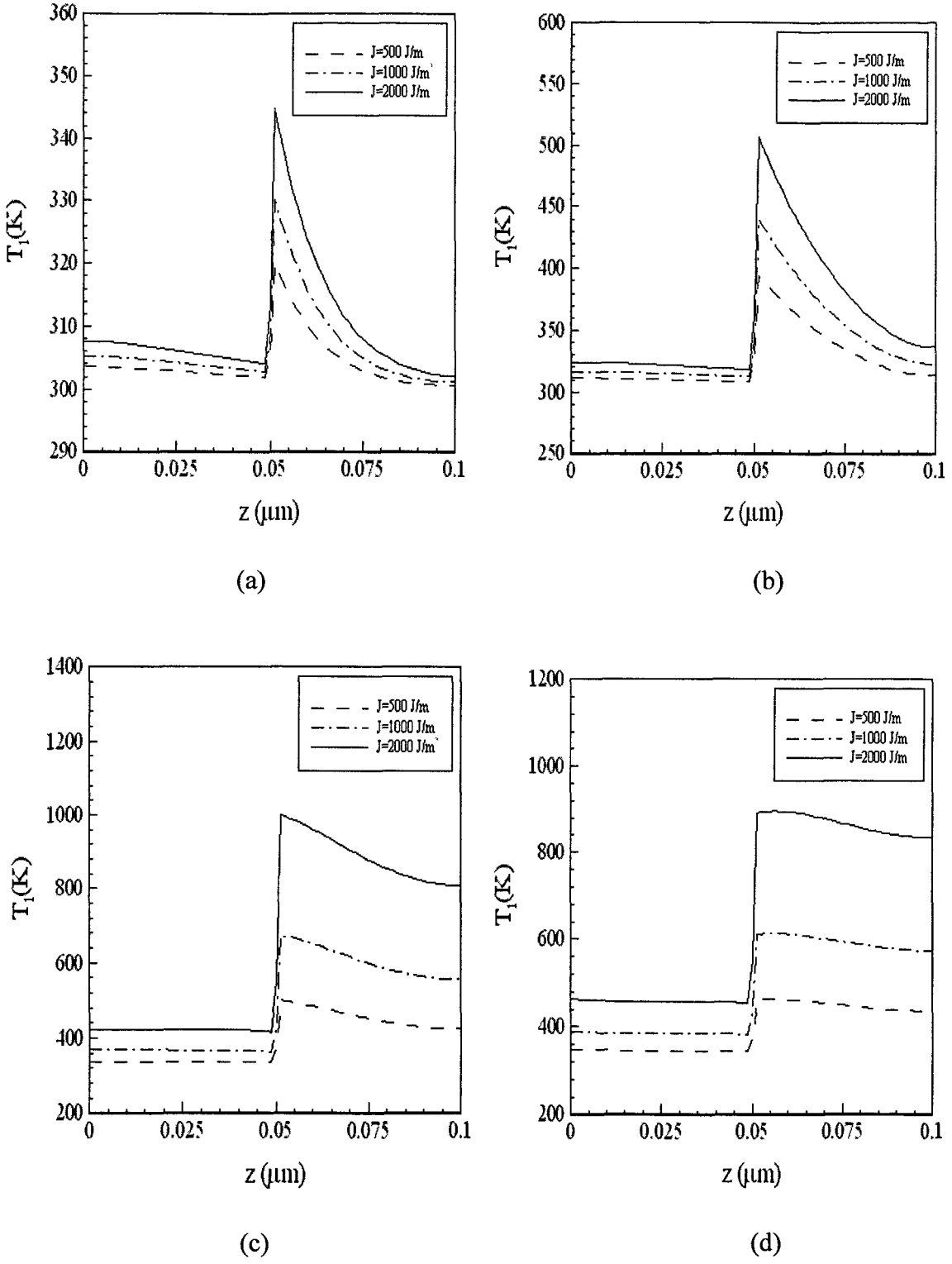

Figure 2.18 Lattice temperature profiles along z at (x_{center}, y_{center}) at different times (a) t = 0.25 ps, (b) t = 0.5 ps, (c) t = 10 ps, and (d) t = 20 ps with a mesh of 20 × 20 × 80 and three different laser fluences (J) of 500J/m^2, 1000J/m^2 and 2000J/m^2.

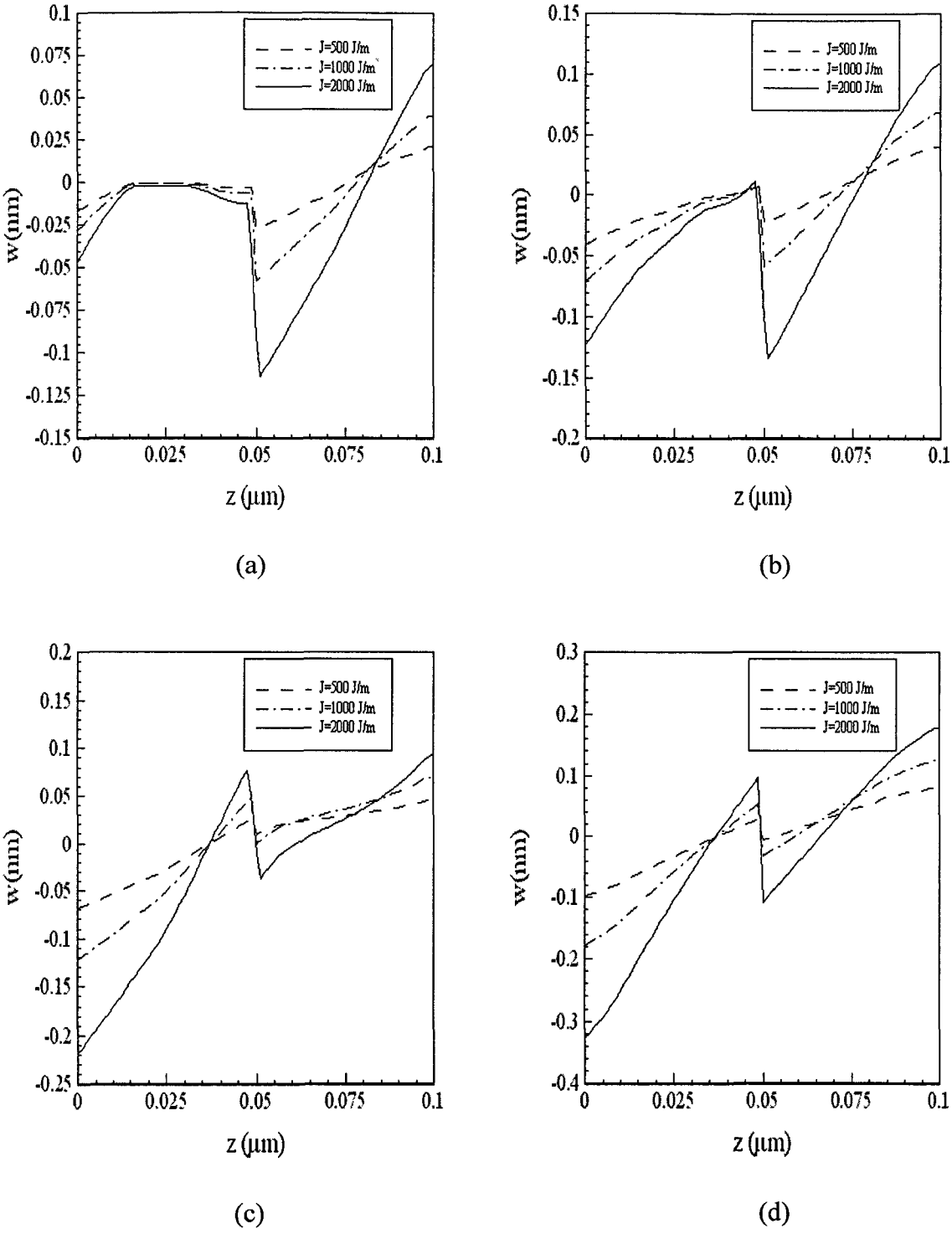

Figure 2.19 Displacement (w) profiles along z at (x_{center}, y_{center}) at different times (a) t = 5 ps, (b) t = 10 ps, (c) t = 15 ps, and (d) t = 20 ps with a mesh of 20 × 20 × 80 and three different laser fluences (J) of 500J/m^2, 1000J/m^2 and 2000J/m^2.

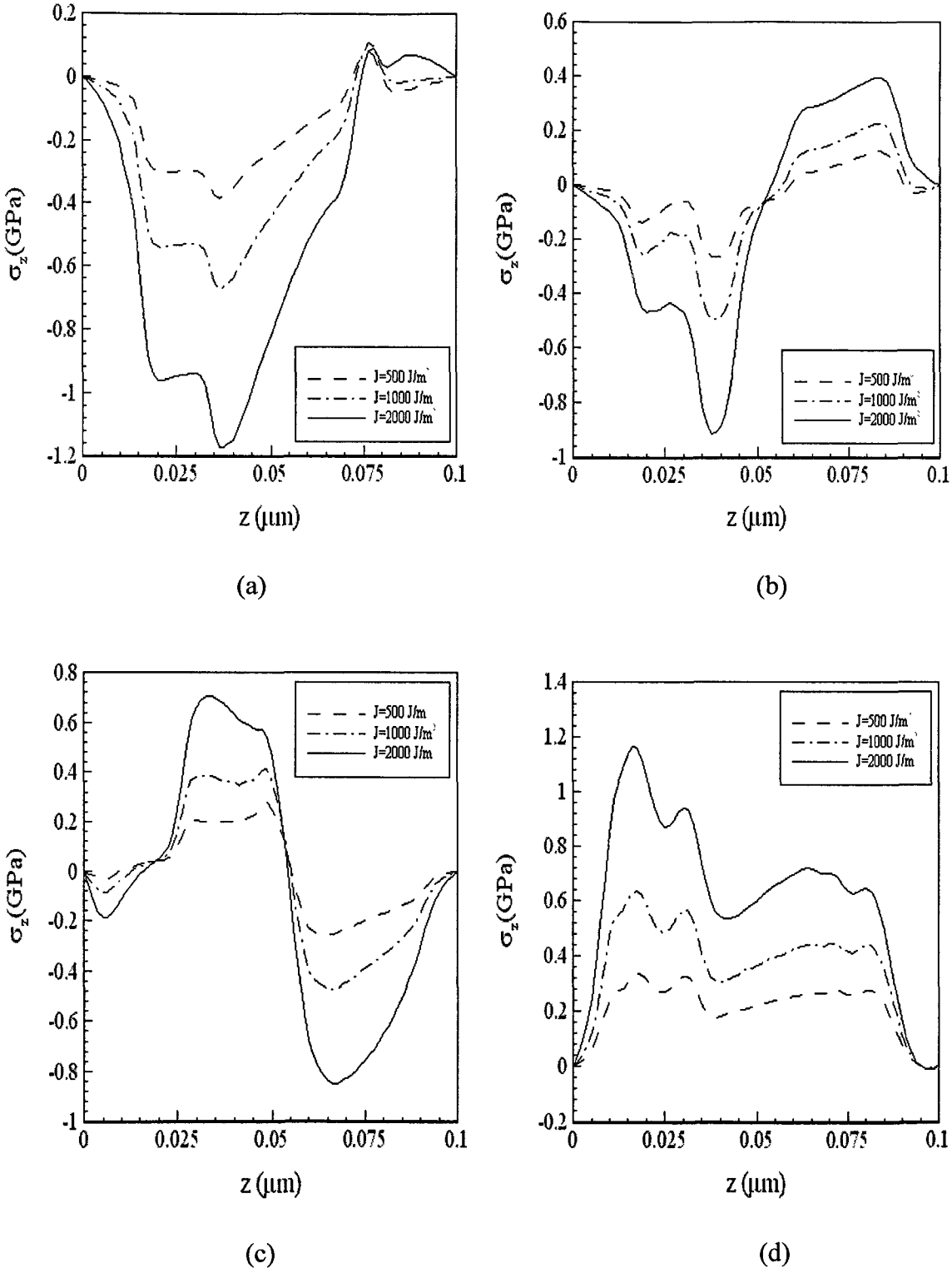

Figure 2.20 Normal stress (σ_z) profiles along z at (x_{center}, y_{center}) at different times (a) t = 5 ps, (b) t = 10 ps, (c) t = 15 ps, and (d) t = 20 ps with a mesh of 20 × 20 × 80 and three different laser fluences (J) of 500J/m^2, 1000J/m^2 and 2000J/m^2.

It should be pointed out that in [8], Energy Equations (2.79) and (2.80) were solved using Crank-Nicolson method because the Crank-Nicolson is unconditionally stable. This similar proof for unconditional stability can be seen in [57]; the generalized Crank-Nicolson schemes were developed for solving parabolic two-step micro heat transfer in a 3D double-layered thin film. In [57], the energy equations for the double-layered thin film were written as follows:

$$C_e^{(m)} \frac{\partial T_e^{(m)}}{\partial t} = k_e^{(m)} \Delta T_e^{(m)} - G_m \left(T_e^{(m)} - T_l^{(m)}\right) + S_m, \tag{2.88}$$

$$C_l^{(m)} \frac{\partial T_l^{(m)}}{\partial t} = G_m (T_e^{(m)} - T_l^{(m)}), \tag{2.89}$$

and generalized the Crank-Nicolson finite difference schemes were written as follows:

$$\begin{aligned} & C_e^{(m)} \frac{(T_e^{(m)})_{i,j,k}^{n+1} - (T_e^{(m)})_{i,j,k}^{n-1}}{2T_0} \\ & = k_e^{(m)} \left[\frac{1}{4\Delta x^2} \delta_x^2 + \frac{1}{4\Delta y^2} \delta_y^2 + \frac{1}{4\Delta z^2} \delta_z^2 \right] \left[(T_e^{(m)})_{i,j,k}^{n+1} + 2(T_e^{(m)})_{i,j,k}^{n\backslash} + (T_e^{(m)})_{i,j,k}^{n-1} \right], \\ & - \frac{G_m}{4} \left\{ \left[(T_e^{(m)})_{i,j,k}^{n+1} + 2(T_e^{(m)})_{i,j,k}^{n\backslash} + (T_e^{(m)})_{i,j,k}^{n-1} \right] \right. \\ & \left. - \left[(T_l^{(m)})_{i,j,k}^{n+1} + 2(T_l^{(m)})_{i,j,k}^{n\backslash} + (T_l^{(m)})_{i,j,k}^{n-1} \right] \right\} + S_{ijk}^n, \end{aligned} \tag{2.90}$$

$$\begin{aligned} C_l^{(m)} \frac{(T_l^{(m)})_{i,j,k}^{n+1} - (T_l^{(m)})_{i,j,k}^{n-1}}{2\Delta t} = & \frac{G_m}{4} \left\{ \left[(T_e^{(m)})_{i,j,k}^{n+1} + 2(T_e^{(m)})_{i,j,k}^{n\backslash} + (T_e^{(m)})_{i,j,k}^{n-1} \right] \right. \\ & \left. - \left[(T_l^{(m)})_{i,j,k}^{n+1} + 2(T_l^{(m)})_{i,j,k}^{n\backslash} + (T_l^{(m)})_{i,j,k}^{n-1} \right] \right\}. \end{aligned} \tag{2.91}$$

The above scheme has been proved to be unconditionally stable using the discrete energy method.

2.2.5 Some Other Methods To Obtain Interface Stress

In 1994, Dr. Nguyen from UC-Berkeley published a paper [58]. In this paper, It demonstrated that:

For the usual case a substrate that is elastically isotropic in the plane of the film, the biaxial stress in the film is given by the Stoney equation:

$$\sigma = \frac{E_s t_s^2}{6(1-\gamma)t_f} K \tag{2.92}$$

For the case, the total thickness of the films is much less than that of the substrate, where E and γ are the substrate biaxial modulus and poison ratio, t_s and t_f are the substrate and film thickness, and K is the substrate curvature.

In a multilayer stack, the thin film approximation assumes that the interaction between the layers is negligible. The average stress in a multilayer stack is:

$$\sigma = \frac{E_s t_s^2}{6(1-\gamma)t} \sum_i K_i = \frac{E_s t_s^2}{6(1-\gamma)t} \sum_i \frac{6(1-\gamma)t_i}{E_s t_s^2} \sigma_i = \frac{1}{t} \sum_i t_i \sigma_i , \tag{2.93}$$

where t is the total thickness of the multilayer structure. The equation above assumes that the interactions between the layers are negligible. Each layer is assumed to cause a fixed bending amount K_i to occur, independent from the bending caused by adjacent layers. For a periodic multilayer stack of N bilayers of thickness $(t_A + t_B)$, then $t = N(t_A + t_B)$, so:

$$\sigma = \frac{1}{N(t_A + t_B)} N(t_A \sigma_A + t_B \sigma_B) = \frac{t_A \sigma_A + t_B \sigma_B}{t_A + t_B} . \tag{2.94}$$

The average stress, thus, is independent of the bilayer period, and the number of bilayers N, and depends on the layer stress and the relative thickness of the layers. The

evolution of stress in *Mo* and *Si* films is shown in Figure 2.21 for thickness ranging from 5nm to approximately one micron. Stress variation with period in *Mo/Si* multilayers is shown in Figure 2.22. the total thickness of the multilayers is kept constant at 280nm.

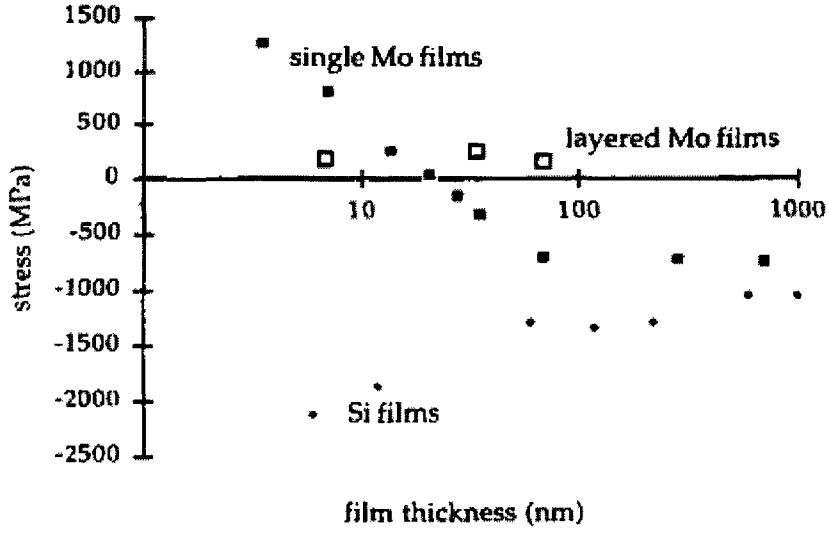

Figure 2.21 Stress evolution in single *Mo* (filled squares), layered *Mo* (open squares), and *Si* films (Diamonds).

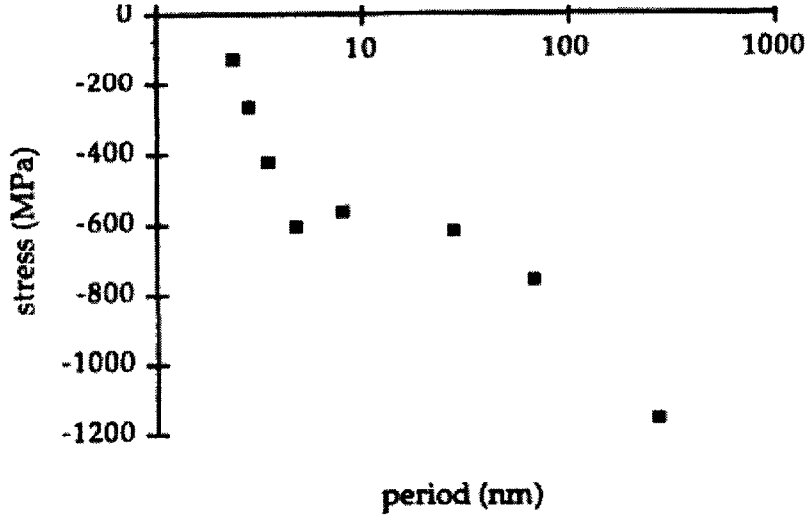

Figure 2.22 Stress variation with period in *Mo/Si* multilayers. Total thickness=280nm.

In 2000, Dr. Schweitz from University of Aarhus, Denmark, published a paper [58]. It demonstrated that specular high-angle x-ray diffraction in Bragg-Brentano geometry and transmission electron microscopy on cross-sectional specimens were performed in order to get information about the microstructure of multilayers. Using the Stoney formula,

$$\sigma = \frac{Y_s d_s^2}{6 d_f}\left(\frac{1}{R_c} - \frac{1}{R_s}\right), \tag{2.95}$$

where Y_s, d_s, d_f, R_c and R_s are the biaxial modulus of the substrate, the thickness of the substrate and thin film, and the radius of curvature of the composite and bare substrate, respectively. The total stress of the thin films was found from the radius of curvature.

The total stress of a multilayered thin film σ is composed of the intralayer stress $\bar{\sigma}$ and interface stress *f*. For multilayers with a modulation period of Λ the difference between the total stress and the intralayer stress thus becomes

$$\sigma - \bar{\sigma} = \frac{2}{\Lambda} f, \tag{2.96}$$

where the factor of 2 arises due to the presence of two interfaces per modulation period. Hence, the interface stress can be obtained from the slope in $\sigma - \bar{\sigma}$ versus Λ^{-1} plot as seen in Figure 2.23.

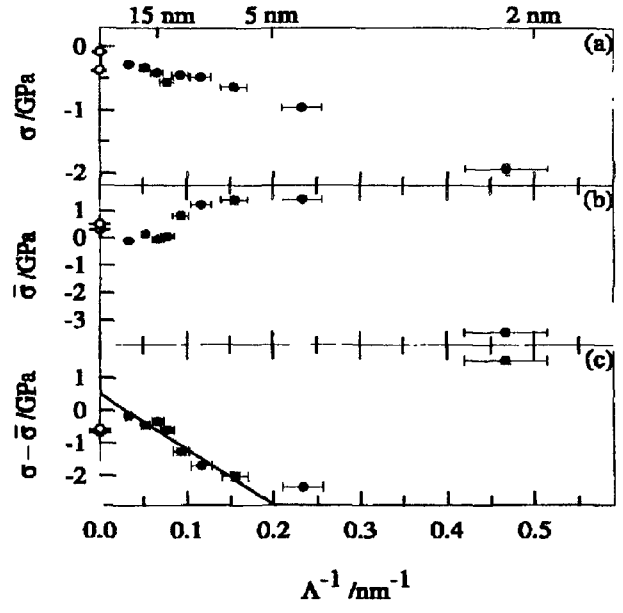

Figure 2.23 The total stress (a) the average intralayer stress (b) the difference in stress as found using profilometry and in-plane x-ray diffraction (c) versus the actual reciprocal modulation period.

The intralayer stress is determined using the $\sin^2\psi$ method. The strain in the direction described by the angles ψ (the angle between the lattice-plane normal and the sample-surface normal) and ϕ (the angle between the projected lattice plane normal and an in-plane axis) can be expressed as:

$$\begin{aligned}(\varepsilon_{33})_{\phi\psi} &= \frac{d_{\phi\psi} - d_0}{d_0} \\ &= \varepsilon_{11}\cos^2(\phi)\sin^2(\psi) + \varepsilon_{12}\cos(2\phi)\sin^2(\psi) + \varepsilon_{22}\sin^2(\phi)\sin^2(\psi) \\ &+ \varepsilon_{33}\cos^2(\psi) + \varepsilon_{13}\cos(\phi)\sin(2\psi) + \varepsilon_{23}\sin(\phi)\sin(2\psi),\end{aligned} \tag{2.97}$$

where $d_{\phi\psi}$ is the lattice spacing and d_0 is the unstressed lattice spacing and ε_{ij} refers to the sample coordinate system.

In Figure 2.24 the lattice parameters for *Au* and *Ni* are plotted versus $\sin^2\psi$ for sample having a modulation period of 8.6nm. The lattice parameters are indeed observed to depend linearly on $\sin^2\psi$.

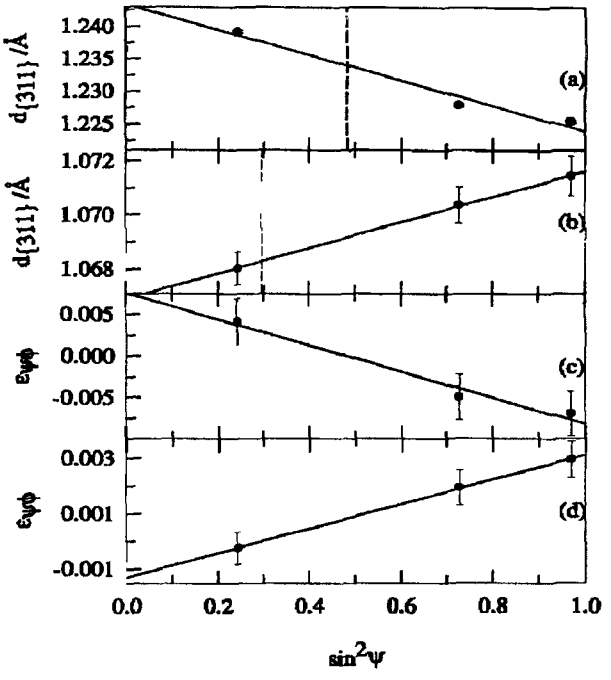

Figure 2.24 The lattice spacing and the crystallographic strains of the planes versus $\sin^2\psi$ for *Au* (a) and (c) and *Ni* (b) and (d).

In 2006, Dr. Lavitas from Texas Tech University published a paper [59]. In this paper, the author and his colleagues predicted virtual melting as an alternative mechanism of stress relaxation and loss of coherence at a moving solid-solid interface. For the internal stresses and their elastic energy, the authors considered a transforming volume *Vn* as a penny-shaped ellipsoid with axes *a*, *b* and an aspect ratio $n = a/b << 1$ (see

Figure 2.25). The components σ_{ij} of the stress tensor due to the components of the transformation strain tensor ε_{ij}^t , i, j =1, 2, and 3, in the volume Vn in isotropic approximation are:

$$\frac{\sigma_{11}}{2\mu} = \frac{-\nu}{1-\nu}(\varepsilon_{11}^t + \varepsilon_{22}^t) - \varepsilon_{11}^t + n\frac{\pi}{32(1-\nu)}(13\varepsilon_{11}^t + (16\nu-1)\varepsilon_{22}^t - 4(2\nu-1)\varepsilon_{33}^t),$$

$$\frac{\sigma_{22}}{2\mu} = \frac{-\nu}{1-\nu}(\varepsilon_{11}^t + \varepsilon_{22}^t) - \varepsilon_{22}^t + n\frac{\pi}{32(1-\nu)}((16\nu-1)\varepsilon_{11}^t + 13\varepsilon_{22}^t - 4(2\nu-1)\varepsilon_{33}^t),$$

$$\frac{\sigma_{33}}{2\mu} = -n\frac{\pi}{8(1-\nu)}((2\nu+1)(\varepsilon_{11}^t + \varepsilon_{22}^t) + 2\varepsilon_{33}^t),$$

$$\frac{\sigma_{23}}{2\mu} = -n\frac{\pi(\nu-2)}{4(1-\nu)}\varepsilon_{23}^t,$$

$$\frac{\sigma_{31}}{2\mu} = -n\frac{\pi(\nu-2)}{4(1-\nu)}\varepsilon_{31}^t,$$

$$\frac{\sigma_{12}}{2\mu} = -\varepsilon_{12}^t + n\frac{\pi(7-8\nu)}{16(1-\nu)}\varepsilon_{12}^t. \qquad (2.98)$$

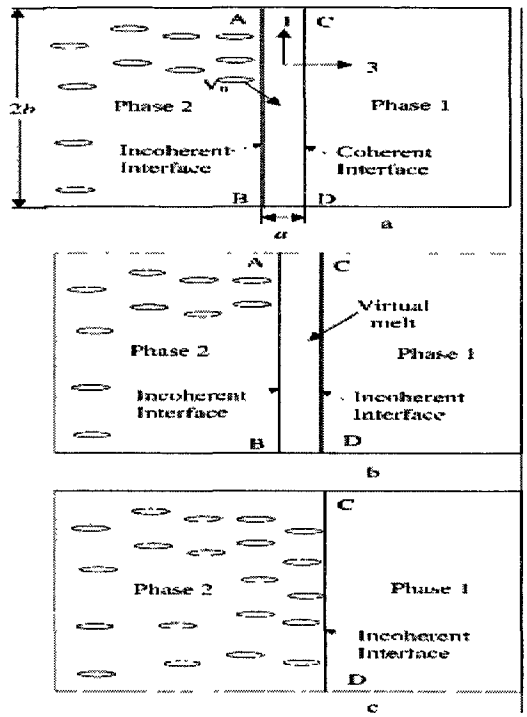

Figure 2.25 Scheme of the solid-solid-phase transformation 1 → 2 in the volume *Vn* via the virtual melting mechanism.

From these three papers, we can see that the interface conditions are complex and not reasonable for the work considered here. From Equation (2.93), it is calculated the average value of the stress which cannot show the stress distribution across the interface. From Equation (2.97), it is calculated the internal stress in some certain situation. Thus, we avoid seeking a mathematical model for stress change across the interface and obtain successfully the stress change across the interface based on only the fourth-power law for radiation and using an iterative numerical method.

2.3 Conclusion

Although Dai et al. have developed a very promising mathematical model for single layered thin film induced by radiation heating; the single metal layer often cannot satisfy all mechanical, thermal and electronic requirements. Because of multilayers, the imperfect thermal contact between layers may occur sometimes and, hence, the stress and displacement caused by the hot-electron blast effect across the interface between layers may change sharply or be discontinuous across the interface, resulting in possible thermal damage. Thus, the purpose of this dissertation is to extend the research to the case that considers 3D double-layered thin films with imperfect interfacial thermal contact exposed by ultrashort-pulsed lasers and to develop a model, and its numerical method that may be more accurate in predicting the thermal damage of the double-layered thin metal films induced by radiation heating.

CHAPTER THREE

3D DOUBLE-LAYERED MATHEMATICAL MODEL

This chapter considers 3D double-layered thin films with imperfect interfacial thermal contact exposed to ultrashort-pulsed lasers. The governing dynamic equations of motion and energy equations for obtaining the temperature distributions, stresses, strains and displacements in the double-layered thin films are then set up. The solutions of these equations will predict the metal thermal damage induced by radiation heating.

3.1 Double-Layered Structure and Governing Equations

We considered a sub-micron metal film consisting of two material layers to illustrate the general effects of the hot-electron blast across the interface, justifying the use of 3D models in describing ultrafast heating and deformation. The coordinate system is provided in Figure 3.1.

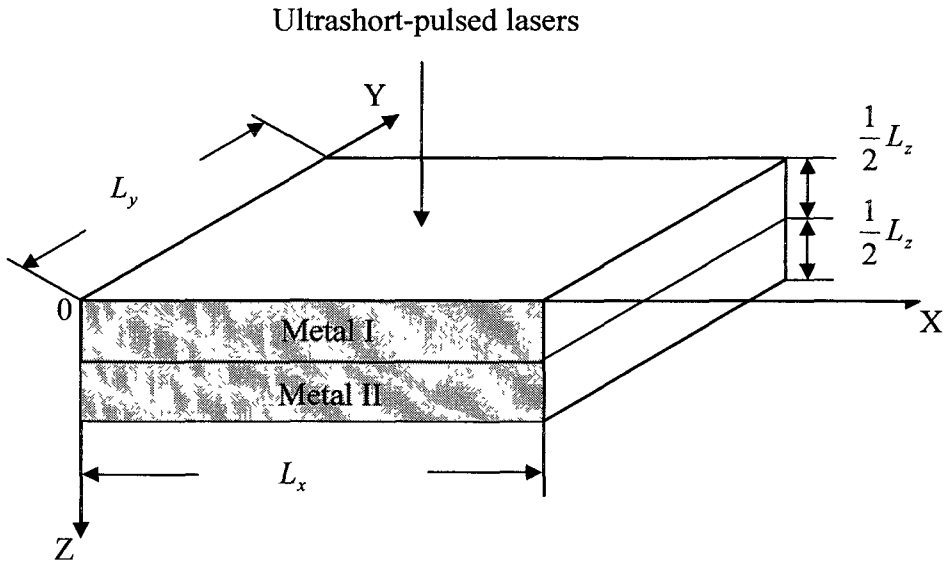

Figure 3.1 A 3D double-layered thin film irradiated by ultrashort-pulsed lasers.

The general governing equations for studying thermal deformation in metal thin film can be expressed as follows:

(1) Dynamic Equations of Motion [42], [55], [60]

$$\rho^{(m)}\frac{\partial^2 u^{(m)}}{\partial t^2}=\frac{\partial \sigma_x^{(m)}}{\partial x}+\frac{\partial \sigma_{xy}^{(m)}}{\partial y}+\frac{\partial \sigma_{xz}^{(m)}}{\partial z}, \tag{3.1}$$

$$\rho^{(m)}\frac{\partial^2 v^{(m)}}{\partial t^2}=\frac{\partial \sigma_{xy}^{(m)}}{\partial x}+\frac{\partial \sigma_y^{(m)}}{\partial y}+\frac{\partial \sigma_{yz}^{(m)}}{\partial z}, \tag{3.2}$$

$$\rho^{(m)}\frac{\partial^2 w^{(m)}}{\partial t^2}=\frac{\partial \sigma_{xz}^{(m)}}{\partial x}+\frac{\partial \sigma_{yz}^{(m)}}{\partial y}+\frac{\partial \sigma_z^{(m)}}{\partial z}, \tag{3.3}$$

where

$$\sigma_x^{(m)}=\lambda^{(m)}(\varepsilon_x^{(m)}+\varepsilon_y^{(m)}+\varepsilon_z^{(m)})+2\mu^{(m)}\varepsilon_x^{(m)}-(3\lambda^{(m)}+2\mu^{(m)})\alpha_T^{(m)}(T_l^{(m)}-T_0), \tag{3.4a}$$

$$\sigma_y^{(m)}=\lambda^{(m)}(\varepsilon_x^{(m)}+\varepsilon_y^{(m)}+\varepsilon_z^{(m)})+2\mu^{(m)}\varepsilon_y^{(m)}-(3\lambda^{(m)}+2\mu^{(m)})\alpha_T^{(m)}(T_l^{(m)}-T_0), \tag{3.4b}$$

$$\sigma_z^{(m)} = \lambda^{(m)}(\varepsilon_x^{(m)} + \varepsilon_y^{(m)} + \varepsilon_z^{(m)}) + 2\mu^{(m)}\varepsilon_z^{(m)} - (3\lambda^{(m)} + 2\mu^{(m)})\alpha_T^{(m)}(T_l^{(m)} - T_0), \tag{3.4c}$$

$$\sigma_{xy}^{(m)} = \mu^{(m)}\gamma_{xy}^{(m)},\ \sigma_{xz}^{(m)} = \mu^{(m)}\gamma_{xz}^{(m)}, \sigma_{yz}^{(m)} = \mu^{(m)}\gamma_{yz}^{(m)}, \tag{3.4d}$$

$$\varepsilon_x^{(m)} = \frac{\partial u^{(m)}}{\partial x},\ \varepsilon_y^{(m)} = \frac{\partial v^{(m)}}{\partial y},\ \varepsilon_z^{(m)} = \frac{\partial w^{(m)}}{\partial z}, \tag{3.4e}$$

$$\gamma_{xy}^{(m)} = \frac{\partial u^{(m)}}{\partial y} + \frac{\partial v^{(m)}}{\partial x},\ \gamma_{xz}^{(m)} = \frac{\partial u^{(m)}}{\partial z} + \frac{\partial w^{(m)}}{\partial x}, \gamma_{yz}^{(m)} = \frac{\partial v^{(m)}}{\partial z} + \frac{\partial w^{(m)}}{\partial y}. \tag{3.4f}$$

Here, m = 1, 2, denotes layer 1 and layer 2, respectively; $u^{(m)}, v^{(m)}$, and $w^{(m)}$ are the displacements in the x, y, z directions, respectively; $\varepsilon_x^{(m)}, \varepsilon_y^{(m)}$, and $\varepsilon_z^{(m)}$ are the normal strains in the x, y, and z directions, respectively; $\gamma_{xy}^{(m)}$ is the shear strain in the xy - plane, $\gamma_{xz}^{(m)}$ is the shear strain in the xz - plane, $\gamma_{yz}^{(m)}$ is the shear strain in the yz - plane; $\sigma_x^{(m)}, \sigma_y^{(m)}$, and $\sigma_z^{(m)}$ are the normal stresses in the x, y, and z directions, respectively; $\sigma_{xy}^{(m)}$ is the shear stress in the xy - plane, $\sigma_{xz}^{(m)}$ is the shear stress in the xz - plane, and $\sigma_{yz}^{(m)}$ is the shear stress in the yz - plane; $T_e^{(m)}$ and $T_l^{(m)}$ are electron and lattice temperatures, respectively; T_0 is the initial temperature; $\rho^{(m)}$ is the density; $\lambda^{(m)} = K^{(m)} - \frac{2}{3}\mu^{(m)}$ [25] and $\mu^{(m)}$ are Lame's coefficients; and $\alpha_T^{(m)}$ is the thermal expansion coefficient.

(2) Energy Equations [9], [42], [55], [60]

$$\begin{aligned} & C_e^{(m)}(T_e)\frac{\partial T_e^{(m)}}{\partial t} \\ & = \frac{\partial}{\partial x}(k_e^{(m)}(T_e,T_l)\frac{\partial T_e^{(m)}}{\partial x}) + \frac{\partial}{\partial y}(k_e^{(m)}(T_e,T_l)\frac{\partial T_e^{(m)}}{\partial y}) + \frac{\partial}{\partial z}(k_e^{(m)}(T_e,T_l)\frac{\partial T_e^{(m)}}{\partial z}) \\ & -G^{(m)}(T_e^{(m)} - T_l^{(m)}) + Q, \end{aligned} \tag{3.5}$$

$$C_l^{(m)}\frac{\partial T_l^{(m)}}{\partial t} = G^{(m)}(T_e^{(m)} - T_l^{(m)}), \tag{3.6}$$

where the heat source introduced by [1], [9] is extended for a Gaussian laser beam focusing at (x_0, y_0) on the top surface as

$$Q(x,y,z,t) = \sqrt{\frac{\beta}{\pi}}\frac{1-R}{t_p z_s}\exp\left[-\frac{z}{z_s} - \frac{(x-x_0)^2+(y-y_0)^2}{r_s^2} - \beta\left(\frac{t-2t_p}{t_p}\right)^2\right]. \tag{3.7}$$

Here, $C_e^{(m)}(T_e) = C_{e0}^{(m)}\left(\frac{T_e^{(m)}}{T_0}\right)$ is the electron heat capacity, $k_e^{(m)}(T_e,T_l) = k_0^{(m)}\left(\frac{T_e^{(m)}}{T_l^{(m)}}\right)$ is the thermal conductivity, $G^{(m)}$ is the electron-lattice coupling factor, $C_l^{(m)}$ is the lattice heat capacity, Q is the energy absorption rate, J is the laser fluence, R is the surface reflectivity, t_p is the laser pulse duration, z_s is the optical penetration depth, and r_s is the spatial profile parameter. In addition, β is the constant which equals $4 \times \ln(2)$. Therefore, we can estimate $\sqrt{\frac{\beta}{\pi}}$ as $0.94J$ and β as 2.77. These two values will be applied to the specific case in this dissertation research.

This dissertation research considered a specific 3D double-layered thin film which is made up of gold and chromium with imperfect interfacial thermal contact between layers in Cartesian coordinates, exposed to an ultrashort-pulsed laser, The

governing equations for studying thermal deformation in metal thin film can be modified and expressed as follows:

(1) Dynamic Equations of Motion [1], [8], [11], [12], [16], [30], [48]

$$\rho^{(m)}\frac{\partial^2 u^{(m)}}{\partial t^2}=\frac{\partial \sigma_x^{(m)}}{\partial x}+\frac{\partial \sigma_{xy}^{(m)}}{\partial y}+\frac{\partial \sigma_{xz}^{(m)}}{\partial z}+2\Lambda^{(m)}T_e^{(m)}\frac{\partial T_e^{(m)}}{\partial x}, \tag{3.8}$$

$$\rho^{(m)}\frac{\partial^2 v^{(m)}}{\partial t^2}=\frac{\partial \sigma_{xy}^{(m)}}{\partial x}+\frac{\partial \sigma_y^{(m)}}{\partial y}+\frac{\partial \sigma_{yz}^{(m)}}{\partial z}+2\Lambda^{(m)}T_e^{(m)}\frac{\partial T_e^{(m)}}{\partial y}, \tag{3.9}$$

$$\rho^{(m)}\frac{\partial^2 w^{(m)}}{\partial t^2}=\frac{\partial \sigma_{xz}^{(m)}}{\partial x}+\frac{\partial \sigma_{yz}^{(m)}}{\partial y}+\frac{\partial \sigma_z^{(m)}}{\partial z}+2\Lambda^{(m)}T_e^{(m)}\frac{\partial T_e^{(m)}}{\partial z}, \tag{3.10}$$

where

$$\sigma_x^{(m)}=\lambda^{(m)}(\varepsilon_x^{(m)}+\varepsilon_y^{(m)}+\varepsilon_z^{(m)})+2\mu^{(m)}\varepsilon_x^{(m)}-(3\lambda^{(m)}+2\mu^{(m)})\alpha_T^{(m)}(T_l^{(m)}-T_0), \tag{3.11a}$$

$$\sigma_y^{(m)}=\lambda^{(m)}(\varepsilon_x^{(m)}+\varepsilon_y^{(m)}+\varepsilon_z^{(m)})+2\mu^{(m)}\varepsilon_y^{(m)}-(3\lambda^{(m)}+2\mu^{(m)})\alpha_T^{(m)}(T_l^{(m)}-T_0), \tag{3.11b}$$

$$\sigma_z^{(m)}=\lambda^{(m)}(\varepsilon_x^{(m)}+\varepsilon_y^{(m)}+\varepsilon_z^{(m)})+2\mu^{(m)}\varepsilon_z^{(m)}-(3\lambda^{(m)}+2\mu^{(m)})\alpha_T^{(m)}(T_l^{(m)}-T_0), \tag{3.11c}$$

$$\sigma_{xy}^{(m)}=\mu^{(m)}\gamma_{xy}^{(m)},\ \sigma_{xz}^{(m)}=\mu^{(m)}\gamma_{xz}^{(m)},\sigma_{yz}^{(m)}=\mu^{(m)}\gamma_{yz}^{(m)}, \tag{3.11d}$$

$$\varepsilon_x^{(m)}=\frac{\partial u^{(m)}}{\partial x},\ \varepsilon_y^{(m)}=\frac{\partial v^{(m)}}{\partial y},\ \varepsilon_z^{(m)}=\frac{\partial w^{(m)}}{\partial z}, \tag{3.11e}$$

$$\gamma_{xy}^{(m)}=\frac{\partial u^{(m)}}{\partial y}+\frac{\partial v^{(m)}}{\partial x},\ \gamma_{xz}^{(m)}=\frac{\partial u^{(m)}}{\partial z}+\frac{\partial w^{(m)}}{\partial x},\gamma_{yz}^{(m)}=\frac{\partial v^{(m)}}{\partial z}+\frac{\partial w^{(m)}}{\partial y}. \tag{3.11f}$$

Here, as shown in Figure 3.2, m = 1, 2, denotes layer 1 and layer 2, respectively; $u^{(m)}, v^{(m)}$, and $w^{(m)}$ are the displacements in the x, y, and z directions, respectively; $\varepsilon_x^{(m)}$, $\varepsilon_y^{(m)}$, and $\varepsilon_z^{(m)}$ are the normal strains in the x, y, and z directions, respectively; $\gamma_{xy}^{(m)}$ is the shear strain in the xy - plane, $\gamma_{xz}^{(m)}$ is the shear strain in the xz - plane, $\gamma_{yz}^{(m)}$ is the shear strain in the yz - plane; $\sigma_x^{(m)}, \sigma_y^{(m)}$, and $\sigma_z^{(m)}$ are the normal stresses in the x, y, and z

directions, respectively; $\sigma_{xy}^{(m)}$ is the shear stress in the xy - plane, $\sigma_{xz}^{(m)}$ is the shear stress in the xz - plane, and $\sigma_{yz}^{(m)}$ is the shear stress in the yz - plane; $T_e^{(m)}$ and $T_l^{(m)}$ are electron and lattice temperatures, respectively; T_0 is the initial temperature; $\rho^{(m)}$ is the density; $\Lambda^{(m)}$ is the electron-blast coefficient; $\lambda^{(m)} = K^{(m)} - \frac{2}{3}\mu^{(m)}$ [25] and $\mu^{(m)}$ are Lame's coefficients; and $\alpha_T^{(m)}$ is the thermal expansion coefficient.

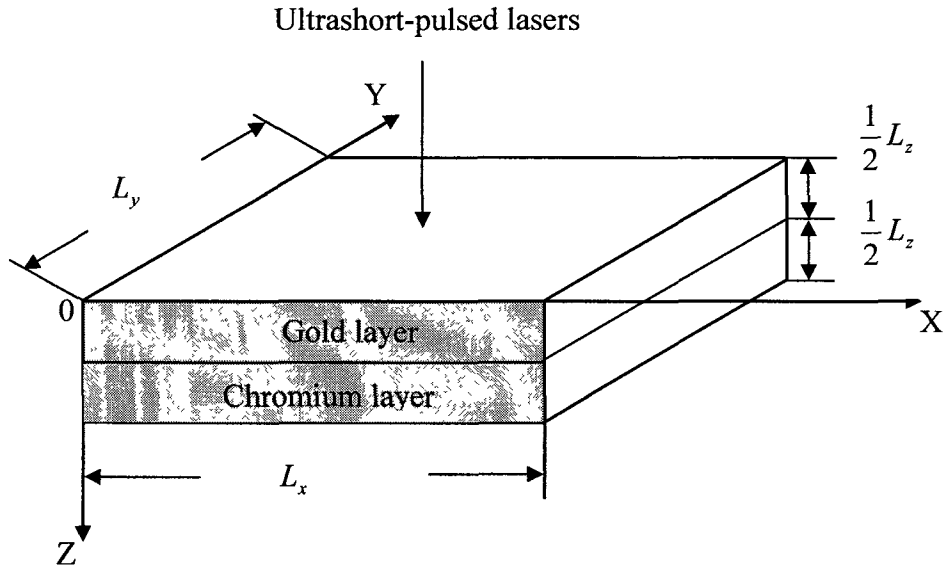

Figure 3.2 A 3D double-layered thin film with the dimension of 100 μm × 100 μm × 0.1μm, irradiated by ultrashort-pulsed lasers.

(2) Energy Equations [1], [8], [11], [12], [47]

$$\begin{aligned} & C_e^{(m)}(T_e)\frac{\partial T_e^{(m)}}{\partial t} \\ & = \frac{\partial}{\partial x}(k_e^{(m)}(T_e,T_l)\frac{\partial T_e^{(m)}}{\partial x}) + \frac{\partial}{\partial y}(k_e^{(m)}(T_e,T_l)\frac{\partial T_e^{(m)}}{\partial y}) + \frac{\partial}{\partial z}(k_e^{(m)}(T_e,T_l)\frac{\partial T_e^{(m)}}{\partial z}) \\ & -G^{(m)}(T_e^{(m)} - T_l^{(m)}) + Q, \end{aligned} \tag{3.12}$$

$$C_l^{(m)}\frac{\partial T_l^{(m)}}{\partial t} = G^{(m)}(T_e^{(m)} - T_l^{(m)}) - (3\lambda^{(m)} + 2\mu^{(m)})\alpha_T^{(m)}T_0\frac{\partial}{\partial t}(\varepsilon_x^{(m)} + \varepsilon_y^{(m)} + \varepsilon_Z^{(m)}), \tag{3.13}$$

where the heat source introduced by [9] is extended for a Gaussian laser beam focusing at (x_0, y_0) on the top surface as

$$Q(x,y,z,t) = 0.94J\frac{1-R}{t_p z_s}\exp\left[-\frac{z}{z_s} - \frac{(x-x_0)^2 + (y-y_0)^2}{r_s^2} - 2.77\left(\frac{t-2t_p}{t_p}\right)^2\right]. \tag{3.14}$$

Here, $C_e^{(m)}(T_e) = C_{e0}^{(m)}\left(\frac{T_e^{(m)}}{T_0}\right)$ is the electron heat capacity, $k_e^{(m)}(T_e,T_l) = k_0^{(m)}\left(\frac{T_e^{(m)}}{T_l^{(m)}}\right)$ is the thermal conductivity, $G^{(m)}$ is the electron-lattice coupling factor, $C_l^{(m)}$ is the lattice heat capacity, Q is the energy absorption rate, J is the laser fluence, R is the surface reflectivity, t_p is the laser pulse duration, z_s is the optical penetration depth, and r_s is the spatial profile parameter. Equations (3.12) and (3.13) are often referred to as parabolic two-step heat transport equations [55], [60]. It should be pointed out that the term $(3\lambda^{(m)} + 2\mu^{(m)})\alpha_T^{(m)}T_0\frac{\partial}{\partial t}(\varepsilon_x^{(m)} + \varepsilon_y^{(m)} + \varepsilon_Z^{(m)})$ is added in Equation (3.13) to consider the coupling effect between lattice temperature and strain rate.

3.2 Initial, Boundary and Interfacial Conditions

The boundary conditions are assumed to be stress free [1], [9] and no heat is lost from the surface in the short time response because insulated boundary conditions are imposed. From [36], we have

$$\sigma_x^{(m)} = 0,\ \sigma_{xy}^{(m)} = 0,\ \sigma_{xz}^{(m)} = 0,\ \text{at } x = 0, L_x, \tag{3.15a}$$

$$\sigma_y^{(m)} = 0,\ \sigma_{xy}^{(m)} = 0,\ \sigma_{yz}^{(m)} = 0,\ \text{at } y = 0, L_y, \tag{3.15b}$$

$$\sigma_z^{(m)} = 0,\ \sigma_{xz}^{(m)} = 0,\ \sigma_{yz}^{(m)} = 0,\ \text{at } z = 0, L_z, \tag{3.15c}$$

$$\frac{\partial T_e^{(m)}}{\partial \vec{n}} = 0,\ \frac{\partial T_l^{(m)}}{\partial \vec{n}} = 0, \tag{3.15d}$$

where $\vec{n}$ is the unit outward normal vector on the boundary.

The interfacial conditions are assumed to be imperfect thermal contact at $z = \frac{L_z}{2}$ (the discontinuity of temperature and heat flux across the interface), thus the nonlinear interfacial condition for T_e can be expressed by the fourth-power for radiation as follows [19], [20], [21]:

$$-k_e^{(1)} \frac{\partial T_e^{(1)}}{\partial z} = -k_e^{(2)} \frac{\partial T_e^{(2)}}{\partial z} = \sigma\left[\left(T_e^{(1)}\right)^4 - \left(T_e^{(2)}\right)^4\right], \tag{3.16}$$

where $\sigma = 5.669 \times 10^{-8}\ \mathrm{W/m^2K^4}$ is Stefan-Boltzman's constant. Once T_e is obtained, T_l at interface can be obtained based on Equation (3.13). Conversely, the interfacial conditions for stress and displacement are expressed as:

$$u^{(1)} = u^{(2)}, v^{(1)} = v^{(2)}, w^{(1)} \neq w^{(2)}, \tag{3.17a}$$

$$\sigma_z^{(1)} \neq \sigma_z^{(2)}, \sigma_{xz}^{(1)} = \sigma_{xz}^{(2)}, \sigma_{yz}^{(1)} = \sigma_{yz}^{(2)}. \tag{3.17b}$$

The initial conditions are assumed to be:

$$T_e^{(m)} = T_l^{(m)} = T_0, u^{(m)} = v^{(m)} = w^{(m)} = 0,$$
$$u_t^{(m)} = v_t^{(m)} = w_t^{(m)} = 0. \tag{3.18}$$

It should be pointed out that the laser beam is applied on the top surface ($z = 0$) at $t = 0$, and the peak intensity occurs when $t = 2t_p$.

It can be seen that finding an analytical solution of Equation (3.8)-(3.14) was very difficult because of the complicated system and the nonlinear equation (see Equation (3.16)). Thus, a numerical method for solving the above governing equations was necessary, in order to obtain the temperature distributions, stresses, strains and displacements in the double-layered metal structure.

CHAPTER FOUR

NUMERICAL METHODS

This chapter will develop a numerical method, which includes a Crank-Nicolson type of finite difference scheme for solving the 3D double-layered thin films with imperfect interfacial thermal contact model for obtaining the temperature distributions, stresses, strains and displacements in the thin films. The finite difference scheme will be stable and the solution is grid independent. The iteration will be convergent.

4.1 Finite Difference Scheme

Following the approach in [8], [13], [14], [16], we first introduce three velocity components v_1, v_2, and v_3 into the model, and then re-write the dynamic equations of motion, Equations (3.1)- (3.4), as follows:

$$v_1^{(m)} = \frac{\partial u^{(m)}}{\partial t},\ v_2^{(m)} = \frac{\partial v^{(m)}}{\partial t},\ v_3^{(m)} = \frac{\partial w^{(m)}}{\partial t}, \tag{4.1}$$

$$\rho^{(m)} \frac{\partial v_1^{(m)}}{\partial t} = \frac{\partial \sigma_x^{(m)}}{\partial x} + \frac{\partial \sigma_{xy}^{(m)}}{\partial y} + \frac{\partial \sigma_{xz}^{(m)}}{\partial z} + 2\Lambda^{(m)} T_e^{(m)} \frac{\partial T_e^{(m)}}{\partial x}, \tag{4.2}$$

$$\rho^{(m)} \frac{\partial v_2^{(m)}}{\partial t} = \frac{\partial \sigma_{xy}^{(m)}}{\partial x} + \frac{\partial \sigma_y^{(m)}}{\partial y} + \frac{\partial \sigma_{yz}^{(m)}}{\partial z} + 2\Lambda^{(m)} T_e^{(m)} \frac{\partial T_e^{(m)}}{\partial y}, \tag{4.3}$$

$$\rho^{(m)} \frac{\partial v_3^{(m)}}{\partial t} = \frac{\partial \sigma_{xz}^{(m)}}{\partial x} + \frac{\partial \sigma_{yz}^{(m)}}{\partial y} + \frac{\partial \sigma_z^{(m)}}{\partial z} + 2\Lambda^{(m)} T_e^{(m)} \frac{\partial T_e^{(m)}}{\partial z}, \tag{4.4}$$

$$\frac{\partial \varepsilon_x^{(m)}}{\partial t} = \frac{\partial v_1^{(m)}}{\partial x}, \frac{\partial \varepsilon_y^{(m)}}{\partial t} = \frac{\partial v_2^{(m)}}{\partial y}, \frac{\partial \varepsilon_z^{(m)}}{\partial t} = \frac{\partial v_3^{(m)}}{\partial z}, \tag{4.5a}$$

$$\begin{aligned} &\frac{\partial \gamma_{xy}^{(m)}}{\partial t} = \frac{\partial v_1^{(m)}}{\partial y} + \frac{\partial v_2^{(m)}}{\partial x}, \frac{\partial \gamma_{xz}^{(m)}}{\partial t} = \frac{\partial v_1^{(m)}}{\partial z} + \frac{\partial v_3^{(m)}}{\partial x}, \\ &\frac{\partial \gamma_{yz}^{(m)}}{\partial t} = \frac{\partial v_2^{(m)}}{\partial z} + \frac{\partial v_3^{(m)}}{\partial y}. \end{aligned} \tag{4.5b}$$

To develop a finite difference scheme, we then design a staggered grid as shown in Figure 4.1, where $v_1^{(m)}$ is placed at $(x_{i+\frac{1}{2}}, y_j, z_k)$, $v_2^{(m)}$ is placed at $(x_i, y_{j+\frac{1}{2}}, z_k)$, $v_3^{(m)}$ is placed at $(x_i, y_j, z_{k+\frac{1}{2}})$, $\gamma_{xy}^{(m)}$ and $\sigma_{xy}^{(m)}$ are placed at $(x_{i+\frac{1}{2}}, y_{j+\frac{1}{2}}, z_k)$, $\gamma_{xz}^{(m)}$ and $\sigma_{xz}^{(m)}$ are placed at $(x_{i+\frac{1}{2}}, y_j, z_{k+\frac{1}{2}})$, $\gamma_{yz}^{(m)}$ and $\sigma_{yz}^{(m)}$ are placed at $(x_i, y_{j+\frac{1}{2}}, z_{k+\frac{1}{2}})$, while $\varepsilon_x^{(m)}$, $\varepsilon_y^{(m)}$, $\varepsilon_z^{(m)}, \sigma_x^{(m)}, \sigma_y^{(m)}, \sigma_z^{(m)}, T_e^{(m)}$ and $T_l^{(m)}$ are at (x_i, y_j, z_k). Here, i, j, and k are indices with $1 \le i \le N_x + 1$, $1 \le j \le N_y + 1$, and $1 \le k \le N_z + 1$, such that $N_x \Delta x = L_x$, $N_y \Delta y = L_y$ and $N_z \Delta z = L_z$, where $\Delta x, \Delta y$ and Δz are spatial step sizes. We denote $(v_1^{(m)})^n_{i+\frac{1}{2},j,k}$, $(v_2^{(m)})^n_{i,j+\frac{1}{2},k}$, and $(v_3^{(m)})^n_{i,j,k+\frac{1}{2}}$ to be numerical approximations of $v_1^{(m)}((i+\frac{1}{2})\Delta x, j\Delta y, k\Delta z, n\Delta t)$, $v_2^{(m)}(i\Delta x, (j+\frac{1}{2})\Delta y, k\Delta z, n\Delta t)$ and $v_3^{(m)}(i\Delta x, j\Delta y, (k+\frac{1}{2})\Delta z, n\Delta t)$, respectively, where Δt is the time increment. Similar notations are used for other variables.

The staggered grid is important to understand the variables locations as shown in Figure 4.1.

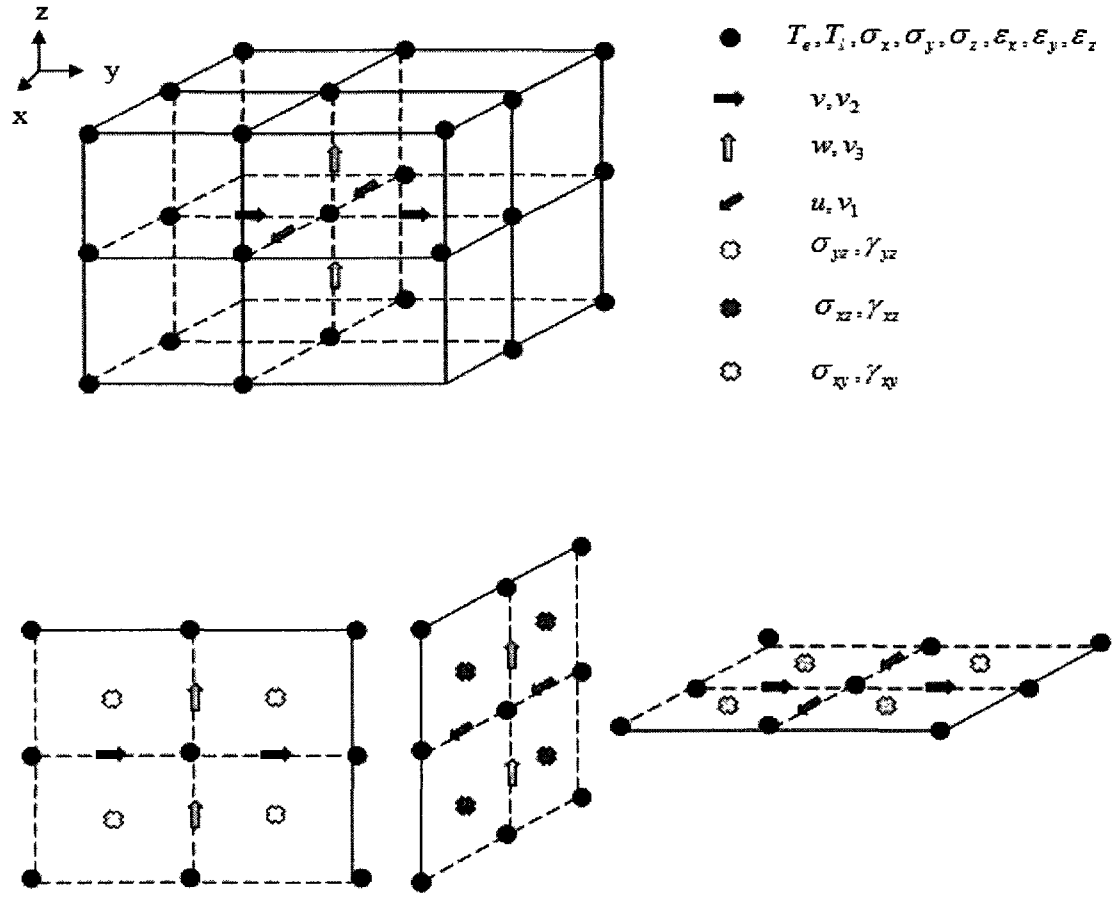

Figure 4.1 A 3D staggered grid for a thin film and locations of variables.

Furthermore, we introduce the finite difference operators, Δ_{-t} and δ_x, as follows:

$$\Delta_{-t} u^n_{i,j,k} = u^n_{i,j,k} - u^{n-1}_{i,j,k},$$

$$\delta_x u^n_{i,j,k} = u^n_{i+\frac{1}{2},j,k} - u^n_{i-\frac{1}{2},j,k}.$$

Finally, δ_y and δ_z are defined similarly to δ_x.

It should be pointed out that the staggered-grid method is often employed in computational fluid dynamics to prevent the solution from oscillations [12]. For example, if v_1 and ε_x in Equation (4.5a) are placed at the same location, employing a central finite difference scheme may produce a velocity component v_1, a wave solution implying oscillation.

To avoid non-physical oscillations in the solution, we further employ a fourth-order compact finite difference scheme for obtaining stress derivatives, $\frac{\partial \sigma_x}{\partial x}$, $\frac{\partial \sigma_{xy}}{\partial y}$, $\frac{\partial \sigma_{xz}}{\partial z}$ and etc. in Equations (4.2)- (4.4).

For example, we calculate $\frac{\partial \sigma_x}{\partial x}$ as follows:

$$a\frac{\partial \sigma_x(i-1)}{\partial x} + b\frac{\partial \sigma_x(i)}{\partial x} + a\frac{\partial \sigma_x(i+1)}{\partial x} = \frac{\sigma_x(i+1/2) - \sigma_x(i-1/2)}{\Delta x}, \quad 2+\frac{1}{2} \le i \le N_x - \frac{1}{2}, \tag{4.6}$$

where a and b are unknown constants. Here, we omit indices j, k, and n for simplicity. Using the Taylor series expansion, we obtain

$$\sigma_x(i+1/2) = \sigma_x(i) + \frac{\Delta x}{2}\frac{\partial \sigma_x(i)}{\partial x} + \frac{\Delta x^2}{2!2^2}\frac{\partial^2 \sigma_x(i)}{\partial x^2} + \frac{\Delta x^3}{3!2^3}\frac{\partial^3 \sigma_x(i)}{\partial x^3} + \frac{\Delta x^4}{4!2^4}\frac{\partial^4 \sigma_x(i)}{\partial x^4} + O(\Delta x^5), \tag{4.7a}$$

$$\sigma_x(i-1/2) = \sigma_x(i) - \frac{\Delta x}{2}\frac{\partial \sigma_x(i)}{\partial x} + \frac{\Delta x^2}{2!2^2}\frac{\partial^2 \sigma_x(i)}{\partial x^2} - \frac{\Delta x^3}{3!2^3}\frac{\partial^3 \sigma_x(i)}{\partial x^3} + \frac{\Delta x^4}{4!2^4}\frac{\partial^4 \sigma_x(i)}{\partial x^4} + O(\Delta x^5), \tag{4.7b}$$

$$\frac{\partial \sigma_x(i+1)}{\partial x} = \frac{\partial \sigma_x(i)}{\partial x} + \Delta x\frac{\partial^2 \sigma_x(i)}{\partial x^2} + \frac{\Delta x^2}{2}\frac{\partial^3 \sigma_x(i)}{\partial x^3} + \frac{\Delta x^3}{3!}\frac{\partial^4 \sigma_x(i)}{\partial x^4} + O(\Delta x^4), \tag{4.7c}$$

$$\frac{\partial \sigma_x(i-1)}{\partial x} = \frac{\partial \sigma_x(i)}{\partial x} - \Delta x\frac{\partial^2 \sigma_x(i)}{\partial x^2} + \frac{\Delta x^2}{2}\frac{\partial^3 \sigma_x(i)}{\partial x^3} - \frac{\Delta x^3}{3!}\frac{\partial^4 \sigma_x(i)}{\partial x^4} + O(\Delta x^4). \tag{4.7d}$$

Substituting the above equations into Equation (4.6) and comparing the corresponding terms, we obtain

$$2a + b = 1,\ a = \frac{1}{24},\ b = \frac{11}{12}, \tag{4.8}$$

with a truncation error of $O(\Delta x^4)$. It should be pointed out that the dissipative term $\frac{\partial^3 \sigma_x(i)}{\partial x^3}$ has been eliminated from the truncation error. Hence, $\frac{\partial \sigma_x(i)}{\partial x}$ can be obtained by solving the following tridiagonal system

$$\frac{1}{24}\frac{\partial \sigma_x(i-1)}{\partial x} + \frac{11}{12}\frac{\partial \sigma_x(i)}{\partial x} + \frac{1}{24}\frac{\partial \sigma_x(i+1)}{\partial x} = \frac{\sigma_x(i+\frac{1}{2}) - \sigma_x(i-\frac{1}{2})}{\Delta x}, \quad 2+\frac{1}{2} \le i \le N_x - \frac{1}{2}, \tag{4.9}$$

where

$$\frac{\partial \sigma_x(\frac{3}{2})}{\partial x} = \frac{\sigma_x(2) - \sigma_x(1)}{\Delta x},\ \frac{\partial \sigma_x(N_x + \frac{1}{2})}{\partial x} = \frac{\sigma_x(N_x+1) - \sigma_x(N_x)}{\Delta x}. \tag{4.10}$$

Using a similar argument, we can evaluate other stress derivatives in Equations (4.1)-(4.5). Hence, the implicit finite difference schemes for solving Equations (4.1)-(4.5) can be written as follows:

$$\rho\frac{1}{\Delta t}\Delta_{-t}(v_1)^{n+1}_{i+\frac{1}{2},j,k} = \frac{\partial(\sigma_x^{n+1})_{i+\frac{1}{2},j,k}}{\partial x} + \frac{\partial(\sigma_{xy}^{n+1})_{i+\frac{1}{2},j,k}}{\partial y} + \frac{\partial(\sigma_{xz}^{n+1})_{i+\frac{1}{2},j,k}}{\partial z} + \Lambda\frac{1}{\Delta x}\delta_x(T_e^2)^{n+1}_{i+\frac{1}{2},j,k}, \tag{4.11}$$

$$\rho\frac{1}{\Delta t}\Delta_{-t}(v_2)^{n+1}_{i,j+\frac{1}{2},k} = \frac{\partial(\sigma_y^{n+1})_{i,j+\frac{1}{2},k}}{\partial y} + \frac{\partial(\sigma_{xy}^{n+1})_{i,j+\frac{1}{2},k}}{\partial x} + \frac{\partial(\sigma_{yz}^{n+1})_{i,j+\frac{1}{2},k}}{\partial z} + \Lambda\frac{1}{\Delta y}\delta_y(T_e^2)^{n+1}_{i,j+\frac{1}{2},k}, \tag{4.12}$$

$$\rho\frac{1}{\Delta t}\Delta_{-t}(v_3)^{n+1}_{i,j,k+\frac{1}{2}} = \frac{\partial(\sigma_z^{n+1})_{i,j,k+\frac{1}{2}}}{\partial z} + \frac{\partial(\sigma_{xz}^{n+1})_{i,j,k+\frac{1}{2}}}{\partial x} + \frac{\partial(\sigma_{yz}^{n+1})_{i,j,k+\frac{1}{2}}}{\partial y} + \Lambda\frac{1}{\Delta z}\delta_z(T_e^2)^{n+1}_{i,j,k+\frac{1}{2}}, \tag{4.13}$$

$$\frac{1}{\Delta t}\Delta_{-t}(\varepsilon_x)^{n+1}_{i,j,k} = \frac{1}{\Delta x}\delta_x(v_1)^{n+1}_{i,j,k}, \tag{4.14a}$$

$$\frac{1}{\Delta t}\Delta_{-t}(\varepsilon_y)^{n+1}_{i,j,k} = \frac{1}{\Delta y}\delta_y(v_2)^{n+1}_{i,j,k}, \tag{4.14b}$$

$$\frac{1}{\Delta t}\Delta_{-t}(\varepsilon_z)^{n+1}_{i,j,k} = \frac{1}{\Delta z}\delta_z(v_3)^{n+1}_{i,j,k}, \tag{4.14c}$$

$$\frac{1}{\Delta t}\Delta_{-t}(\gamma_{xy})^{n+1}_{i+\frac{1}{2},j+\frac{1}{2},k} = \frac{1}{\Delta y}\delta_y(v_1)^{n+1}_{i+\frac{1}{2},j+\frac{1}{2},k} + \frac{1}{\Delta x}\delta_x(v_2)^{n+1}_{i+\frac{1}{2},j+\frac{1}{2},k}, \tag{4.15a}$$

$$\frac{1}{\Delta t}\Delta_{-t}(\gamma_{xz})^{n+1}_{i+\frac{1}{2},j,k+\frac{1}{2}} = \frac{1}{\Delta z}\delta_z(v_1)^{n+1}_{i+\frac{1}{2},j,k+\frac{1}{2}} + \frac{1}{\Delta x}\delta_x(v_3)^{n+1}_{i+\frac{1}{2},j,k+\frac{1}{2}}, \tag{4.15b}$$

$$\frac{1}{\Delta t}\Delta_{-t}(\gamma_{yz})^{n+1}_{i,j+\frac{1}{2},k+\frac{1}{2}} = \frac{1}{\Delta z}\delta_z(v_2)^{n+1}_{i,j+\frac{1}{2},k+\frac{1}{2}} + \frac{1}{\Delta y}\delta_y(v_3)^{n+1}_{i,j+\frac{1}{2},k+\frac{1}{2}}, \tag{4.15c}$$

where Equstions (3.4a)-(3.4d) are discretized as:

$$(\sigma_x)_{i,j,k}^{n+1} = \lambda[(\varepsilon_x)_{i,j,k}^{n+1} + (\varepsilon_y)_{i,j,k}^{n+1} + (\varepsilon_z)_{i,j,k}^{n+1}] + 2\mu(\varepsilon_x)_{i,j,k}^{n+1} - (3\lambda + 2\mu)\alpha_T[(T_l)_{i,j,k}^{n+1} - T_0], \tag{4.16a}$$

$$(\sigma_y)_{i,j,k}^{n+1} = \lambda[(\varepsilon_x)_{i,j,k}^{n+1} + (\varepsilon_y)_{i,j,k}^{n+1} + (\varepsilon_z)_{i,j,k}^{n+1}] + 2\mu(\varepsilon_y)_{i,j,k}^{n+1} - (3\lambda + 2\mu)\alpha_T[(T_l)_{i,j,k}^{n+1} - T_0], \tag{4.16b}$$

$$(\sigma_z)_{i,j,k}^{n+1} = \lambda[(\varepsilon_x)_{i,j,k}^{n+1} + (\varepsilon_y)_{i,j,k}^{n+1} + (\varepsilon_z)_{i,j,k}^{n+1}] + 2\mu(\varepsilon_z)_{i,j,k}^{n+1} - (3\lambda + 2\mu)\alpha_T[(T_l)_{i,j,k}^{n+1} - T_0], \tag{4.16c}$$

$$(\sigma_{xy})_{i+\frac{1}{2},j+\frac{1}{2},k}^{n+1} = \mu(\gamma_{xy})_{i+\frac{1}{2},j+\frac{1}{2},k}^{n+1}, \tag{4.17a}$$

$$(\sigma_{xz})_{i+\frac{1}{2},j,k+\frac{1}{2}}^{n+1} = \mu(\gamma_{xz})_{i+\frac{1}{2},j,k+\frac{1}{2}}^{n+1}, \tag{4.17b}$$

$$(\sigma_{xy})_{i,j+\frac{1}{2},k+\frac{1}{2}}^{n+1} = \mu(\gamma_{xy})_{i,j+\frac{1}{2},k+\frac{1}{2}}^{n+1}. \tag{4.17c}$$

The displacements $u^{(m)}$, $v^{(m)}$ and $w^{(m)}$ are then obtained as follows:

$$\frac{1}{\Delta t}\Delta_{-t}u_{i+\frac{1}{2},j,k}^{n+1} = (v_1)_{i+\frac{1}{2},j,k}^{n+1}, \tag{4.18a}$$

$$\frac{1}{\Delta t}\Delta_{-t}v_{i,j+\frac{1}{2},k}^{n+1} = (v_2)_{i,j+\frac{1}{2},k}^{n+1}, \tag{4.18b}$$

$$\frac{1}{\Delta t}\Delta_{-t}w_{i,j,k+\frac{1}{2}}^{n+1} = (v_3)_{i,j,k+\frac{1}{2}}^{n+1}. \tag{4.18c}$$

The energy equations, Equations (3.5)-(3.6), are solved using the Crank-Nicholson finite difference method [62]. As such, Equation (3.5)-(3.6) are discretized as follows:

$$
\begin{aligned}
&C_{e0}^{(m)}\frac{(T_e^{(m)})_{i,j,k}^{n+1}+(T_e^{(m)})_{i,j,k}^{n}}{2T_0}\cdot\frac{1}{\Delta t}\Delta_{-t}(T_e^{(m)})_{i,j,k}^{n+1}\\
&=\frac{1}{2\Delta x^2}((k_e^{(m)})_{i+\frac{1}{2},j,k}^{n+1}\delta_x(T_e^{(m)})_{i+\frac{1}{2},j,k}^{n+1}-(k_e^{(m)})_{i-\frac{1}{2},j,k}^{n+1}\delta_x(T_e^{(m)})_{i-\frac{1}{2},j,k}^{n+1})\\
&\quad+\frac{1}{2\Delta x^2}((k_e^{(m)})_{i+\frac{1}{2},j,k}^{n}\delta_x(T_e^{(m)})_{i+\frac{1}{2},j,k}^{n}-(k_e^{(m)})_{i-\frac{1}{2},j,k}^{n}\delta_x(T_e^{(m)})_{i-\frac{1}{2},j,k}^{n})\\
&\quad+\frac{1}{2\Delta y^2}((k_e^{(m)})_{i,j+\frac{1}{2},k}^{n+1}\delta_y(T_e^{(m)})_{i,j+\frac{1}{2},k}^{n+1}-(k_e^{(m)})_{i,j-\frac{1}{2},k}^{n+1}\delta_y(T_e^{(m)})_{i,j-\frac{1}{2},k}^{n+1})\\
&\quad+\frac{1}{2\Delta y^2}((k_e^{(m)})_{i,j+\frac{1}{2},k}^{n}\delta_y(T_e^{(m)})_{i,j+\frac{1}{2},k}^{n}-(k_e^{(m)})_{i,j-\frac{1}{2},k}^{n}\delta_y(T_e^{(m)})_{i,j-\frac{1}{2},k}^{n})\\
&\quad+\frac{1}{2\Delta z^2}((k_e^{(m)})_{i,j,k+\frac{1}{2}}^{n+1}\delta_z(T_e^{(m)})_{i,j,k+\frac{1}{2}}^{n+1}-(k_e^{(m)})_{i,j,k-\frac{1}{2}}^{n+1}\delta_z(T_e^{(m)})_{i,j,k-\frac{1}{2}}^{n+1})\\
&\quad+\frac{1}{2\Delta z^2}((k_e^{(m)})_{i,j,k+\frac{1}{2}}^{n}\delta_z(T_e^{(m)})_{i,j,k+\frac{1}{2}}^{n}-(k_e^{(m)})_{i,j,k-\frac{1}{2}}^{n}\delta_z(T_e^{(m)})_{i,j,k-\frac{1}{2}}^{n})\\
&\quad-G^{(m)}(\frac{(T_e^{(m)})_{i,j,k}^{n+1}+(T_e^{(m)})_{i,j,k}^{n}}{2}-\frac{(T_l^{(m)})_{i,j,k}^{n+1}+(T_l^{(m)})_{i,j,k}^{n}}{2})+Q_{i,j,k}^{n+\frac{1}{2}},
\end{aligned}
\tag{4.19}
$$

$$
\begin{aligned}
&C_l^{(m)}\frac{1}{\Delta t}\Delta_{-t}(T_l^{(m)})_{i,j,k}^{n+1}\\
&=G^{(m)}(\frac{(T_e^{(m)})_{i,j,k}^{n+1}+(T_e^{(m)})_{i,j,k}^{n}}{2}-\frac{(T_l^{(m)})_{i,j,k}^{n+1}+(T_l^{(m)})_{i,j,k}^{n}}{2})\\
&\quad-(3\lambda^{(m)}+2\mu^{(m)})\frac{\alpha_T^{(m)}}{\Delta t}T_0(\Delta_{-t}(\varepsilon_x^{(m)})_{i,j,k}^{n+1}+\Delta_{-t}(\varepsilon_y^{(m)})_{i,j,k}^{n+1}+\Delta_{-t}(\varepsilon_z^{(m)})_{i,j,k}^{n+1}).
\end{aligned}
\tag{4.20}
$$

It should be pointed out that the Crank-Nicolson method is employed because it is unconditionally stable for solving heat conduction equations [58]. The unconditionally stability indicates that there is no restriction on mesh ratio. The unconditionally stability is particularly important because the dimension in the considered domain is in sub-micro

It should be pointed out that the Crank-Nicolson method is employed because it scale and the grid size will be very small. Unconditional stability will allow us to choose grid sizes and time step without any restrictions.

We can obtain the lattice temperature from Equation (4.21):

$$(T_l)_{i,J,k}^{n+1} = \frac{d}{(1+d)}(T_e^{)})_{i,J,k}^{n+1} + \frac{d}{(1+d)}((T_e)_{i,J,k}^{n} - (T_l)_{i,J,k}^{n}) + \frac{1}{(1+d)}(T_l)_{i,J,k}^{n} - \frac{ee}{(1+d)}\left[((\varepsilon_x)_{i,J,k}^{n+1} + (\varepsilon_y)_{i,J,k}^{n+1} + (\varepsilon_z)_{i,J,k}^{n+1}) - ((\varepsilon_x)_{i,J,k}^{n} + (\varepsilon_y)_{i,J,k}^{n} + (\varepsilon_z)_{i,J,k}^{n})\right], \tag{4.21}$$

where

$$d = \frac{G \cdot \Delta t}{2C_l}, \tag{4.22}$$

$$ee = \frac{(3\lambda + 2\mu)\alpha_T \cdot T_0}{C_l}. \tag{4.23}$$

Then we can easily calculate the electron temperature from Equation (4.24):

$$
\begin{aligned}
(T_e)_{i,j,k}^{n+1} = & \frac{1}{(a+b_1+b_2+b_3+b_4+b_5+b_6+\frac{G\Delta t}{2}-\frac{G\Delta t}{2}\frac{d}{(1+d)})} \\
& \times (b_1(T_e)_{i+1,j,k}^{n+1}+b_2(T_e)_{i-1,j,k}^{n+1}+b_3(T_e)_{i,j+1,k}^{n+1}+b_4(T_e)_{i,j-1,k}^{n+1} \\
& + b_5(T_e)_{i,j,k+1}^{n+1}+b_6(T_e)_{i,j,k-1}^{n+1} \\
& + c_1((T_e)_{i+1,j,k}^{n}-(T_e)_{i,j,k}^{n})-((T_e)_{i,j,k}^{n}-(T_e)_{i-1,j,k}^{n}) \\
& + c_3((T_e)_{i,j+1,k}^{n}-(T_e)_{i,j,k}^{n})-c_4((T_e)_{i,j,k}^{n}-(T_e)_{i,j-1,k}^{n}) \\
& + c_5((T_e)_{i,j,k+1}^{n}-(T_e)_{i,j,k}^{n})-c_6((T_e)_{i,j,k}^{n}-(T_e)_{i,j,k-1}^{n}) \\
& + \frac{G\Delta t}{2}\frac{d}{(1+d)}((T_e)_{i,j,k}^{n}-(T_l)_{i,j,k}^{n})+\frac{G\Delta t}{2}\frac{1}{(1+d)}(T_l)_{i,j,k}^{n}-\frac{G\Delta t}{2}\frac{ee}{(1+d)} \\
& \times\left[((\varepsilon_x)_{i,j,k}^{n+1}+(\varepsilon_y)_{i,j,k}^{n+1}+(\varepsilon_z)_{i,j,k}^{n+1})-((\varepsilon_x)_{i,j,k}^{n}+(\varepsilon_y)_{i,j,k}^{n}+(\varepsilon_z)_{i,j,k}^{n})\right] \qquad (4.24) \\
& - \frac{G\Delta t}{2}((T_e)_{i,j,k}^{n}-(T_l)_{i,j,k}^{n})+Q_{i,j,k}\Delta t+a(T_e)_{i,j,k}^{n}),
\end{aligned}
$$

where the electron heat capacity $C_e(T_e)$ can be obtained below [8], [16]:

$$
C_e(T_e) = C_{e0}(\frac{T_e}{T_0}) = C_{e0}\frac{T_e{}_{i,j,k}^{n+1}+T_e{}_{i,j,k}^{n}}{2T_0}, \qquad (4.25)
$$

the thermal conductivity $k_e(T_e, T_l)$ is calculated based on

$$
k_e(T_e, T_l) = k_0(\frac{T_e}{T_l}), \qquad (4.26)
$$

and constants a, b_i (i=1,...,6) and c_i (i=1,...,6) are given as follows:

$$a = C_{e0}\frac{(T_e)^{n+1}_{i,j,k} + (T_e)^{n}_{i,j,k}}{2T_0}, \tag{4.27}$$

$$b_1 = \frac{(k_e)^{n+1}_{i+\frac{1}{2},j,k}}{2\Delta x^2}\cdot\Delta t = k_0\frac{(\frac{(T_e)^{n+1}_{i+1,j,k}}{(T_l)^{n+1}_{i+1,j,k}} + \frac{(T_e)^{n+1}_{i,j,k}}{(T_l)^{n+1}_{i,j,k}})}{2}\cdot\frac{\Delta t}{2\Delta x^2}, \tag{4.28}$$

$$b_2 = \frac{(k_e)^{n+1}_{i-\frac{1}{2},j,k}}{2\Delta x^2}\cdot\Delta t = k_0\frac{(\frac{(T_e)^{n+1}_{i,j,k}}{(T_l)^{n+1}_{i,j,k}} + \frac{(T_e)^{n+1}_{i-1,j,k}}{(T_l)^{n+1}_{i-1,j,k}})}{2}\cdot\frac{\Delta t}{2\Delta x^2}, \tag{4.29}$$

$$b_3 = \frac{(k_e)^{n+1}_{i,j+\frac{1}{2},k}}{2\Delta y^2}\cdot\Delta t = k_0\frac{(\frac{(T_e)^{n+1}_{i,j+1,k}}{(T_l)^{n+1}_{i,j+1,k}} + \frac{(T_e)^{n+1}_{i,j,k}}{(T_l)^{n+1}_{i,j,k}})}{2}\cdot\frac{\Delta t}{2\Delta y^2}, \tag{4.30}$$

$$b_4 = \frac{(k_e)^{n+1}_{i,j-\frac{1}{2},k}}{2\Delta y^2}\cdot\Delta t = k_0\frac{(\frac{(T_e)^{n+1}_{i,j,k}}{(T_l)^{n+1}_{i,j,k}} + \frac{(T_e)^{n+1}_{i,j-1,k}}{(T_l)^{n+1}_{i,j-1,k}})}{2}\cdot\frac{\Delta t}{2\Delta y^2}, \tag{4.31}$$

$$b_5 = \frac{(k_e)^{n+1}_{i,j,k+\frac{1}{2}}}{2\Delta z^2}\cdot\Delta t = k_0\frac{(\frac{(T_e)^{n+1}_{i,j,k+1}}{(T_l)^{n+1}_{i,j,k+1}} + \frac{(T_e)^{n+1}_{i,j,k}}{(T_l)^{n+1}_{i,j,k}})}{2}\cdot\frac{\Delta t}{2\Delta z^2}, \tag{4.32}$$

$$b_6 = \frac{(k_e)^{n+1}_{i,j,k-\frac{1}{2}}}{2\Delta z^2}\cdot\Delta t = k_0\frac{(\frac{(T_e)^{n+1}_{i,j,k}}{(T_l)^{n+1}_{i,j,k}} + \frac{(T_e)^{n+1}_{i,j,k-1}}{(T_l)^{n+1}_{i,j,k-1}})}{2}\cdot\frac{\Delta t}{2\Delta z^2}, \tag{4.33}$$

$$c_1 = \frac{(k_e)^{n}_{i+\frac{1}{2},j,k}}{2\Delta x^2}\cdot\Delta t = k_0\frac{(\frac{(T_e)^{n}_{i+1,j,k}}{(T_l)^{n}_{i+1,j,k}} + \frac{(T_e)^{n}_{i,j,k}}{(T_l)^{n}_{i,j,k}})}{2}\cdot\frac{\Delta t}{2\Delta x^2}, \tag{4.34}$$

$$c_2 = \frac{(k_e)^{n}_{i-\frac{1}{2},j,k}}{2\Delta x^2}\cdot\Delta t = k_0\frac{(\frac{(T_e)^{n}_{i,j,k}}{(T_l)^{n}_{i,j,k}} + \frac{(T_e)^{n}_{i-1,j,k}}{(T_l)^{n}_{i-1,j,k}})}{2}\cdot\frac{\Delta t}{2\Delta x^2}, \tag{4.35}$$

$$c_3 = \frac{(k_e)^{n}_{i,j+\frac{1}{2},k}}{2\Delta y^2}\cdot\Delta t = k_0\frac{(\frac{(T_e)^{n}_{i,j+1,k}}{(T_l)^{n}_{i,j+1,k}} + \frac{(T_e)^{n}_{i,j,k}}{(T_l)^{n}_{i,j,k}})}{2}\cdot\frac{\Delta t}{2\Delta y^2}, \tag{4.36}$$

$$c_4 = \frac{(k_e)^n_{i,j-\frac{1}{2},k}}{2\Delta y^2}\cdot\Delta t = k_0\frac{\left(\frac{(T_e)^n_{i,j,k}}{(T_l)^n_{i,j,k}} + \frac{(T_e)^n_{i,j-1,k}}{(T_l)^n_{i,j-1,k}}\right)}{2}\cdot\frac{\Delta t}{2\Delta y^2}, \tag{4.37}$$

$$c_5 = \frac{(k_e)^n_{i,j,k+\frac{1}{2}}}{2\Delta z^2}\cdot\Delta t = k_0\frac{\left(\frac{(T_e)^n_{i,j,k+1}}{(T_l)^n_{i,j,k+1}} + \frac{(T_e)^n_{i,j,k}}{(T_l)^n_{i,j,k}}\right)}{2}\cdot\frac{\Delta t}{2\Delta z^2}, \tag{4.38}$$

$$c_6 = \frac{(k_e)^n_{i,j,k-\frac{1}{2}}}{2\Delta z^2}\cdot\Delta t = k_0\frac{\left(\frac{(T_e)^n_{i,j,k}}{(T_l)^n_{i,j,k}} + \frac{(T_e)^n_{i,j,k-1}}{(T_l)^n_{i,j,k-1}}\right)}{2}\cdot\frac{\Delta t}{2\Delta z^2}. \tag{4.39}$$

4.2 Discrete Initial, Boundary and Interfacial Conditions

To complete the formulation of our numerical method, we now turn our attention to the approximation of initial, boundary and interfacial conditions:

$$(\sigma_x)^n_{1,j,k} = (\sigma_x)^n_{N_x+1,j,k} = 0,\ 1\le j\le N_y+1,\ 1\le k\le N_z+1, \tag{4.40a}$$

$$(\sigma_{xy})^n_{1+\frac{1}{2},j+\frac{1}{2},k} = (\sigma_{xy})^n_{N_x+\frac{1}{2},j+\frac{1}{2},k} = 0,\ 1\le j\le N_y,\ 1\le k\le N_z, \tag{4.40b}$$

$$(\sigma_{xz})^n_{1+\frac{1}{2},j,k+\frac{1}{2}} = (\sigma_{xz})^n_{N_x+\frac{1}{2},j,k+\frac{1}{2}} = 0,\ 1\le j\le N_y,\ 1\le k\le N_z, \tag{4.40c}$$

$$(\sigma_{yz})^n_{1,j+\frac{1}{2},k+\frac{1}{2}} = (\sigma_{yz})^n_{N_x,j+\frac{1}{2},k+\frac{1}{2}} = 0,\ 1\le j\le N_y,\ 1\le k\le N_z, \tag{4.40d}$$

$$(\sigma_y)^n_{i,1,k} = (\sigma_y)^n_{i,N_y+1,k} = 0,\ 1\le i\le N_x+1,\ 1\le k\le N_z+1, \tag{4.41a}$$

$$(\sigma_{xy})^n_{i+\frac{1}{2},1+\frac{1}{2},k} = (\sigma_{xy})^n_{i+\frac{1}{2},N_y+\frac{1}{2},k} = 0,\ 1\le i\le N_x,\ 1\le k\le N_z, \tag{4.41b}$$

$$(\sigma_{xz})^n_{i+\frac{1}{2},1,k+\frac{1}{2}} = (\sigma_{xz})^n_{i+\frac{1}{2},N_y,k+\frac{1}{2}} = 0,\ 1\le i\le N_x,\ 1\le k\le N_z, \tag{4.41c}$$

$$(\sigma_{yz})^n_{i,1+\frac{1}{2},k+\frac{1}{2}} = (\sigma_{yz})^n_{i,N_y+\frac{1}{2},k+\frac{1}{2}} = 0,\ 1\le i\le N_x,\ 1\le k\le N_z, \tag{4.41d}$$

$$(\sigma_z)^n_{i,j,1} = (\sigma_z)^n_{i,j,N_z+1} = 0,\ 1\le i\le N_x+1,\ 1\le j\le N_y+1, \tag{4.42a}$$

$$(\sigma_{xy})^n_{i+\frac{1}{2},J+\frac{1}{2},1} = (\sigma_{xy})^n_{i+\frac{1}{2},J+\frac{1}{2},N_z} = 0,\ 1 \le i \le N_x,\ 1 \le j \le N_y, \tag{4.42b}$$

$$(\sigma_{xz})^n_{i+\frac{1}{2},J,1+\frac{1}{2}} = (\sigma_{xz})^n_{i+\frac{1}{2},J,N_z+\frac{1}{2}} = 0,\ 1 \le i \le N_x,\ 1 \le j \le N_y, \tag{4.42c}$$

$$(\sigma_{yz})^n_{i,J+\frac{1}{2},1+\frac{1}{2}} = (\sigma_{yz})^n_{i,J+\frac{1}{2},N_z+\frac{1}{2}} = 0,\ 1 \le i \le N_x,\ 1 \le j \le N_y, \tag{4.42d}$$

$$(T_e)^n_{1,J,k} = (T_e)^n_{2,J,k},\ (T_e)^n_{N_x+1,J,k} = (T_e)^n_{N_x,J,k}, \tag{4.43a}$$

$$(T_e)^n_{i,1,k} = (T_e)^n_{i,2,k},\ (T_e)^n_{i,N_y+1,k} = (T_e)^n_{i,N_y,k}, \tag{4.43b}$$

$$(T_e)^n_{i,J,1} = (T_e)^n_{i,J,2},\ (T_e)^n_{i,J,N_z+1} = (T_e)^n_{i,J,N_z}, \tag{4.43c}$$

$$(T_l)^n_{1,J,k} = (T_l)^n_{2,J,k},\ (T_l)^n_{N_x+1,J,k} = (T_l)^n_{N_x,J,k}, \tag{4.44a}$$

$$(T_l)^n_{i,1,k} = (T_l)^n_{i,2,k},\ (T_l)^n_{i,N_y+1,k} = (T_l)^n_{i,N_y,k}, \tag{4.44b}$$

$$(T_l)^n_{i,J,1} = (T_l)^n_{i,J,2},\ (T_l)^n_{i,J,N_z+1} = (T_l)^n_{i,J,N_z}, \tag{4.44c}$$

where $1 \le i \le N_x + 1,\ 1 \le j \le N_y + 1,\ 1 \le k \le N_z + 1$, for any time level n. The initial conditions are approximated as

$$u^0_{i+\frac{1}{2},J,k} = v^0_{i,J+\frac{1}{2},k} = w^0_{i,J,k+\frac{1}{2}} = 0, \tag{4.45a}$$

$$(v_1)^0_{i+\frac{1}{2},J,k} = (v_2)^0_{i,J+\frac{1}{2},k} = (v_3)^0_{i,J,k+\frac{1}{2}} = 0, \tag{4.45b}$$

$$(T_e)^0_{i,J,k} = (T_l)^0_{i,J,k} = T_0, \tag{4.45b}$$

$$(\varepsilon_x)^0_{i+\frac{1}{2},J,k} = (\varepsilon_y)^0_{i,J+\frac{1}{2},k} = (\varepsilon_z)^0_{i,J,k+\frac{1}{2}} = 0, \tag{4.45d}$$

$$(\sigma_x)^0_{i+\frac{1}{2},J,k} = (\sigma_y)^0_{i,J+\frac{1}{2},k} = (\sigma_z)^0_{i,J,k+\frac{1}{2}} = 0, \tag{4.45e}$$

$$(\sigma_{xy})^0_{i+\frac{1}{2},J+\frac{1}{2},k} = (\gamma_{xy})^0_{i+\frac{1}{2},J+\frac{1}{2},k} = 0, \tag{4.45f}$$

$$(\sigma_{xz})^0_{i+\frac{1}{2},j,k+\frac{1}{2}} = (\gamma_{xz})^0_{i+\frac{1}{2},j,k+\frac{1}{2}} = 0, \tag{4.45g}$$

$$(\sigma_{yz})^0_{i,j+\frac{1}{2},k+\frac{1}{2}} = (\gamma_{yz})^0_{i,j+\frac{1}{2},k+\frac{1}{2}} = 0. \tag{4.45h}$$

where $1 \le i \le N_x + 1,\ 1 \le j \le N_y + 1,\ 1 \le k \le N_z + 1$, for any time level n.

The discrete interfacial condition for electron temperature is obtained based on Equation (3.9):

$$(k_e^{(1)})^{n+1}_{i,j,N+\frac{1}{2}} \frac{(T_e^{(1)})^{n+1}_{i,j,N+1} - (T_e^{(1)})^{n+1}_{i,j,N}}{\Delta z} = (k_e^{(2)})^{n+1}_{i,j,\frac{3}{2}} \frac{(T_e^{(2)})^{n+1}_{i,j,2} - (T_e^{(2)})^{n+1}_{i,j,1}}{\Delta z}, \tag{4.46a}$$

$$(k_e^{(1)})^{n+1}_{i,j,N+\frac{1}{2}} \frac{(T_e^{(1)})^{n+1}_{i,j,N+1} - (T_e^{(1)})^{n+1}_{i,j,N}}{\Delta z} = \sigma\{[(T_e^{(1)})^{n+1}_{i,j,N+1}]^4 - [(T_e^{(2)})^{n+1}_{i,j,1}]^4\}, \tag{4.46b}$$

$$(T_e^{(1)})^{n+1}_{i,j,N+1} \neq (T_e^{(2)})^{n+1}_{i,j,1}. \tag{4.46c}$$

While the interfacial conditions for velocity components $v_1^{(m)}$, $v_2^{(m)}$ and $v_3^{(m)}$ are obtained based on Equation (3.10a) and (3.10b)

$$(v_1^{(1)})^{n+1}_{i+\frac{1}{2},j,N+1} = (v_1^{(2)})^{n+1}_{i+\frac{1}{2},j,1}, \tag{4.46d}$$

$$(v_2^{(1)})^{n+1}_{i,j+\frac{1}{2},N+1} = (v_2^{(2)})^{n+1}_{i,j+\frac{1}{2},1}, \tag{4.46e}$$

$$(v_3^{(1)})^{n+1}_{i,j,N+\frac{1}{2}} \neq (v_3^{(2)})^{n+1}_{i,j,\frac{3}{2}}, \tag{4.46f}$$

$$(\sigma_z^{(1)})^{n+1}_{i,j,N+1} \neq (\sigma_z^{(2)})^{n+1}_{i,j,1}, \tag{4.46g}$$

$$(\sigma_{xz}^{(1)})^{n+1}_{i+\frac{1}{2},j,N+\frac{1}{2}} = (\sigma_{xz}^{(2)})^{n+1}_{i+\frac{1}{2},j,\frac{3}{2}}, \tag{4.46h}$$

$$(\sigma_{yz}^{(1)})^{n+1}_{i,j+\frac{1}{2},N+\frac{1}{2}} = (\sigma_{yz}^{(2)})^{n+1}_{i,j+\frac{1}{2},\frac{3}{2}}. \tag{4.46i}$$

It should be pointed out that Equations (4.11)-(4.13) are nonlinear since the terms $\delta_x((T_e^{(m)})^{n+1}_{i+\frac{1}{2},j,k})^2$, $\delta_y((T_e^{(m)})^{n+1}_{i,j+\frac{1}{2},k})^2$ and $\delta_z((T_e^{(m)})^{n+1}_{i,j,k+\frac{1}{2}})^2$ are nonlinear. It can also be seen that Equation (4.19) is nonlinear. Furthermore, $(v_3^{(1)})^{n+1}_{i,j,N+\frac{1}{2}} \neq (v_3^{(2)})^{n+1}_{i,j,\frac{3}{2}}$ in Equation (4.46f) and $(\sigma_z^{(1)})^{n+1}_{i,j,N+1} \neq (\sigma_z^{(2)})^{n+1}_{i,j,1}$ in Equation (4.46g) are essentially useless in computation. Therefore, we must solve scheme iteratively. In particular, the interfacial condition in Equations (4.46a) and (4.46b) is iteratively calculated as follows:

$$(T_e^{(1)})^{n+1(new)}_{i,j,N+1} = (T_e^{(1)})^{n+1(old)}_{i,j,N} - \frac{\sigma\Delta z}{a_1}\{[(T_e^{(1)})^{n+1(old)}_{i,j,N+1}]^4 - [(T_e^{(2)})^{n+1(old)}_{i,j,1}]^4\}, \qquad (4.47a)$$

$$(T_e^{(2)})^{n+1(new)}_{i,j,1} = (T_e^{(2)})^{n+1(old)}_{i,j,2} - \frac{a_1}{a_2}[(T_e^{(1)})^{n+1(old)}_{i,j,N+1} - (T_e^{(1)})^{n+1(old)}_{i,j,N}], \qquad (4.47b)$$

where

$$a_1 = k_0^{(1)}\frac{(T_e^{(1)})^{n+1(old)}_{i,j,N+1}}{(T_l^{(1)})^{n+1(old)}_{i,j,N+1}},\ a_2 = k_0^{(2)}\frac{(T_e^{(2)})^{n+1(old)}_{i,j,1}}{(T_l^{(2)})^{n+1(old)}_{i,j,1}}. \qquad (4.47c)$$

4.3 General Algorithm

From the knowledge of numerical solutions for partial differential equations, if a finite difference scheme is consistent (implying that the truncation error goes to zero when the grid size tends to zero) and stable (a small change in the initial data causes only a small change the numerical result), then the numerical solution obtained based on the finite difference scheme is convergent to the exact solution of the partial different equation. Based on the obtained numerical scheme in the previous section, an iterative method for obtaining electron and lattice temperatures, stresses, strains, velocities, and displacements at time level $n + 1$ from time level n can be described as follows:

1. Set the initial values for $(\varepsilon_x^{(m)})^{n+1}$, $(\varepsilon_y^{(m)})^{n+1}$, $(\varepsilon_z^{(m)})^{n+1}$, $(\gamma_{xy}^{(m)})^{n+1}$, $(\gamma_{xz}^{(m)})^{n+1}$ and $(\gamma_{yz}^{(m)})^{n+1}$ by using the obtained values at time level n and solve iteratively Equations (4.19) and (4.20) coupled with the interfacial conditions, Equations (4.46a)-(4.46c), for $(T_e^{(m)})^{n+1}$ and $(T_l^{(m)})^{n+1}$ including the temperature at the interface.
2. Solve for $(\sigma_x^{(m)})^{n+1}$, $(\sigma_y^{(m)})^{n+1}$, $(\sigma_z^{(m)})^{n+1}$, $(\sigma_{xy}^{(m)})^{n+1}$, $(\sigma_{xz}^{(m)})^{n+1}$, and $(\sigma_{yz}^{(m)})^{n+1}$ using Equations (4.16)-(4.17). It should be pointed out that both $(\sigma_z^{(1)})_{i,j,N+1}^{n+1}$, and $(\sigma_z^{(2)})_{i,j,1}^{n+1}$ at the interface are calculated based on Equation (4.16c); therefore, they are certainly different from each other because $(T_l^{(1)})_{i,j,N+1}^{n+1}$ and $(T_l^{(2)})_{i,j,1}^{n+1}$ at the interface are different.
3. Solve for the derivatives of $(\sigma_x^{(m)})^{n+1}$, $(\sigma_y^{(m)})^{n+1}$, $(\sigma_z^{(m)})^{n+1}$, $(\sigma_{xy}^{(m)})^{n+1}$, $(\sigma_{xz}^{(m)})^{n+1}$, and $(\sigma_{yz}^{(m)})^{n+1}$ using Equations (4.9)-(4.10) or similar equations.
4. Solve for $(v_1^{(m)})^{n+1}$, $(v_2^{(m)})^{n+1}$, and $(v_3^{(m)})^{n+1}$ using Equations (4.11)-(4.13).
5. Update $(\varepsilon_x^{(m)})^{n+1}$, $(\varepsilon_y^{(m)})^{n+1}$, $(\varepsilon_z^{(m)})^{n+1}$, $(\gamma_{xy}^{(m)})^{n+1}$, $(\gamma_{xz}^{(m)})^{n+1}$ and $(\gamma_{yz}^{(m)})^{n+1}$ using Equations (4.14)-(4.15).

Given the required accuracy ξ_1 (for temperature) and ξ_2 (for strain), repeat the above steps until a convergent solution is obtained based on the following criteria:

$$\left|(T_e^{(m)})_{i,j,k}^{n+1(new)} - (T_e^{(m)})_{i,j,k}^{n+1(old)}\right| \le \xi_1, \tag{4.48a}$$

$$\left|(\varepsilon_x^{(m)})_{i,j,k}^{n+1(new)} - (\varepsilon_x^{(m)})_{i,j,k}^{n+1(old)}\right| \le \xi_2, \left|(\varepsilon_y^{(m)})_{i,j,k}^{n+1(new)} - (\varepsilon_y^{(m)})_{i,j,k}^{n+1(old)}\right| \le \xi_2, \tag{4.48b}$$

$$\left|(\varepsilon_z^{(m)})_{i,j,k}^{n+1(new)} - (\varepsilon_z^{(m)})_{i,j,k}^{n+1(old)}\right| \le \xi_2, \left|(\gamma_{xy}^{(m)})_{i,j,k}^{n+1(new)} - (\gamma_{xy}^{(m)})_{i,j,k}^{n+1(old)}\right| \le \xi_2, \tag{4.48c}$$

$$\left|(\gamma_{xz}^{(m)})_{i,j,k}^{n+1(new)} - (\gamma_{xz}^{(m)})_{i,j,k}^{n+1(old)}\right| \le \xi_2, \left|(\gamma_{yz}^{(m)})_{i,j,k}^{n+1(new)} - (\gamma_{yz}^{(m)})_{i,j,k}^{n+1(old)}\right| \le \xi_2. \qquad (4.48d)$$

It should be pointed out that the conditions $(v_3^{(1)})_{i,j,N+\frac{1}{2}}^{n+1} \neq (v_3^{(2)})_{i,j,\frac{3}{2}}^{n+1}$ in the Equation (4.46f) and $(\sigma_z^{(1)})_{i,j,N+1}^{n+1} \neq (\sigma_z^{(2)})_{i,j,1}^{n+1}$ in the Equation (4.46g) automatically satisfied the above iterative method.

CHAPTER FIVE

NUMERICAL EXAMPLE

This chapter will test the applicability of the model and its numerical scheme by considering 3D double-layered thin films with imperfect interfacial thermal contact exposed to ultrashort-pulsed lasers. Results will be discussed and compared with the previous work in [8], [16].

5.1 Example Description

To test the applicability of the developed numerical scheme, we investigated the temperature rises and thermal deformations in a 3D double-layered thin film consisting of a gold layer on a chromium padding layer with the dimensions 100 μm ×100 μm ×0.1μm. The thermo physical properties for gold and chromium are listed in Table 1 [1], [8], [62]. We assumed that the laser was focused on the center of the top surface of the thin film. Three different values of laser fluences (J = 500 J/m^2, 1000 J/ m^2 and 2000 J/m^2) were chosen to study the hot-electron blast force. Three meshes of 20 × 20 × 60, 20 × 20 × 80, 20 × 20× 100 for each layer in (x, y, z) for the thin film were used in order to test the convergence of the scheme. The time increment was chosen to be 0.005 ps and T_0 was set to be 300 K. The convergence criteria were chosen to be $\xi_1 = 10^{-8}$ for temperature and $\xi_2 = 10^{-16}$ for deformation.

Table 5.1 Thermophysical properties of gold and chromium

Properties	Unit	Gold	Chromium	Others
ρ	kg/m^3	19300	7190	
Λ	$J/(m^3K^2)$	70	1933	
λ	Pa	199.0×10^9	83.3×10^9	
μ	Pa	27.0×10^9	115.0×10^9	
α_T	$1/K$	14.2×10^{-6}	4.9×10^{-6}	
C_{e0}	$J/(m^3K)$	2.1×10^4	5.8×10^4	
C_l	$J/(m^3K)$	2.5×10^6	3.3×10^6	
G	$W/(m^3K)$	2.6×10^{16}	42×10^{16}	
k_e	$W/(mK)$	315	94	
R				0.93
t_p	s			0.1×10^{-12}
z_s, ζ	m			15.3×10^{-9}
r_s	m			1.0×10^{-6}
J	J/m^2			500, 1000, 2000

5.2 Results and Discussion

Figure 5.1a shows the changes in electron temperature ($\Delta T_e/(\Delta T_e)_{\max}$) at the center ($x_{center} = 50$ μm , $y_{center} = 50$ μm) of the gold surface with a laser fluence of $J = 500$ J/m^2 between the perfect thermal contact [17] and the imperfect thermal contact at the interface. The maximum temperature rise of T_e (i.e., $(\Delta T_e)_{\max}$) for the imperfect thermal contact case is about 4,062 K, which is higher than 3,765 K obtained in [8] and 3,727 K obtained by Tzou et al. [1] for the perfect thermal contact case. This result is as expected because the amount of heat transferred to the chromium layer at the imperfect thermal contact interface should be much smaller than that in the perfect thermal contact case. As a result, the maximum temperature rise of T_e should be higher. The result also explains that the change in electron temperature at the center of the top surface of the

gold layer decreases very slowly after a peak with increasing time, which is significantly different from that in the perfect thermal contact case. Figure 5.1b shows the displacement w at the center (x_{center}, y_{center}) of the gold surface. The negative value of displacement w indicates that the gold layer at the center $(x_{center}, y_{center}, 0)$ is expanding along the negative z direction. Due to the higher temperature in the gold layer for the imperfect thermal contact case, the gold layer at the center $(x_{center}, y_{center}, 0)$ is expanding much more than that in the perfect thermal contact case. Furthermore, it can be seen from both figures that the mesh size had no significant effect on the solution and, hence, the solution is considered to be convergent.

Figures 5.2 and 5.3 show comparisons of electron temperature and lattice temperature along z direction at (x_{center}, y_{center}) between the perfect thermal contact [8] and the imperfect thermal contact at the interface at different times (a) t = 0.25 ps, (b) t = 1 ps, (c) t = 10 ps, and (d) t = 20 ps, which were obtained based on a mesh of 20 × 20 × 80 and three different laser fluences (J = 500 J/m^2, 1000 J/m^2 and 2000 J/m^2). It can be seen that the electron temperature in both cases rises to its maximum at the beginning and then decreases while the lattice temperature rises with time. Figure 5.2 shows clearly that there is a sharp discontinuity of electron temperature at the interface when the imperfect thermal contact exists between two bonded thin layers. Similar temperature discontinuity is observed at the interface for lattice temperature in Figure 5.3. In particular, we see from Figure 5.3 that the lattice temperature profiles between these two cases are completely different. For the perfect thermal contact case, the lattice temperature increases drastically across the interface because the conductivity of chromium is smaller than that of gold. However, for the imperfect thermal contact case,

the lattice temperature in the gold layer is higher than that in the chromium layer. These results indicate that imperfect thermal contact at the interface provides a barrier to thermal energy diffusion across the interface. These two figures also show that electron temperature and lattice temperature are uniform throughout the chromium layer and uniform throughout the gold layer after a long period. The uniform electron and lattice temperatures are probably due to increased rate of collision between electrons and phonons in the gold thin layer as electron energy diffusion is inhibited at the interface.

Figure 5.4 shows the displacement w of the thin film along z at (x_{center}, y_{center}) between the perfect thermal contact [8] and the imperfect thermal contact at the interface at different times (a) t = 5 ps, (b) t = 10 ps, (c) t = 15 ps, and (d) t = 20 ps with a mesh of $20 \times 20 \times 80$ and three different laser fluences (J = 500 J/m^2, 1000 J/m^2 and 2000 J/m^2). The negative value indicates that the displacement moves in the negative z direction, while the positive value implies that it moves in the positive z direction. It can be seen from this figure that for the imperfect thermal contact case the film is expanding, and sharp discontinuity of displacement exists at the interface. The gold layer undergoes severe displacement from negative to positive while the displacement in the chromium layer is almost absent. However, sharp discontinuity of displacement exists at the interface, which may result in shear failure. Severe displacement exists in the gold layer may produce internal damages within the layer. Displacement in the gold layer is more pronounced for bonded films with the imperfect thermal contact.

Figure 5.5 shows the normal stress σ_z along z at (x_{center}, y_{center}) between the perfect thermal contact [8] and the imperfect thermal contact at the interface at different times (a) t = 5 ps, (b) t = 10 ps, (c) t = 15 ps, and (d) t = 20 ps with a mesh of

$20 \times 20 \times 80$ and three different laser fluencies (J = 500 J/m^2, 1000 J/m^2 and 2000 J/m^2). The ultrashort-pulsed laser heating produced severe stress distributions in the gold layer for the imperfect thermal contact case. However, in the chromium layer, stress distribution is less severe which implies that the gold layer may undergo severe structural deformation. Furthermore, it can be seen from Figure 5.5 that the curve of the normal stress σ_z, is smooth and does not appear sustain non-physical oscillations.

Figures 5.6-5.10 were plotted based on the results obtained with a mesh of $20 \times 20 \times 80$ and with a laser fluence of J = 1000 J/m^2 Figures 5.6 and 5.7 show contours of the electron temperature distribution and the lattice temperature distribution in the cross section of $y = y_{center}$ at different times (a) t = 0.25 ps, (b) t = 1 ps,, (c) t = 10 ps and (d) t = 20 ps, respectively. It can be seen from both figures that the heat is mainly transferred along the z direction and with time the electron temperature and lattice temperature drop gradually. The electron temperature in gold film at the surface drops from 6170 K at 0.25 ps to 980 K at 20 ps. The chromium film at the bottom maintains the electron temperature of 300 K. The lattice temperature, which is the atom temperature inside the metal film, increases in gold film at the surface from 305 K at 0.25 ps to 796 K at 20 ps. The chromium film at the bottom maintains a lattice temperature of 300 K. The temperature change across the interface illustrates that the electron temperature and lattice temperature are obviously discontinues at the interface.

Figure 5.8 shows contours of displacements w in the cross section of $y = y_{center}$ at different times (a) t = 5 ps, (b) t = 10 ps, (c) t = 15 ps, and (d) t = 20 ps, respectively. It can be seen from Figure 5.8 that at the beginning of 5 ps, the temperature is transferred through the gold metal but discontinuous as it passes through the interface. Therefore,

the surface and bottom of gold film have energy accumulated, causing the displacement in the z direction to expand along the negative z direction. From 10 ps to 20 ps, the severe displacement along the z direction exists in the gold layer. The displacement along the z direction at the surface of gold film increases from 0.274 nm at 10 ps to 0.954 nm at 20 ps. The displacement along z direction in the chromium film remains zero because the temperature is discontinuous at the interface.

Figure 5.9 shows contours of displacements v in the cross section of $x = x_{center}$ at different times (a) t = 5 ps, (b) t = 10 ps, (c) t = 15 ps, and (d) t = 20 ps, respectively. According to Figure 5.9, the central part of gold film is expanding along the center line in the x direction. At the time of 5 ps, the displacement v is changing from positive to negative because the hot-blast force placed in the positive z direction on the center of the surface which results in shrinkage of the gold metal across the center line in the x direction. From the time of 10 ps to 20 ps, the heat expands the gold film because the displacement v is changing from negative value to positive value. It should be pointed out that there is no expansion in the chromium film and displacement v equal to zero due to the discontinuity of temperature across the interface.

Figure 5.10 shows contours of displacements u in the cross section of $y = y_{center}$ at different times (a) t = 5 ps, (b) t = 10 ps, (c) t = 15 ps, and (d) t = 20 ps, respectively. Figure 5.10 has almost the same properties as Figure 5.9. Thus, according to Figure 5.10, the central part of gold film is expanding along the center line in the y direction. At the time of 5 ps, the displacement u is changing from positive to negative because the hot-blast force placed in the positive z direction on the center of the surface, which results in shrinkage of the gold metal across the center line in the x direction. From the time of 10

ps to 20 ps the heat expands the gold film because the displacement u is changing from negative to positive. It should be pointed out that there is no expansion in the chromium film and displacement u equal to zero due to the discontinuity of temperature across the interface.

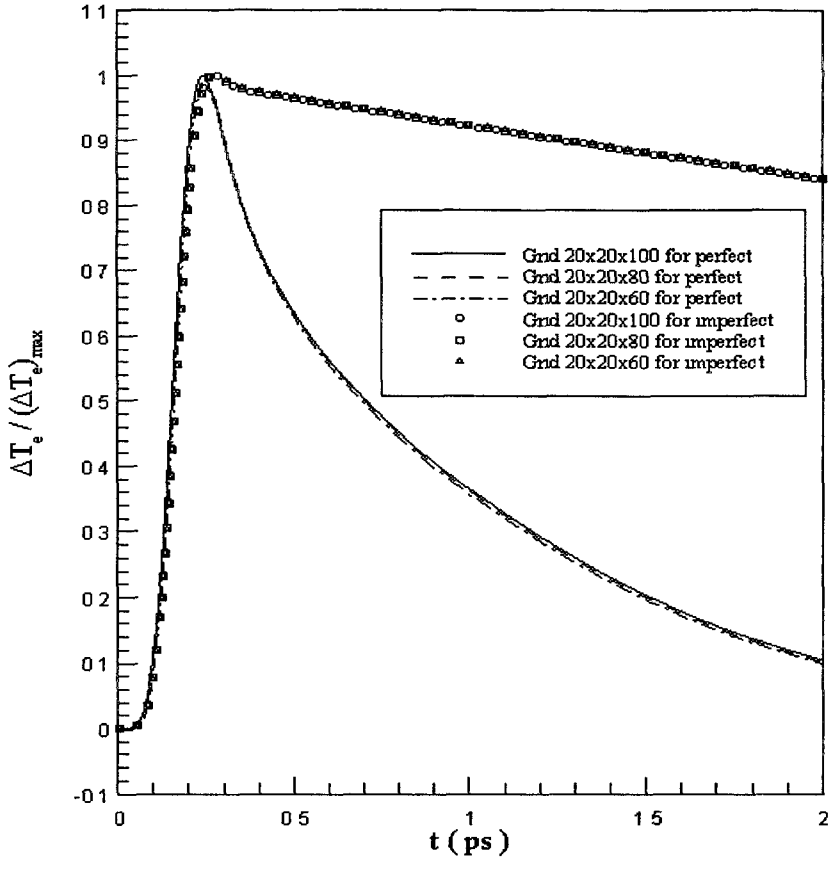

(a)

Figure 5.1a Change in electron temperature versus time with a laser fluence (J) of $500J/m^2$.

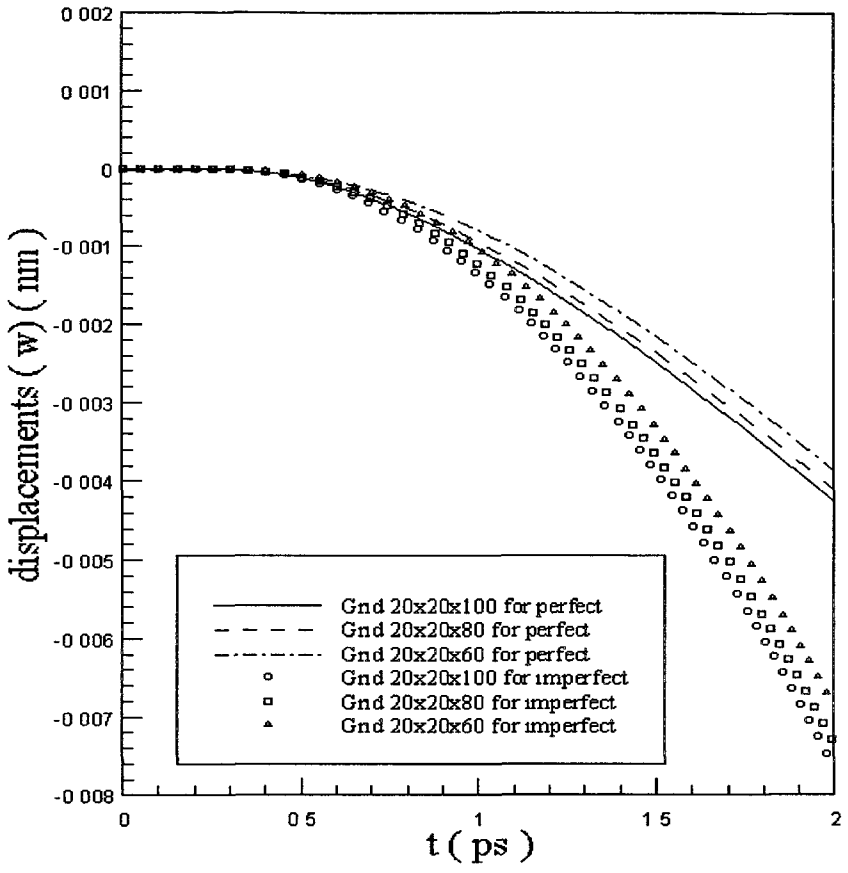

(b)

Figure 5.1b Chang in displacements at the center of top surface of thin versus time with a laser fluence (J) of 500J/m^2. The *w* is the displacement at (x_{center}, y_{center}, 0) of thin film.

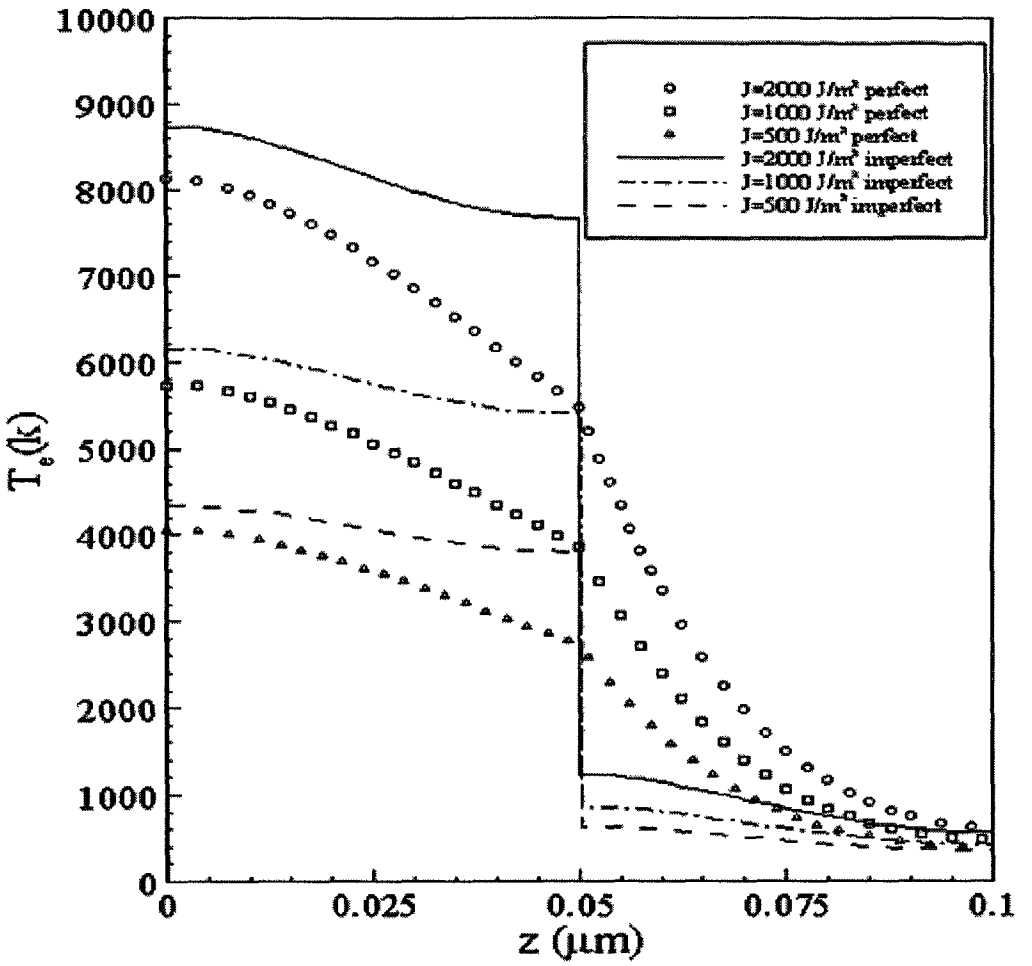

(a)

Figure 5.2a Electron temperature profiles along z at (x_{center}, y_{center},) at the time of t = 0.25 ps with a mesh of $20 \times 20 \times 80$ and three different laser fluences (J) of 500J/m^2, 1000J/m^2 and 2000J/m^2.

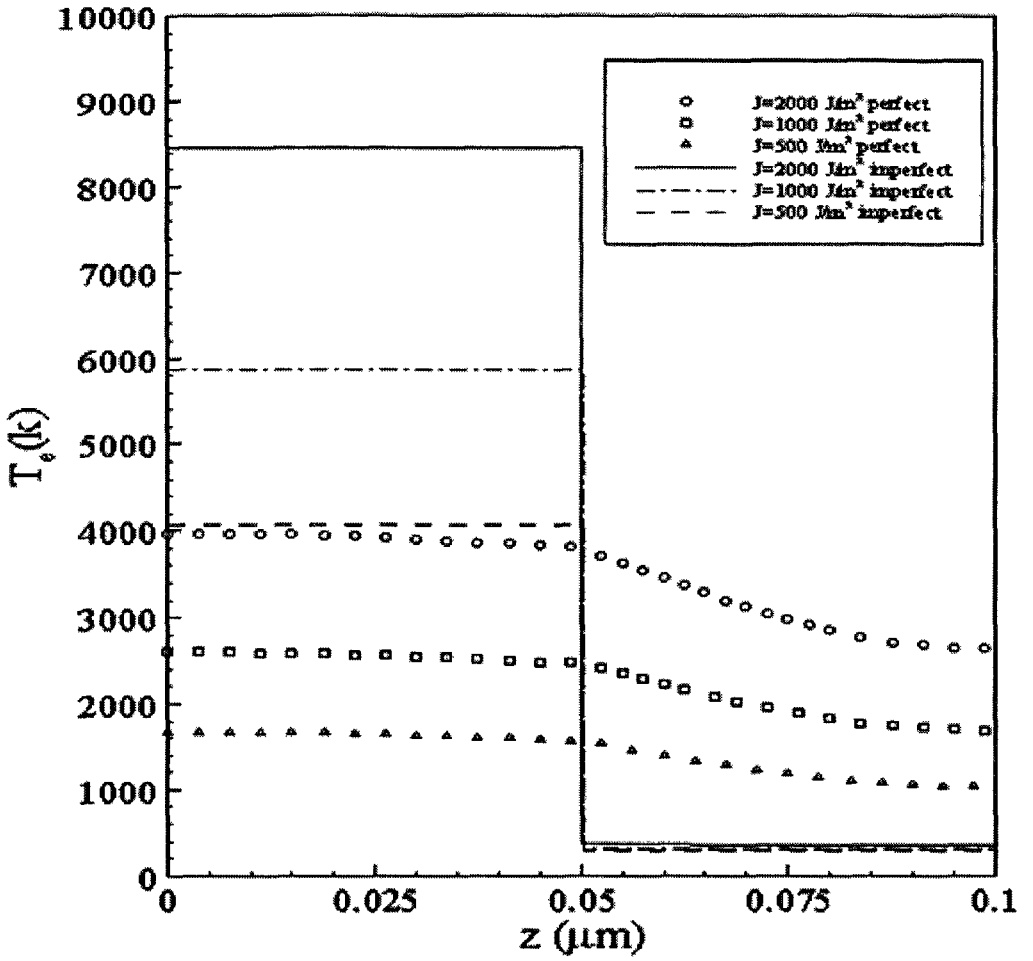

(b)

Figure 5.2b Electron temperature profiles along z at (x_{center}, y_{center},) at the time of t = 1 ps with a mesh of $20 \times 20 \times 80$ and three different laser fluences (J) of 500J/m^2, 1000J/m^2 and 2000J/m^2.

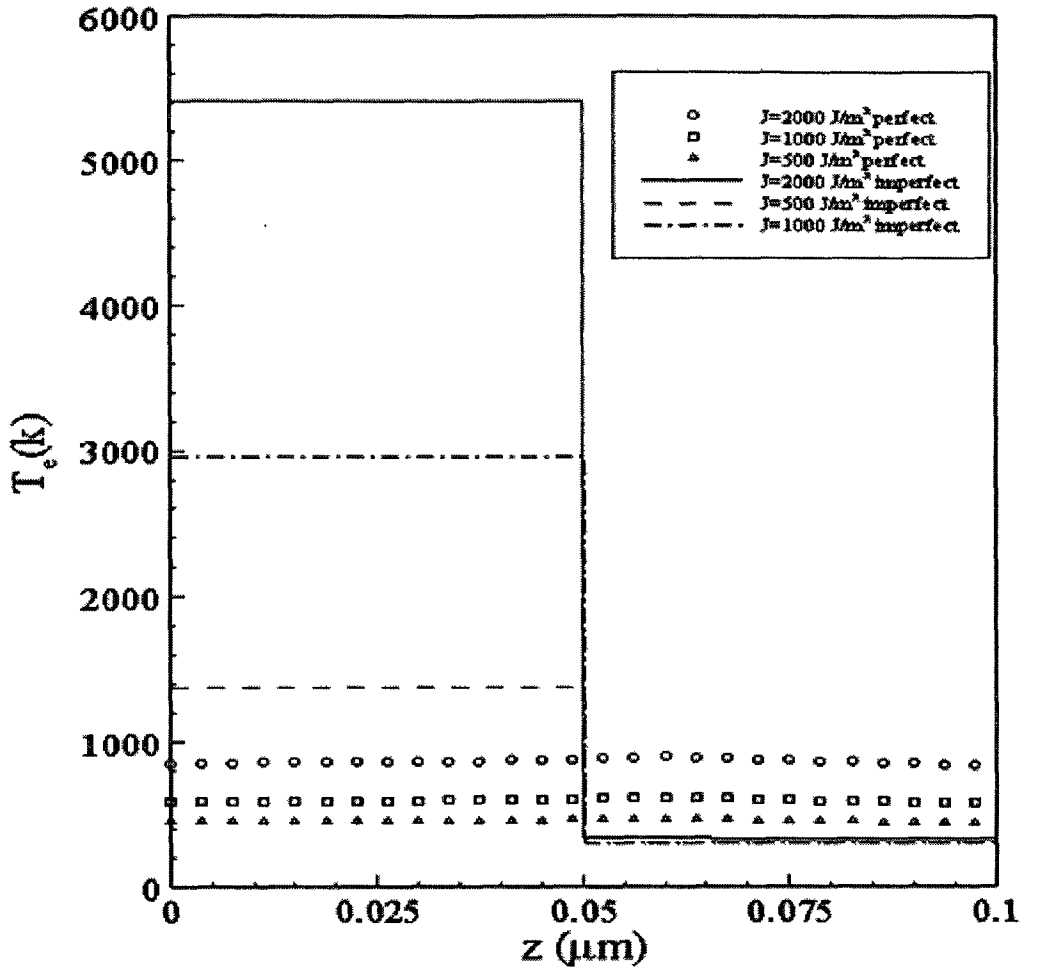

(c)

Figure 5.2c Electron temperature profiles along z at (x_{center}, y_{center},) at the time of t = 10 ps with a mesh of $20 \times 20 \times 80$ and three different laser fluences (J) of 500J/m^2, 1000J/m^2 and 2000J/m^2.

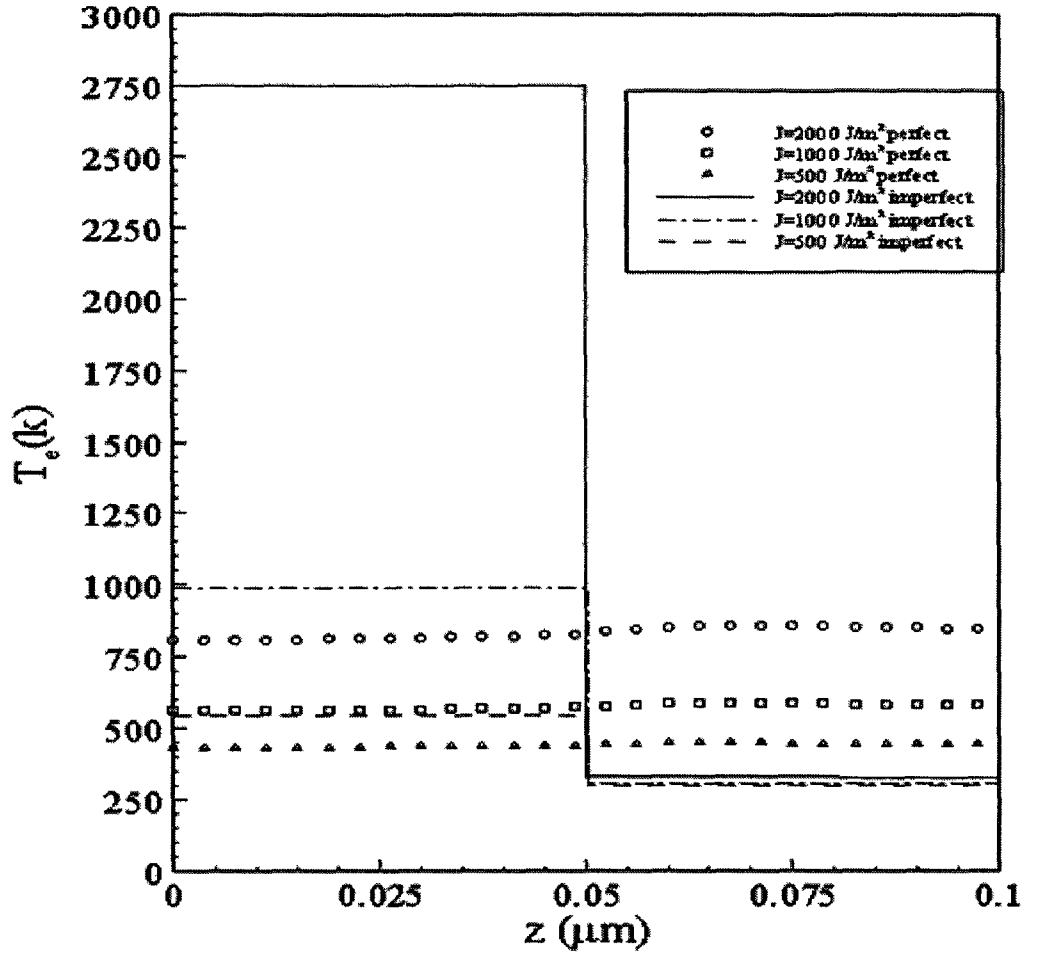

(d)

Figure 5.2d Electron temperature profiles along z at (x_{center}, y_{center},) at the time of t = 20 ps with a mesh of $20 \times 20 \times 80$ and three different laser fluences (J) of 500J/m^2, 1000J/m^2 and 2000J/m^2.

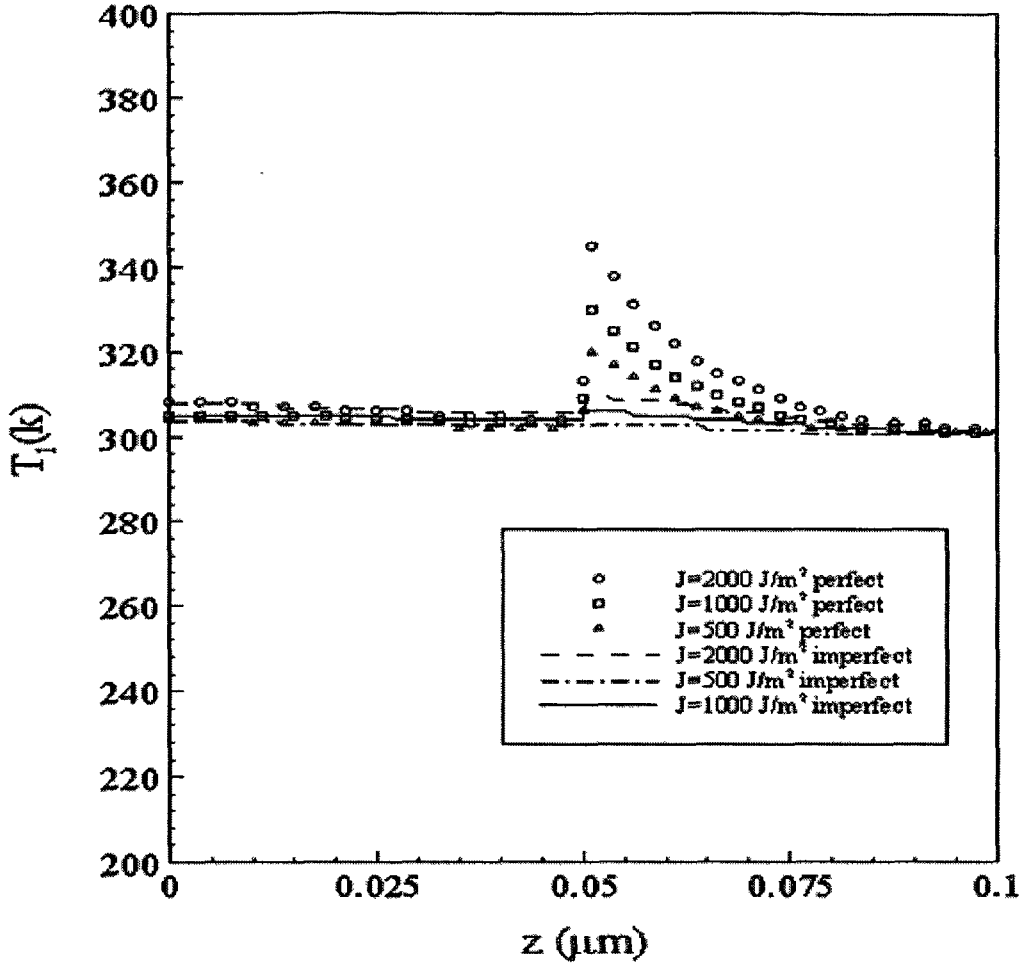

(a)

Figure 5.3a Lattice temperature profiles along z at (x_{center}, y_{center},) at the time of t = 0.25 ps with a mesh of $20 \times 20 \times 80$ and three different laser fluences (J) of 500J/m^2, 1000J/m^2 and 2000J/m^2.

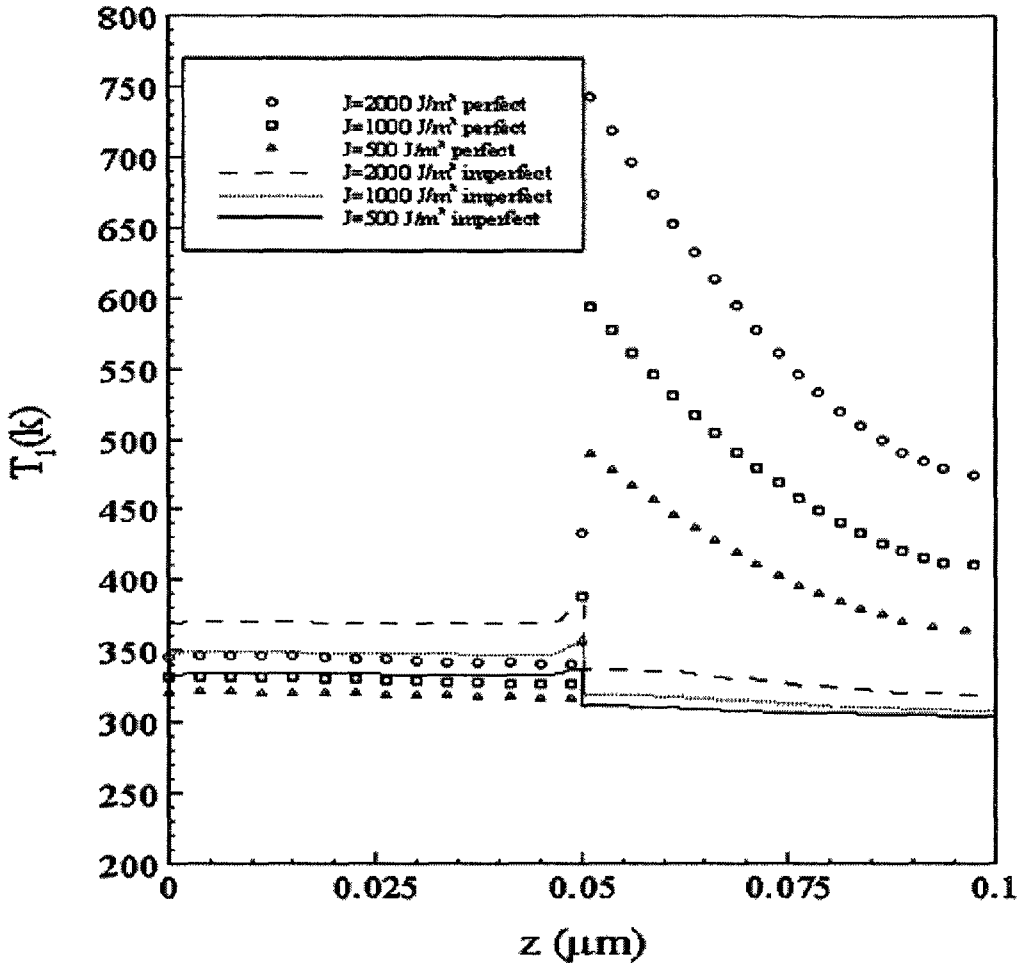

(b)

Figure 5.3b Lattice temperature profiles along z at (x_{center}, y_{center},) at the time of t = 1 ps with a mesh of $20 \times 20 \times 80$ and three different laser fluences (J) of 500J/m^2, 1000J/m^2 and 2000J/m^2.

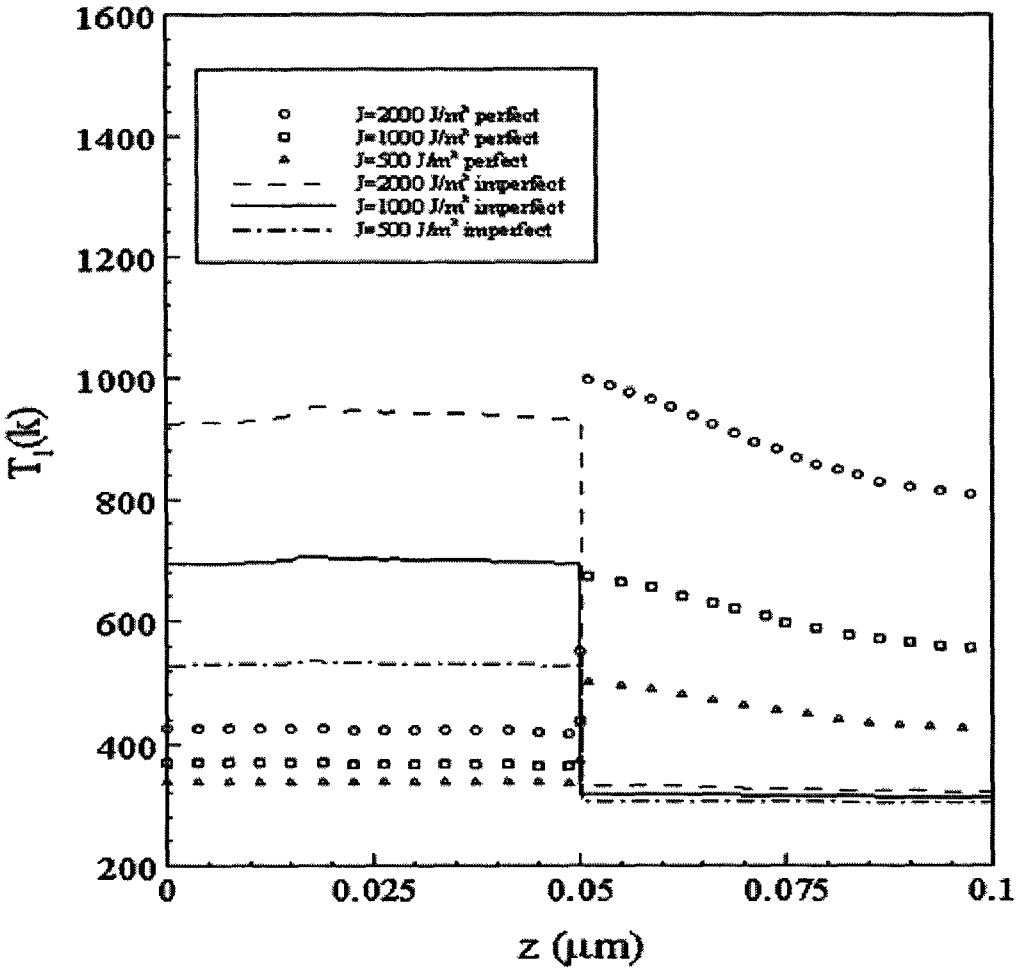

(c)

Figure 5.3c Lattice temperature profiles along z at (x_{center}, y_{center},) at the time of t = 10 ps with a mesh of $20 \times 20 \times 80$ and three different laser fluences (J) of 500J/m^2, 1000J/m^2 and 2000J/m^2.

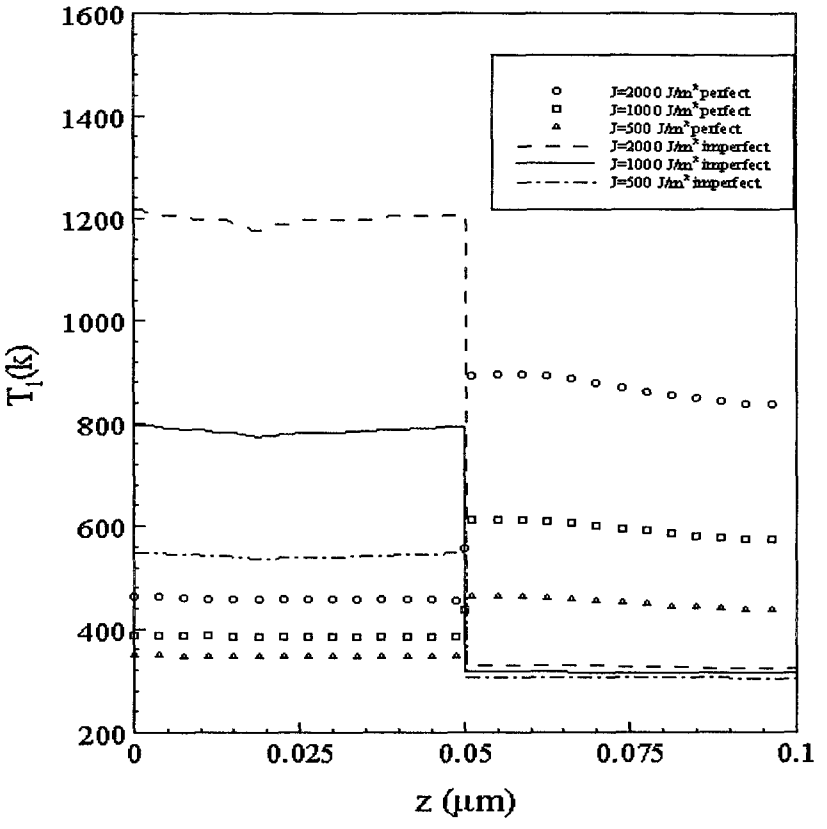

(d)

Figure 5.3d Lattice temperature profiles along z at (x_{center}, y_{center},) at the time of $t = 20$ ps with a mesh of $20 \times 20 \times 80$ and three different laser fluences (J) of 500J/m^2, 1000J/m^2 and 2000J/m^2.

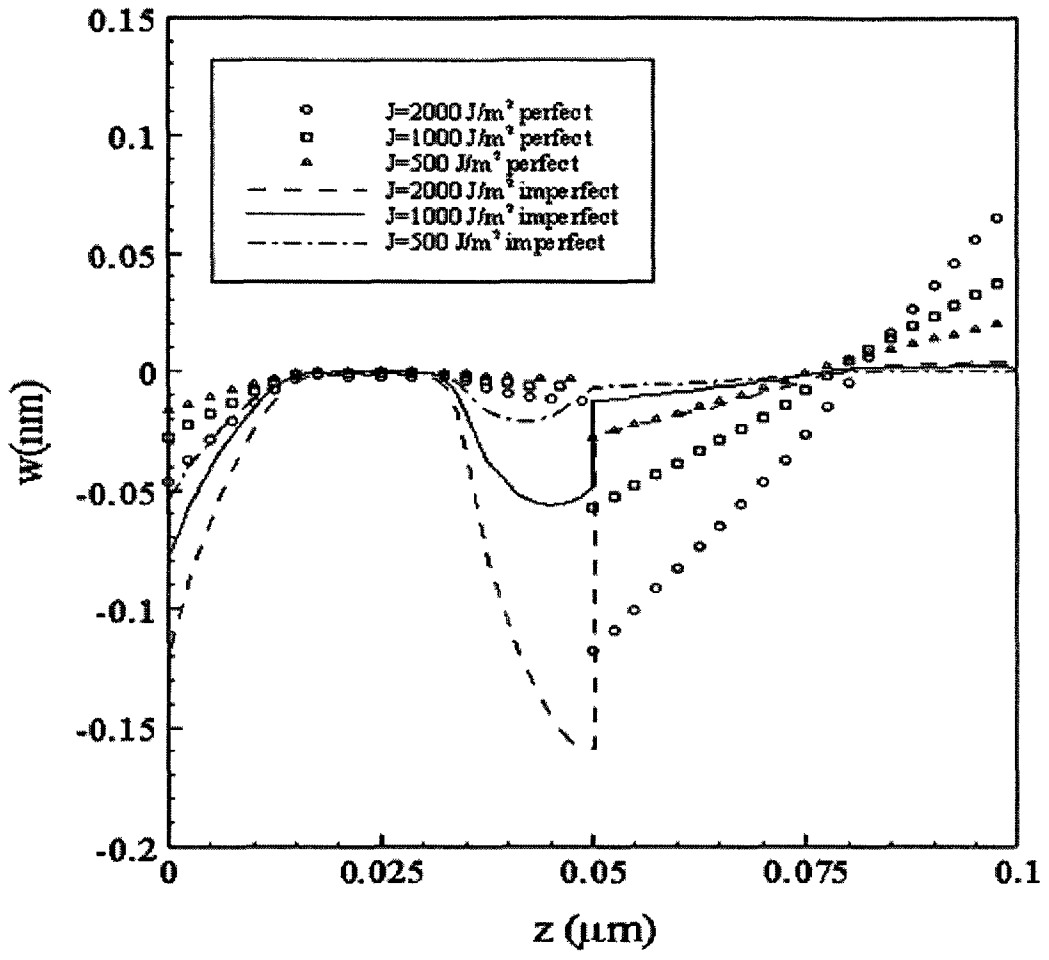

(a)

Figure 5.4a Displacement w profiles along z at (x_{center}, y_{center},) at the time of t = 5 ps with a mesh of $20 \times 20 \times 80$ and three different laser fluences (J) of 500J/m^2, 1000J/m^2 and 2000J/m^2.

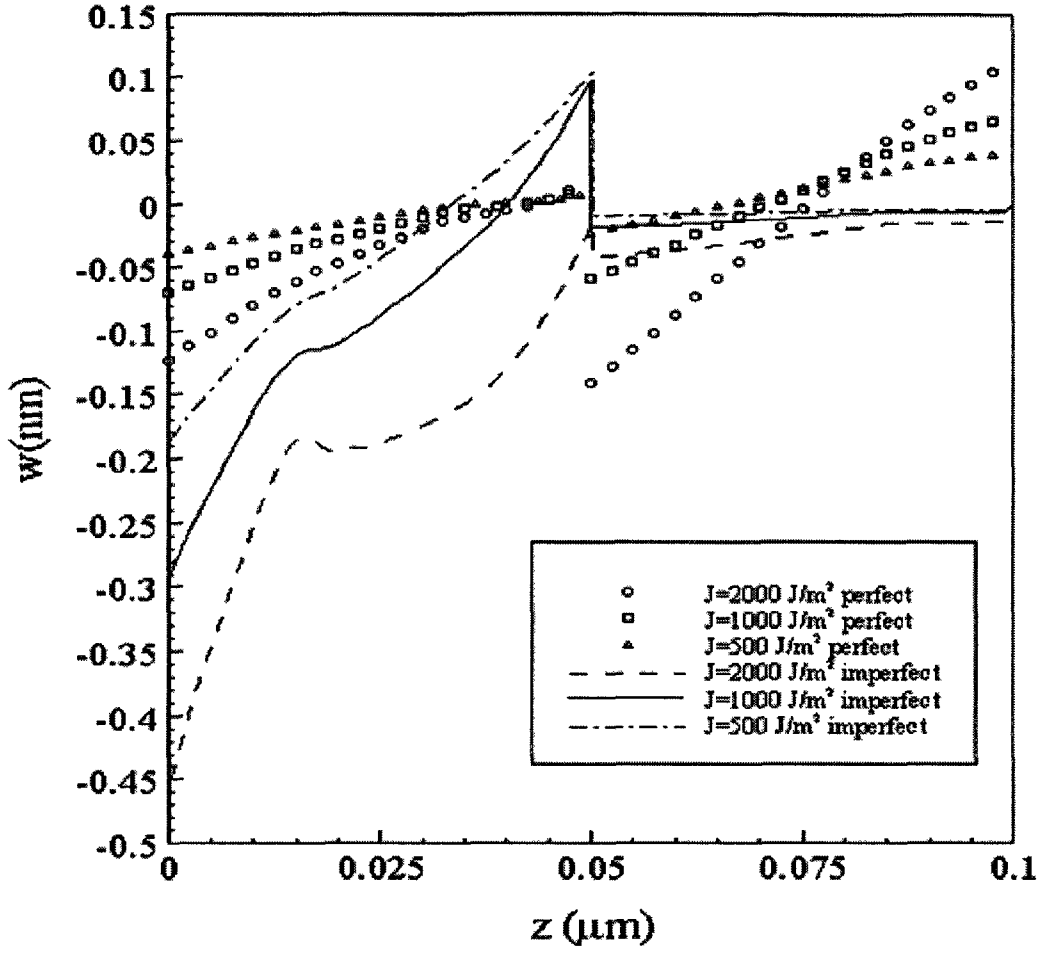

(b)

Figure 5.4b Displacement w profiles along z at (x_{center}, y_{center},) at the time of t = 10 ps with a mesh of $20 \times 20 \times 80$ and three different laser fluences (J) of 500J/m^2, 1000J/m^2 and 2000J/m^2.

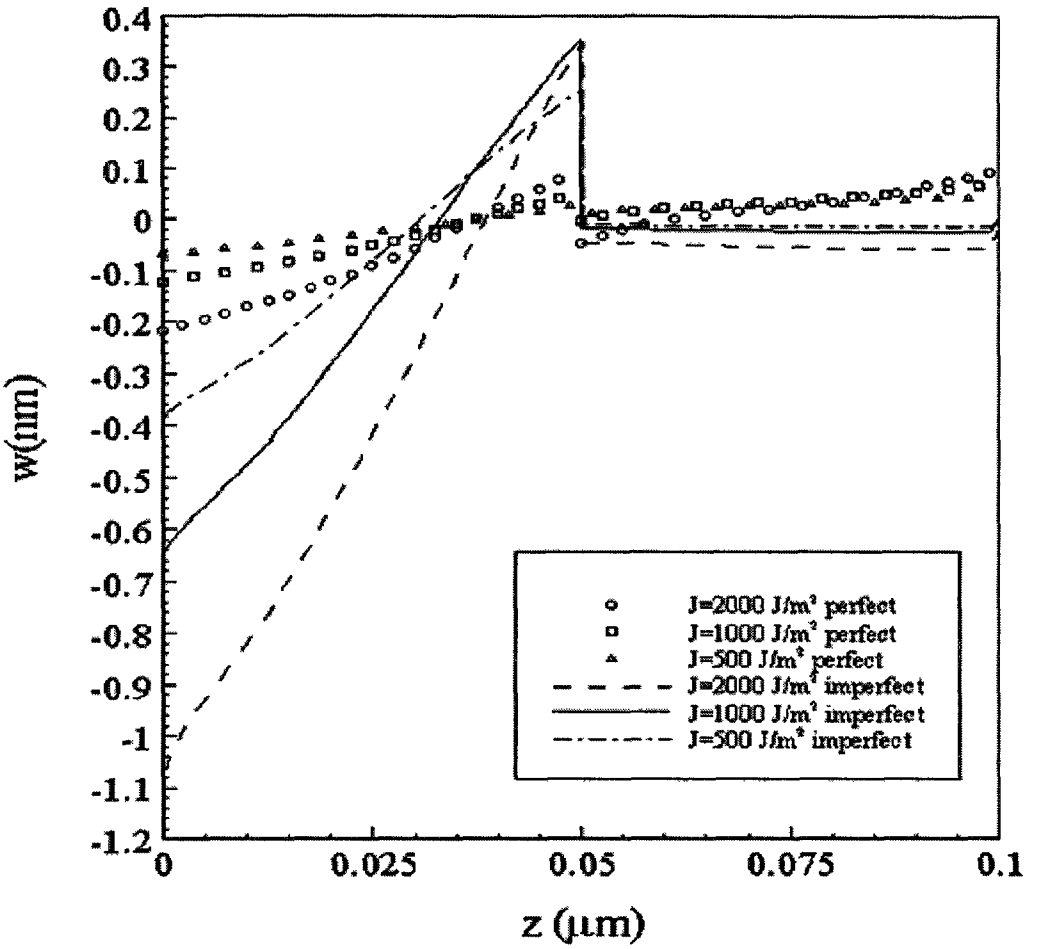

(c)

Figure 5.4c Displacement w profiles along z at (x_{center}, y_{center},) at the time of t = 15 ps with a mesh of $20 \times 20 \times 80$ and three different laser fluences (J) of 500J/m^2, 1000J/m^2 and 2000J/m^2.

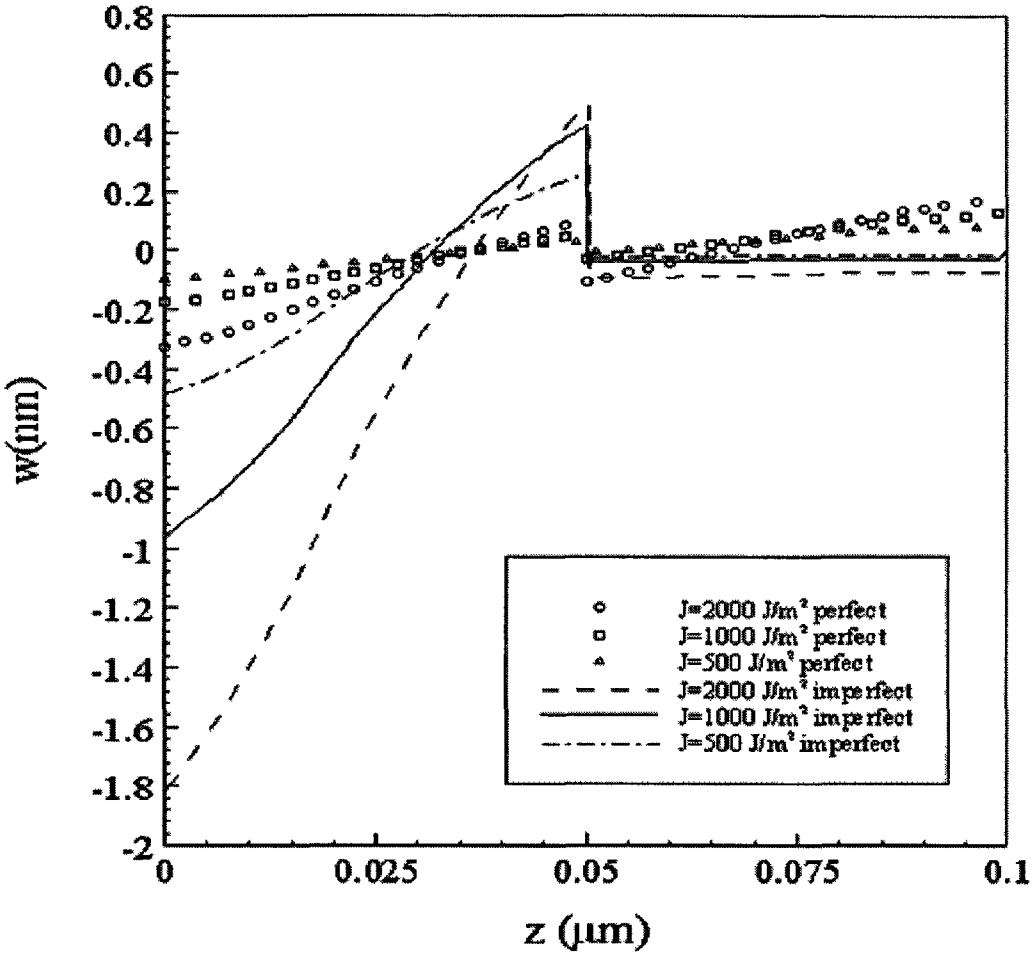

(d)

Figure 5.4d Displacement w profiles along z at (x_{center}, y_{center},) at the time of t = 20 ps with a mesh of $20 \times 20 \times 80$ and three different laser fluences (J) of 500J/m^2, 1000J/m^2 and 2000J/m^2.

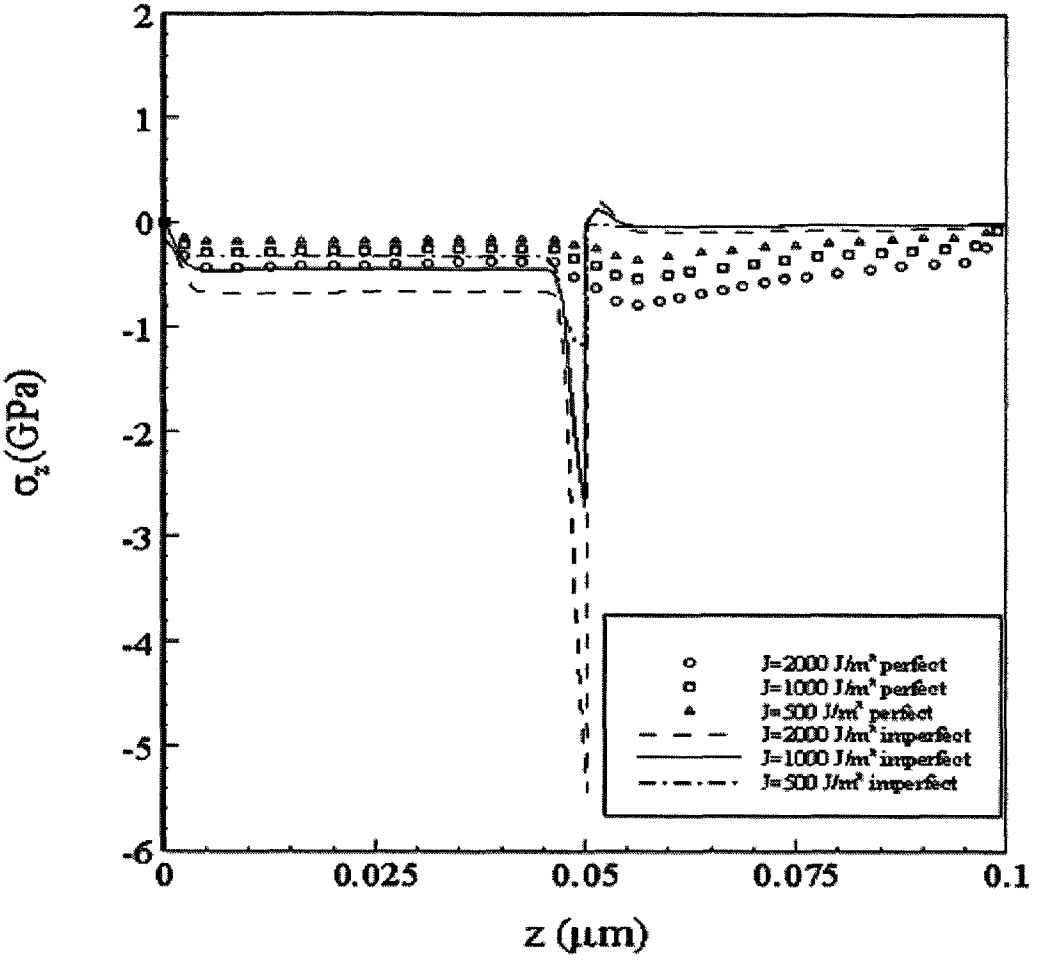

(a)

Figure 5.5a Normal stress (σ_z) profiles along z at (x_{center}, y_{center},) at the time of t = 5 ps with a mesh of $20 \times 20 \times 80$ and three different laser fluences (J) of 500J/m^2, 1000J/m^2 and 2000J/m^2.

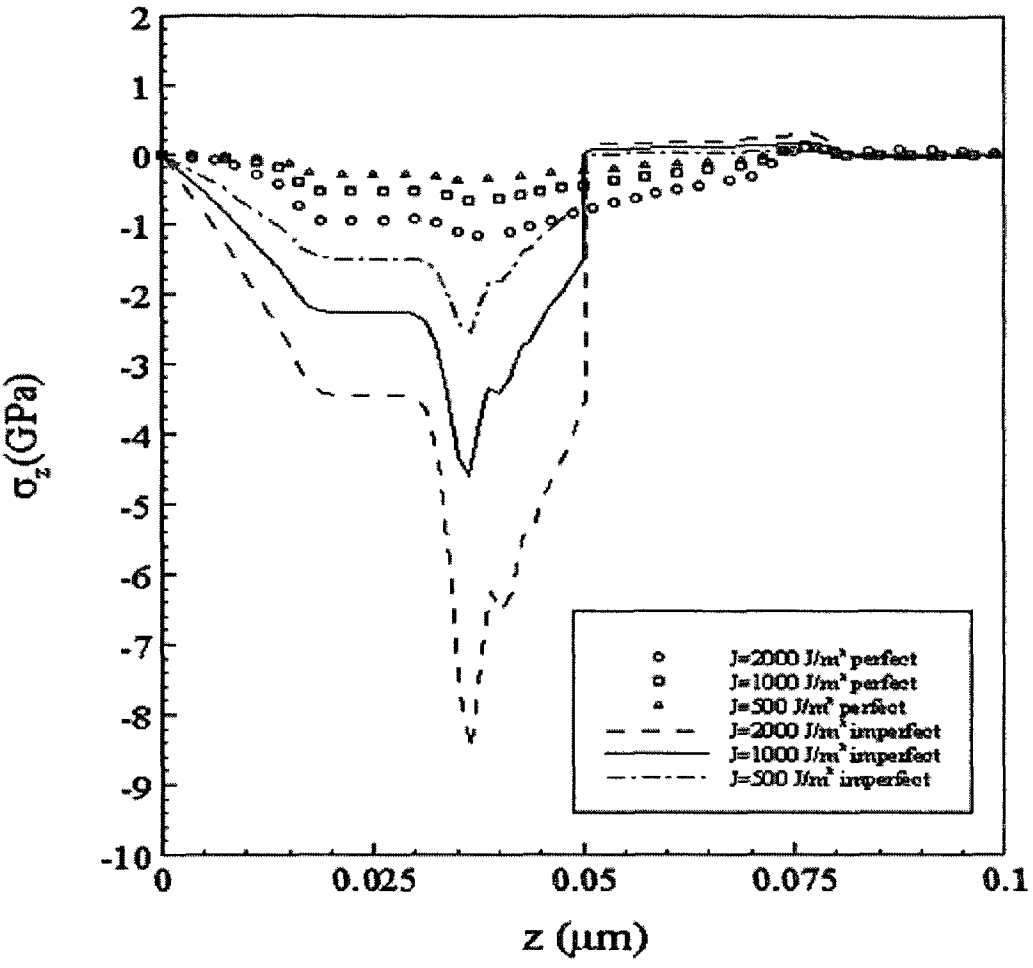

(b)

Figure 5.5b Normal stress (σ_z) profiles along z at (x_{center}, y_{center},) at the time of t = 10 ps with a mesh of $20 \times 20 \times 80$ and three different laser fluences (J) of 500J/m^2, 1000J/m^2 and 2000J/m^2.

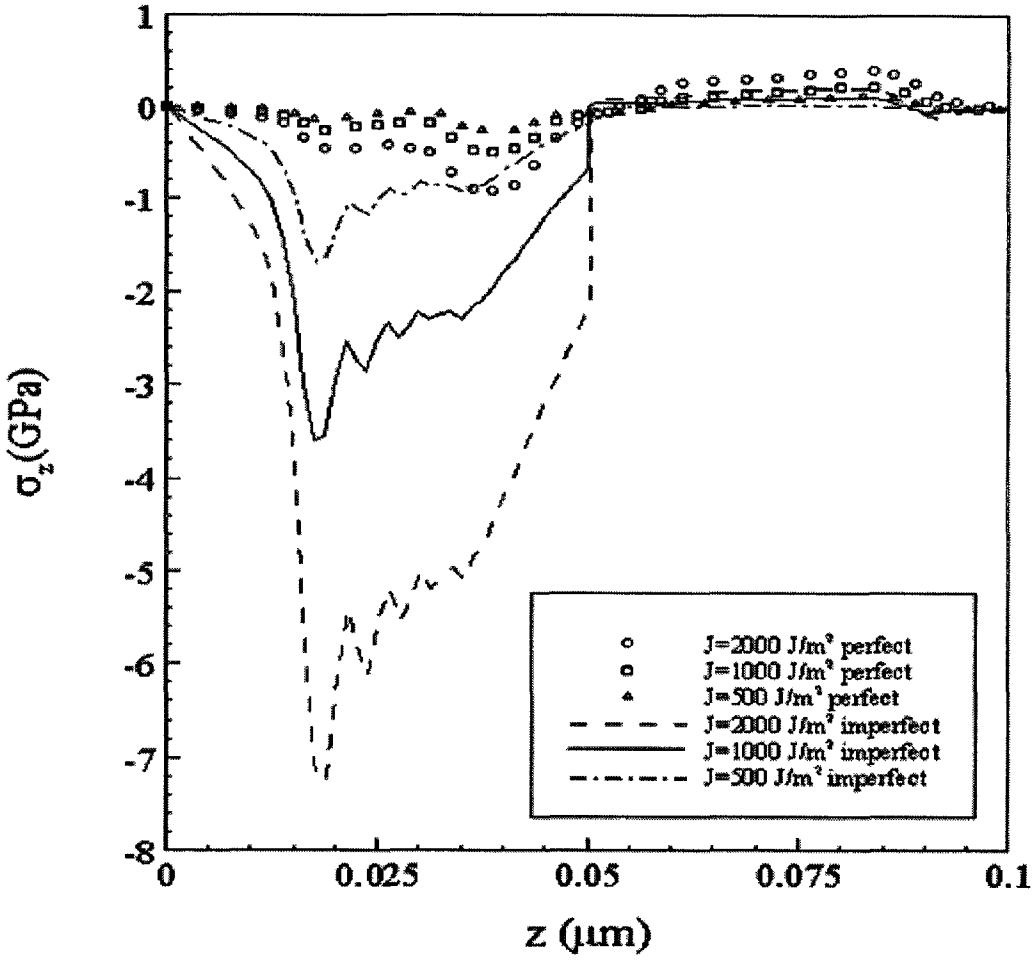

(c)

Figure 5.5c Normal stress (σ_z) profiles along z at (x_{center}, y_{center},) at the time of t = 15 ps with a mesh of $20 \times 20 \times 80$ and three different laser fluences (J) of 500J/m^2, 1000J/m^2 and 2000J/m^2.

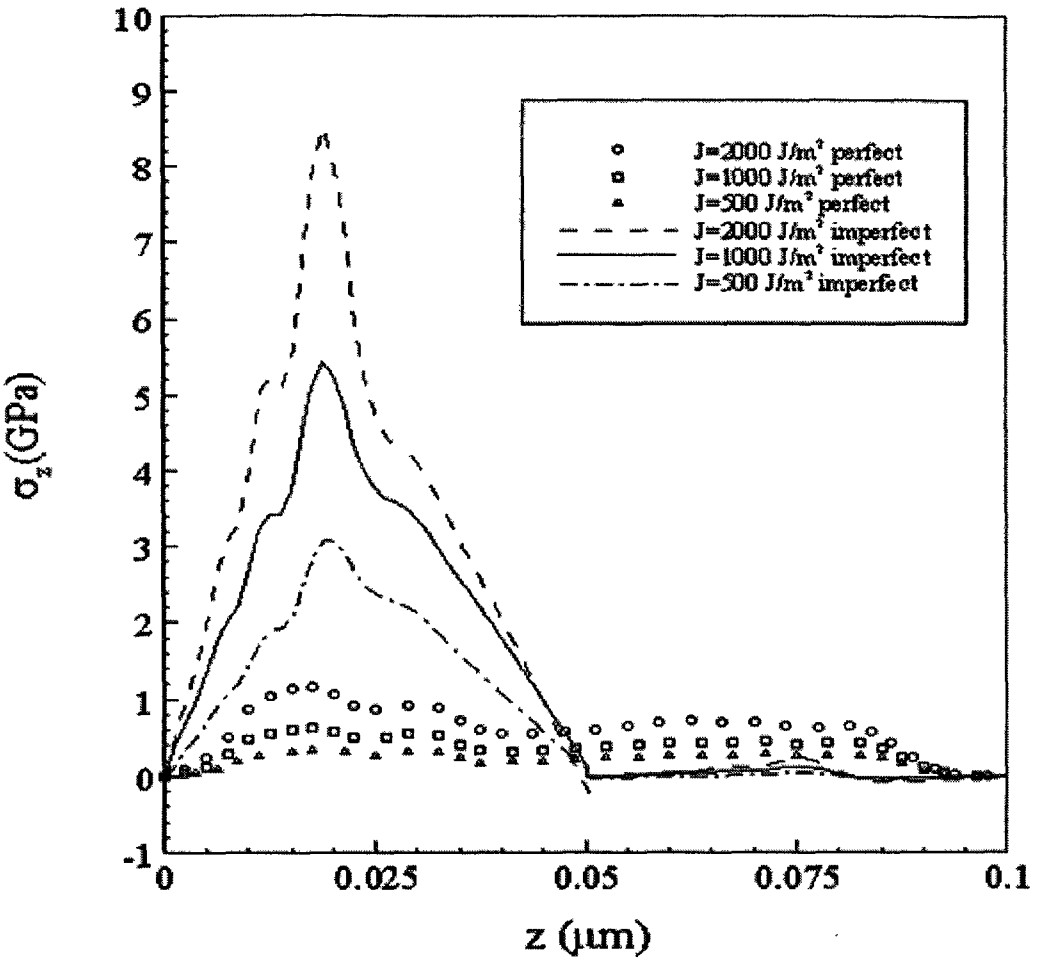

(d)

Figure 5.5d Normal stress (σ_z) profiles along z at (x_{center}, y_{center},) at the time of t = 20 ps with a mesh of $20 \times 20 \times 80$ and three different laser fluences (J) of 500J/m^2, 1000J/m^2 and 2000J/m^2.

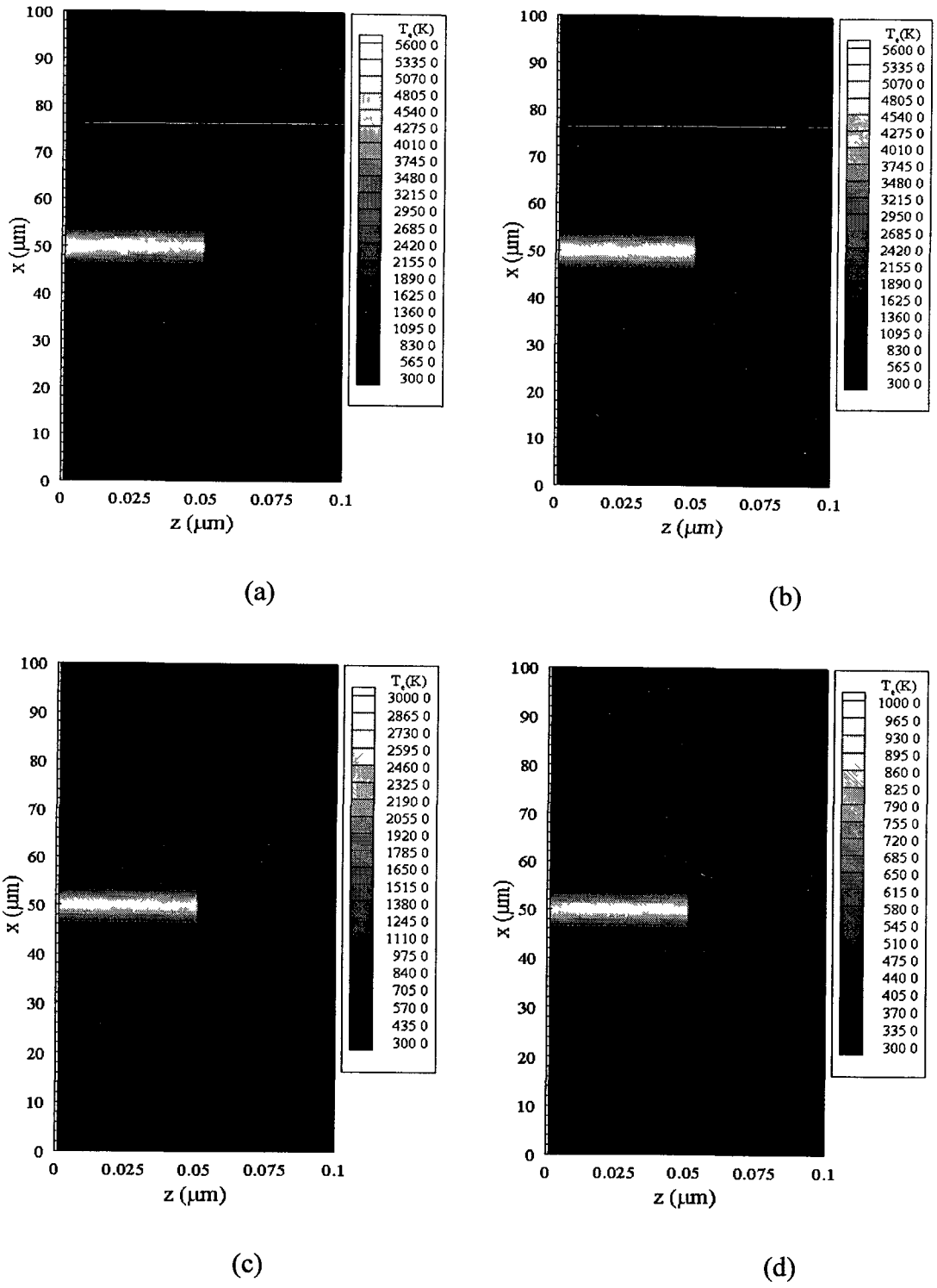

Figure 5.6 Contours of electron temperature distributions in the cross section of $y = 50$ μm at different times (a) $t = 0.25$ ps, (b) $t = 1$ ps, (c) $t = 10$ ps, and (d) $t = 20$ ps with a mesh of $20 \times 20 \times 80$ and three different laser fluences (J) of $1000 J/m^2$.

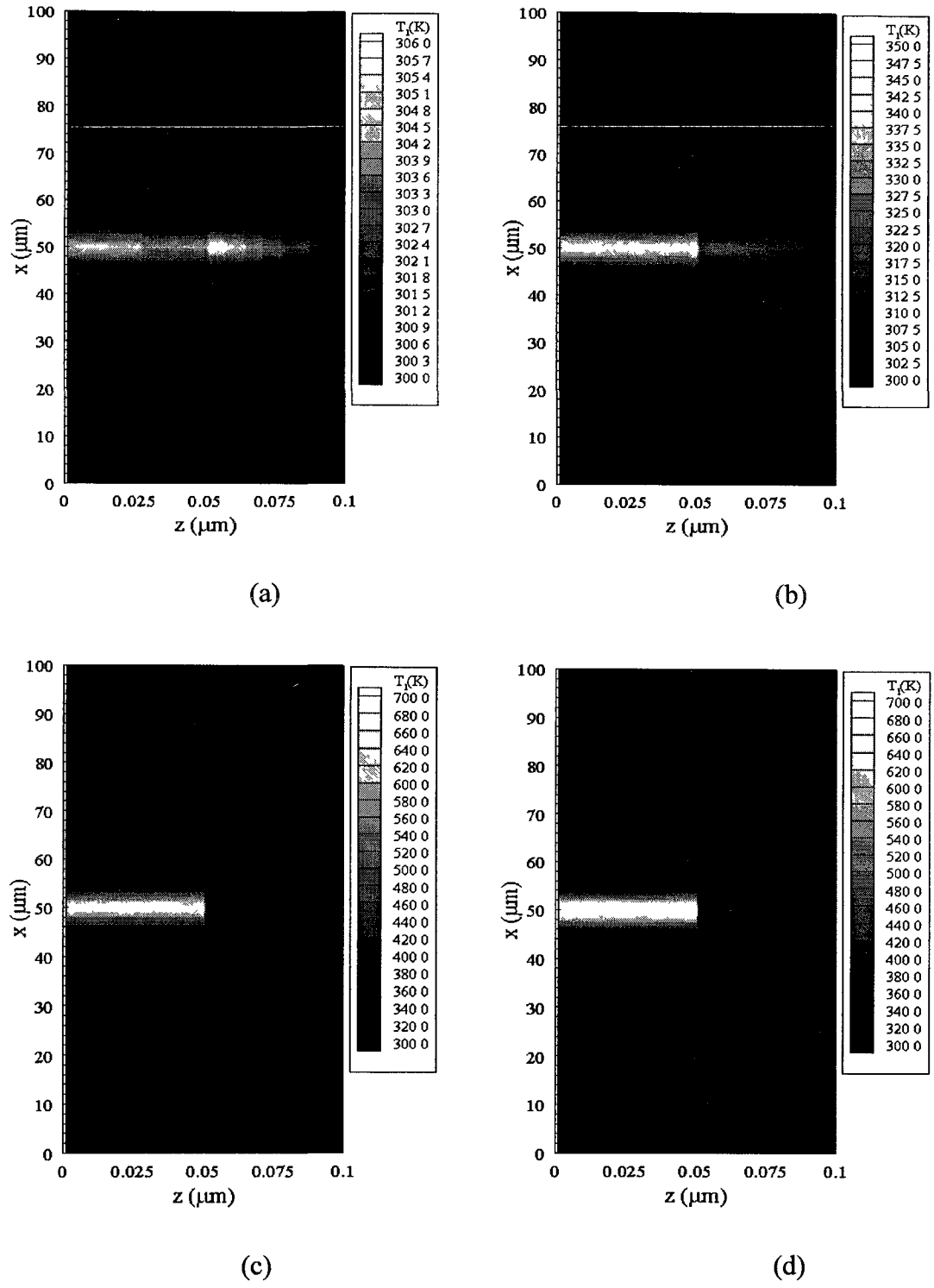

Figure 5.7 Contours of lattice temperature distributions in the cross section of $y = 50$ μm at different times (a) $t = 0.25$ ps, (b) $t = 1$ ps, (c) $t = 10$ ps, and (d) $t = 20$ ps with a mesh of $20 \times 20 \times 80$ and three different laser fluences (J) of 1000J/m^2.

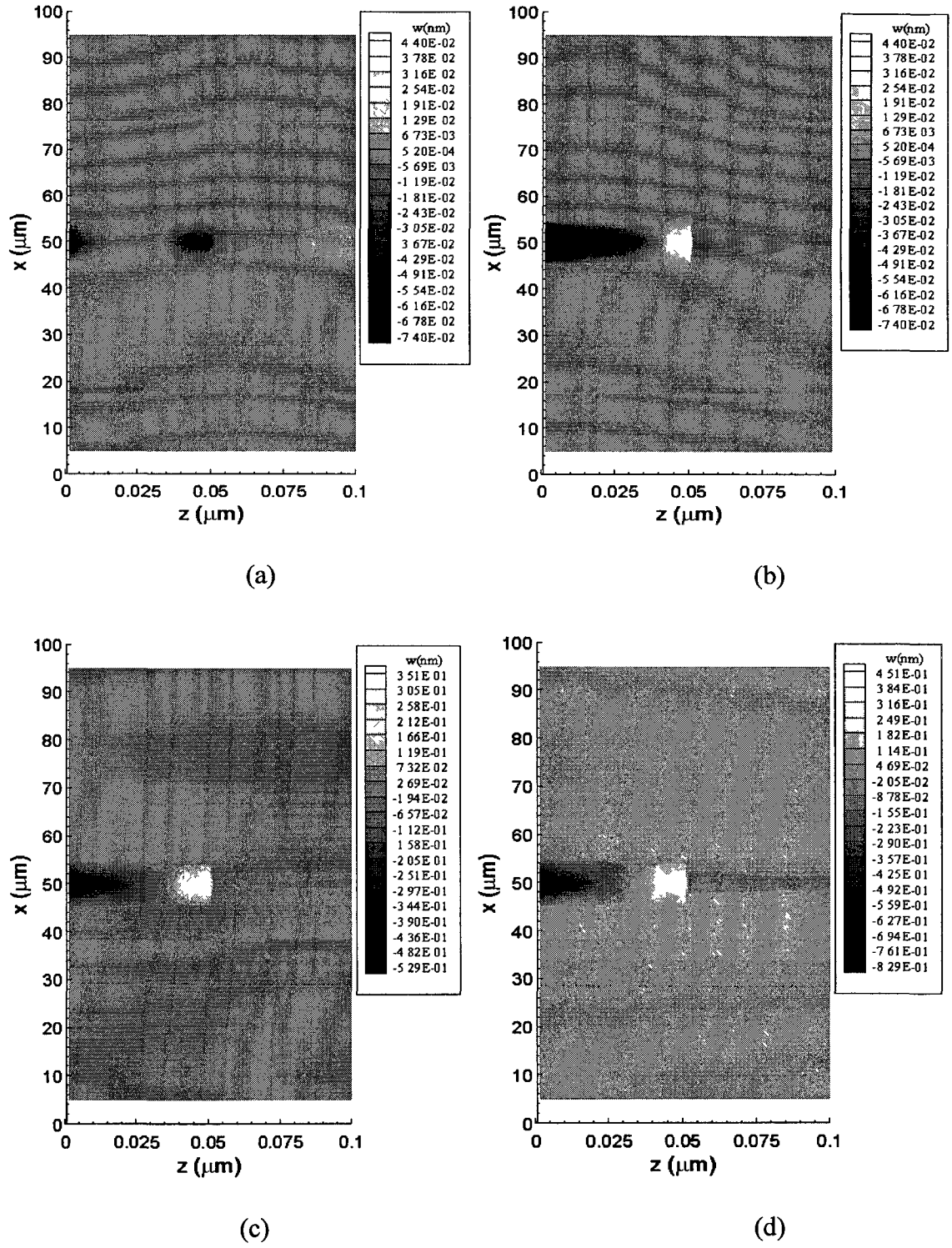

Figure 5.8 Contours of displacement (w) distributions in the cross section of $y = 50$ μm at different times (a) $t = 5$ ps, (b) $t = 10$ ps, (c) $t = 15$ ps, and (d) $t = 20$ ps with a mesh of $20 \times 20 \times 80$ and three different laser fluences (J) of $1000 J/m^2$.

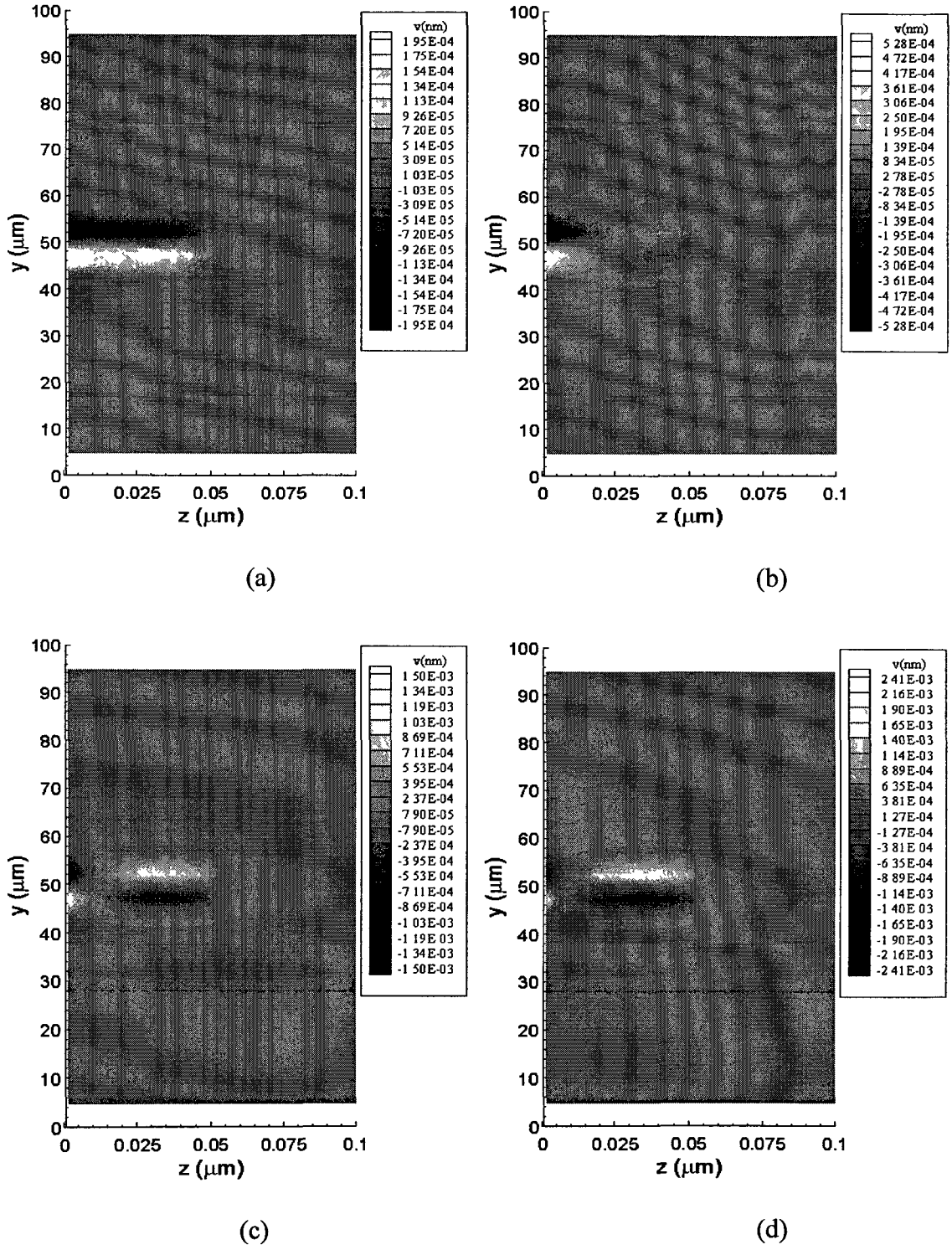

Figure 5.9 Contours of displacement (v) distributions in the cross section of x = 50 μm at different times (a) t = 5 ps, (b) t = 10 ps, (c) t = 15 ps, and (d) t = 20 ps with a mesh of $20 \times 20 \times 80$ and three different laser fluences (J) of 1000J/m^2.

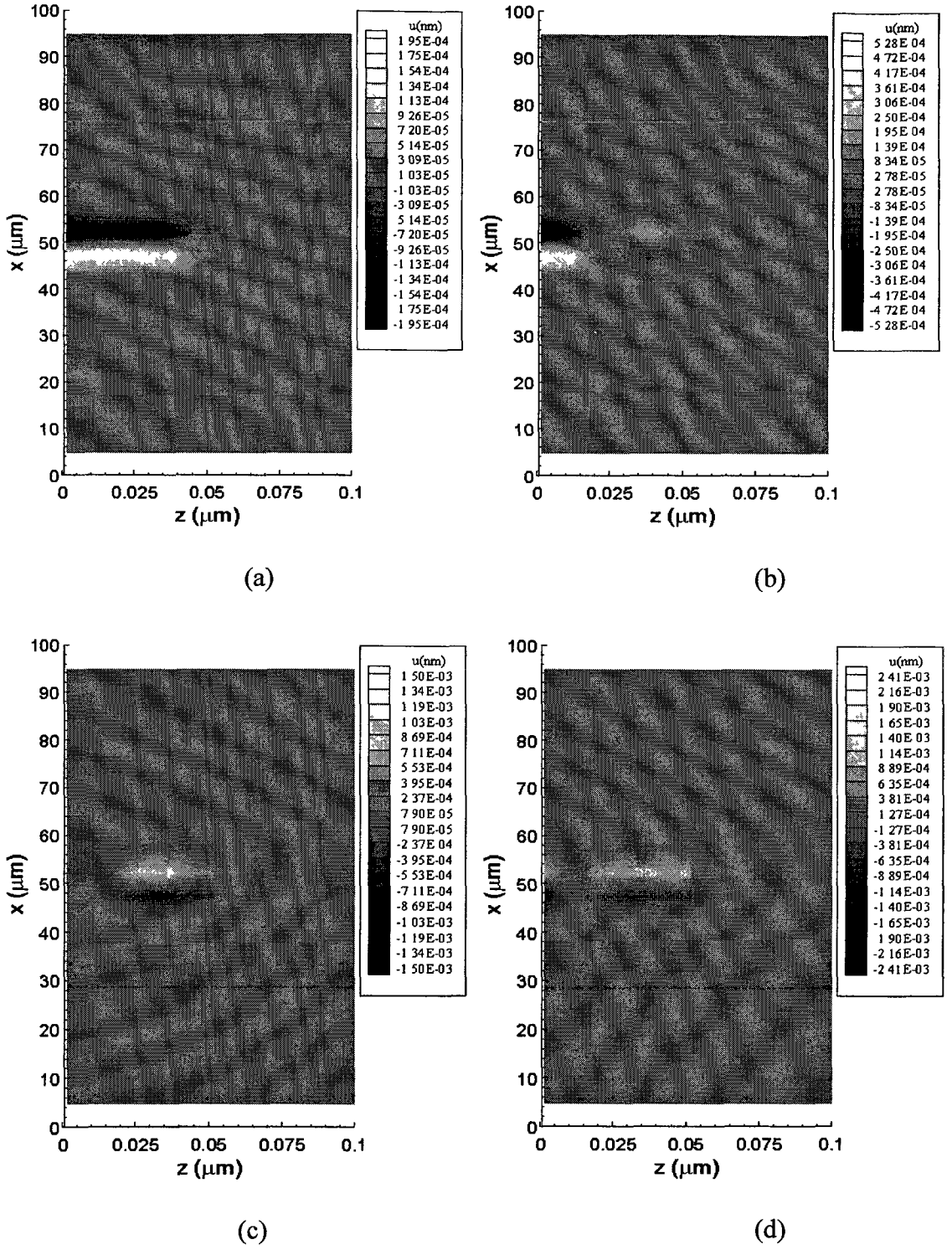

Figure 5.10 Contours of displacement (u) distributions in the cross section of $y = 50$ μm at different times (a) $t = 5$ ps, (b) $t = 10$ ps, (c) $t = 15$ ps, and (d) $t = 20$ ps with a mesh of $20 \times 20 \times 80$ and three different laser fluences (J) of 1000J/m^2.

CHAPTER SIX

CONCLUSION AND FUTURE WORK

In this dissertation, we have presented a numerical method for studying thermal deformation in 3D double-layered metal thin films exposed to ultrashort pulsed lasers, where the interface between layers is an imperfect thermal contact, which gives a nonlinear interfacial condition for temperature. The method, based on the parabolic two-step heat transport equations, accounts for the coupling effect between lattice temperature and strain rate, the fourth-power law for radiation for the interfacial condition, as well as for the hot-electron blast effect in momentum transfer. Some methods allows us to avoid non-physical oscillations in the solution: first, introducing the velocity components into the dynamic equations of motion; second, using a staggered grid where the unknown variables are placed at different locations so that the checker-board solution could be eliminated; third, employing a fourth-order compact scheme to calculate stresses derivatives in the dynamic equations of motion so that the third-order derivatives of stresses did not appear in the truncation error.

Numerical results show that there is a sharp discontinuity of electron temperature at the interface when an imperfect thermal contact exists between two bonded thin layers, and similar temperature discontinuity is observed at the interface for lattice temperature. These results indicate that imperfect thermal contact at the interface

provides a barrier to thermal energy diffusion across the interface. The observed uniform electron and lattice temperatures are probably due to increased rate of collision between electrons and phonons in the gold thin layer as electron energy diffusion is inhibited at the interface. Sharp discontinuity of displacement existing at the interface may result in shear failure. Displacement alteration in the gold layer is more pronounced for bonded films with imperfect thermal contact at the interface. Numerical results also show there are no non-physical oscillations in the solutions.

The further research may apply the obtained mathematical model and its numerical scheme to any multilayered case where the films could be different materials and exposed to ultrafast heating.

APPENDIX A

NOMENCLATURE

C_e	electron heat capcity, $J/(m^3K)$
C_l	lattice heat capcity, $J/(m^3K)$
E	phonon/electron energy, J
G	electron-lattice coupling factor, $W/(m^3K)$
J	laser fluence, J/m^2
K	bulk modulus, Pa
k_e	thermal conductivity, $W/(mK)$
L_x	length of micro thin film in the x - direction, μm
L_y	length of micro thin film in the y - direction, μm
L_z	length of micro thin film in the z - direction, μm
m	index for layer
N_x	number of grid points in the x - direction
N_y	number of grid points in the y - direction
N_z	number of grid points in the z - direction
Q	energy absorption, W/m^2
R	surface reflectivity
r_s	spatial profile parameter of laser,
S	volumetric heat source, W/m^2
T	absolute temperature, K
T_e	electron temperature, K
T_l	lattice temperature, K

t_p	laser pulse duration, s
$u^n_{i,j,k}$	numerical solution of $u(x_i, y_j, z_k, t_n)$
u	displacement in the x - direction, m
v	displacement in the y - direction, m
w	displacement in the z - direction, m
v_1	velocity component in the x - direction, m/s
v_2	velocity component in the y - direction, m/s
v_3	velocity component in the z - direction, m/s
x	Cartesian coordinate
y	Cartesian coordinate
z	Cartesian coordinate
z_s	optical penetration depth, m
$\vec{n}$	unit outward normal vector on the boundary

Greek Symbols

Δt	time increment, s
Δx	rectangular grid size in the x - direction, m
Δy	rectangular grid size in the y - direction, m
Δz	rectangular grid size in the z - direction, m
ζ	optical penetration depth, m
α_T	thermal expansion coefficient
Δ_{-t}	finite difference operator in the t - direction
δ_x	central difference operator

δ_y	central difference operator
δ_z	central difference operator
Δ_x	forward difference operator
Δ_{-x}	backward difference operator
Δ_y	forward difference operator
Δ_{-y}	backward difference operator
Δ_z	forward difference operator
Δ_{-z}	backward difference operator
τ_e	electron relaxation time, ps
τ_l	lattice relaxation time, ps
ε_x	normal strain in the x - direction
ε_y	normal strain in the y - direction
ε_z	normal strain in the z - direction
γ_{xy}	shear strain in the xy - plane
γ_{xz}	shear strain in the xz - plane
γ_{yz}	shear strain in the yz - plane
Λ	electron-blast coefficient, $J/(m^3K^2)$
λ	Lame's constant, Pa
μ	Lame's constant, Pa
ρ	density, kg/m^3
δ	penetration depth nm

σ	Stefan-Boltzmann's constant
σ_x	normal stress in the x - direction
σ_y	normal stress in the y - direction
σ_z	normal stress in the z - direction
σ_{xy}	shear stress in the xy - plane
σ_{xz}	shear stress in the xz - plane
σ_{yz}	shear stress in the yz - plane

Subscripts and Superscripts

0	initial value at $t = 0$
e	electron
i	grid index in the x - direction
j	grid index in the y - direction
k	grid index in the z - direction
l	lattice
n	time level

APPENDIX B

SOURCE CODE OF EXAMPLE

```
C Main program

      implicit double precision (a-h,l,o-z)
      dimension t(4001),t1(4001),x(51),y(51),z(221)
      dimension TEo(41,41,101),TEold(41,41,101),
     $ TLo(41,41,101),TLold(41,41,101),
     $ TEm(4001),TLm(4001),
     $ u1m(4001),u2m(4001),u3m(4001),
     $ v1m(4001),v2m(4001),v3m(4001),

C Ex, Ey, Ez normal strain and shear strain
     $ epxo(41,41,101),epyo(41,41,101),epzo(41,41,101),
     $ epxyo(41,41,101),epxzo(41,41,101),epyzo(41,41,101),
     $  xsaoo(41,41,101),ysaoo(41,41,101),zsaoo(41,41,101),
     $ ssaooxy(41,41,101),ssaooxz(41,41,101),
     $ ssaooyz(41,41,101),
     $ epxn(41,41,101),epyn(41,41,101),epzn(41,41,101),
     $ epxyn(41,41,101),epxzn(41,41,101),epyzn(41,41,101),

C Normal stress and shear stress
     $ saxo(41,41,101),sayo(41,41,101),sazo(41,41,101),
     $ saxyo(41,41,101),saxzo(41,41,101),sayzo(41,41,101),
     $ saxn(41,41,101),sayn(41,41,101),sazn(41,41,101),
     $ saxyn(41,41,101),saxzn(41,41,101),sayzn(41,41,101),

C Velocity and displacement
     $ vxo(41,41,101),vyo(41,41,101),vzo(41,41,101),
     $ vxn(41,41,101),vyn(41,41,101),vzn(41,41,101),
     $ uxo(41,41,101),uyo(41,41,101),uzo(41,41,101),
     $ uxn(41,41,101),uyn(41,41,101),uzn(41,41,101),

C Stress derivative
     $ d(41,41,101),b(221),c(221),a(221),beta(221),
     $ gama(41,41,101),
     $ difx(41,41,101),dify(41,41,101),difz(41,41,101),
     $ difxyx(41,41,101),difxyy(41,41,101),
     $ difxzx(41,41,101),
     $ difxzz(41,41,101),difyzy(41,41,101),
     $ difyzz(41,41,101),

C  Additional set
     $ u1(41,41,101),u2(41,41,101),u3(41,41,101),
     $ u4(41,41,101),
     $ u5(41,41,101),u6(41,41,101),
     $ u7(41,41,101),u8(41,41,101),
     $ u9(41,41,101)

C Data

C Lame constant
      clemta1=199.0d+9
      clemta2=83.3d+9
C Shear modulus
      cmiu1=27.0d+9
      cmiu2=115.0d+9
C Thermal expansion coefficient
      alpha1=14.2d-6
      alpha2=4.9d-6
      open(unit=8, file='etm.txt')
      open(unit=7, file='um.txt')
C dimension
      lx=1.0D-4
      ly=1.0D-4
      lz=1.0D-7
C grid
      nx=20
      ny=20
      nz=81
      nz2=41
      dx=lx/nx
      dy=ly/ny
      dz=lz/nz
C Time increment
      nt=4000
      dt=0.005d-12

      icounter=0
      x(1)=0
      y(1)=0
      z(1)=0

      do i=2,nx+1
      x(i)=x(i-1)+dx
      enddo

      do j=2,ny+1
      y(j)=y(j-1)+dy
      enddo

      do k=2,nz+1
      z(k)=z(k-1)+dz
      enddo

      theta=0.5

C Initial conditions

      do i=1,nx+1
      do j=1,ny+1
      do k=1,nz+1
      TEo(i,j,k)=300.0
      TLo(i,j,k)=300.0
      TEold(i,j,k)=300.0
      TLold(i,j,k)=300.0

      epxo(i,j,k)=0.0
      epyo(i,j,k)=0.0
      epzo(i,j,k)=0.0
      saxo(i,j,k)=0.0
      sayo(i,j,k)=0.0
      sazo(i,j,k)=0.0
      xsaoo(i,j,k)=0.0
      ysaoo(i,j,k)=0.0
      zsaoo(i,j,k)=0.0

      ssaooxy(i,j,k)=0.0
      ssaooxz(i,j,k)=0.0
      ssaooyz(i,j,k)=0.0
      difx(i,j,k)=0.0
      dify(i,j,k)=0.0
      difz(i,j,k)=0.0
      difxyx(i,j,k)=0.0
      difxyy(i,j,k)=0.0
      difxzx(i,j,k)=0.0
```

```
difxzz(i,j,k)=0.0
difyzy(i,j,k)=0.0
difyzz(i,j,k)=0.0
enddo
enddo
enddo

do i=1,nx
do j=1,ny+1
do k=1,nz+1
uxo(i,j,k)=0.0
 vxo(i,j,k)=0.0
 enddo
enddo
enddo

do i=1,nx+1
do j=1,ny
do k=1,nz+1
uyo(i,j,k)=0.0
vyo(i,j,k)=0.0
enddo
enddo
enddo

do i=1,nx+1
do j=1,ny+1
do k=1,nz
uzo(i,j,k)=0.0
vzo(i,j,k)=0.0
enddo
enddo
enddo

do i=1,nx
do j=1,ny
do k=2,nz
epxyo(i,j,k)=0.0
saxyo(i,j,k)=0.0
enddo
enddo
enddo

do i=1,nx
do j=2,ny
do k=1,nz
epxzo(i,j,k)=0.0
saxzo(i,j,k)=0.0
enddo
enddo
enddo

do i=2,nx
do j=1,ny
do k=1,nz
epyzo(i,j,k)=0.0
sayzo(i,j,k)=0.0
enddo
enddo
enddo

n=1
      TEm(n)=0.0
      TLm(n)=0.0

      big=0.0

      write(*,*) 'start'

      do 1 n=1,nt
      t(n)=n*dt
      t1(n)=(n-1)*dt+dt/2.0

C Guess normal and shear strain Ex, Ey, Ez, Exy,
  Eyz, Exz Values

      do i=1,nx+1
      do j=1,ny+1
      do k=1,nz+1
      epxn(i,j,k)=epxo(i,j,k)
      epyn(i,j,k)=epyo(i,j,k)
      epzn(i,j,k)=epzo(i,j,k)
      epxyn(i,j,k)=epxyo(i,j,k)
      epyzn(i,j,k)=epyzo(i,j,k)
      epxzn(i,j,k)=epxzo(i,j,k)
      enddo
      enddo
      enddo

C Iteration

      tol=1d-17
      detuvmax=tol+1d-5
      do while (detuvmax.gt.tol)
      detuvmax=0.0
      det1max=0.0
      det2max=0.0
      det3max=0.0
      det4max=0.0
      det5max=0.0
      det6max=0.0

C Call subroutine calculate temperature

Call temp(nx,ny,nz,nz2,dx,dy,dz,x,y,z,t1(n),dt,TLo,
$  TLold,TEo,TEold,epxn,epyn,epzn,epxo,epyo,epzo)

C Compute normal stress

      do j=1,ny+1
      do k=1,nz+1
      saxn(1,j,k)=0.0
      saxn(nx+1,j,k)=0.0
      end do
      end do

      do i=1,nx+1
      do k=1,nz+1
      sayn(i,1,k)=0.0
      sayn(i,ny+1,k)=0.0
      end do
      end do
```

```
      do j=1,ny+1
      do i=1,nx+1
      sazn(i,j,1)=0.0
      sazn(i,j,nz+1)=0.0
      end do
      end do

      do i=2,nx
      do j=2,ny

C gold

      clemta=clemta1
      cmiu=cmiu1
      alpha=alpha1
      do k=2,nz2
      saxn(i,j,k)=(clemta+2.0*cmiu)*epxn(i,j,k)
$     +clemta*epyn(i,j,k)
$     +clemta*epzn(i,j,k)
$     -(3.0*clemta+2.0*cmiu)*alpha*(TLold(i,j,k)-300.0)

      sayn(i,j,k)=clemta*epxn(i,j,k)
$     +(clemta+2.0*cmiu)*epyn(i,j,k)
$     +clemta*epzn(i,j,k)
$     -(3.0*clemta+2.0*cmiu)*alpha*(TLold(i,j,k)-300.0)

      sazn(i,j,k)=clemta*epxn(i,j,k)
$     +(clemta+2.0*cmiu)*epzn(i,j,k)
$     +clemta*epyn(i,j,k)
$     -(3.0*clemta+2.0*cmiu)*alpha*(TLold(i,j,k)-300.0)
      end do

C Chromium

      clemta=clemta2
      cmiu=cmiu2
      alpha=alpha2
      do k=nz2+2,nz
       saxn(i,j,k)=(clemta+2.0*cmiu)*epxn(i,j,k)
$     +clemta*epyn(i,j,k)
$     +clemta*epzn(i,j,k)
$     -(3.0*clemta+2.0*cmiu)*alpha*(TLold(i,j,k)-300.0)

       sayn(i,j,k)=clemta*epxn(i,j,k)
$     +(clemta+2.0*cmiu)*epyn(i,j,k)
$     +clemta*epzn(i,j,k)
$     -(3.0*clemta+2.0*cmiu)*alpha*(TLold(i,j,k)-300.0)

      sazn(i,j,k)=clemta*epxn(i,j,k)
$     +(clemta+2.0*cmiu)*epzn(i,j,k)
$     +clemta*epyn(i,j,k)
$     -(3.0*clemta+2.0*cmiu)*alpha*(TLold(i,j,k)-300.0)
      end do

      k=nz2+1
      saxn(i,j,k)=(saxn(i,j,k+1)+saxn(i,j,k-1))/2
      sayn(i,j,k)=(sayn(i,j,k+1)+sayn(i,j,k-1))/2
      end do
      end do

C Calculate shear stress

      do j=1,ny
      do k=2,nz
      saxyn(1,j,k)=0.0
      saxyn(nx,j,k)=0.0
      end do
      end do

      do i=1,nx
      do k=2,nz
      saxyn(i,1,k)=0.0
      saxyn(i,ny,k)=0.0
      end do
      end do

      do j=2,ny-1
      do i=2,nx-1
      clemta=clemta1
      cmiu=cmiu1
      alpha=alpha1
      do k=2,nz2
      saxyn(i,j,k)=cmiu*epxyn(i,j,k)
      end do
      clemta=clemta2
      cmiu=cmiu2
      alpha=alpha2
      do k=nz2+2,nz
      saxyn(i,j,k)=cmiu*epxyn(i,j,k)
      end do
      k=nz2+1
      saxyn(i,j,k)=saxyn(i,j,k-1)
      end do
      end do

      do j=2,ny
      do k=1,nz
      saxzn(1,j,k)=0.0
      saxzn(nx,j,k)=0.0
      end do
      end do

      do i=1,nx
      do j=2,ny
      saxzn(i,j,1)=0.0
      saxzn(i,j,nz)=0.0
      end do
      end do

      do j=2,ny
      do i=2,nx-1
      clemta=clemta1
      cmiu=cmiu1
      alpha=alpha1
      do k=2,nz2
      saxzn(i,j,k)=cmiu*epxzn(i,j,k)
      end do
      clemta=clemta2
      cmiu=cmiu2
      alpha=alpha2
      do k=nz2+1,nz-1
      saxzn(i,j,k)=cmiu*epxzn(i,j,k)
      end do
      end do
```

```
      end do

      do i=2,nx
      do k=1,nz
      sayzn(i,1,k)=0.0
      sayzn(i,ny,k)=0.0
      end do
      end do

      do i=2,nx
      do j=1,ny
      sayzn(i,j,1)=0.0
      sayzn(i,j,nz)=0.0
      end do
      end do

      do j=2,ny-1
      do i=2,nx
      clemta=clemta1
      cmiu=cmiu1
      alpha=alpha1
      do k=2,nz2
      sayzn(i,j,k)=cmiu*sayzn(i,j,k)
      end do
      clemta=clemta2
      cmiu=cmiu2
      alpha=alpha2
      do k=nz2+1,nz-1
      sayzn(i,j,k)=cmiu*sayzn(i,j,k)
      end do
      end do
      end do

C Calculate derivative of stress difx

      do k=2,nz
      do j=2,ny
      difx(1,j,k)=(saxn(2,j,k)-saxn(1,j,k))/dx
      difx(nx,j,k)=(saxn(nx+1,j,k)-saxn(nx,j,k))/dx
      end do
      end do

      b(2)=0.0
      a(2)=11.0/12.0
      c(2)=-1.0/24.0

      do k=2,nz
      do j=2,ny
      d(2,j,k)=(saxn(3,j,k)-saxn(2,j,k))/dx
     $ -1.0/24.0*difx(1,j,k)
      end do
      end do

      do i=3,nx-2
      b(i)=-1.0/24.0
      a(i)=11.0/12.0
      c(i)=-1.0/24.0
      do j=2,ny
      do k=2,nz
      d(i,j,k)=(saxn(i+1,j,k)-saxn(i,j,k))/dx
      end do
      end do

      end do

      b(nx-1)=-1.0/24.0
      a(nx-1)=11.0/12.0
      c(nx-1)=0.0

      do k=2,nz
      do j=2,ny
      d(nx-1,j,k)=(saxn(nx,j,k)-saxn(nx-1,j,k))/dx
     $ -1.0/24.0*difx(nx,j,k)
      end do
      end do

      beta(nx)=0.0
      do k=2,nz
      do j=2,ny
      gama(nx,j,k)=0.0
      end do
      end do

      do m=2,nx-1
      i=nx-m+1
      beta(i)=b(i)/(a(i)-c(i)*beta(i+1))
      do j=2,ny
      do k=2,nz
      gama(i,j,k)=(d(i,j,k)+c(i)*gama(i+1,j,k))/(a(i)
     $ -c(i)*beta(i+1))
      end do
      end do
      end do

      do j=2,ny
      do k=2,nz
      u1(1,j,k)=0.0
      end do
      end do

      do i=2,nx-1
      do j=2,ny
      do k=2,nz
      u1(i,j,k)=beta(i)*u1(i-1,j,k)+gama(i,j,k)
      difx(i,j,k)=u1(i,j,k)
      end do
      end do
      end do

      do i=1,nx
      a(i)=0
      b(i)=0
      c(i)=0
      beta(i)=0
      do j=1,ny
      do k=1,nz
      gama(i,j,k)=0.0
      d(i,j,k)=0.0
      end do
      end do
      end do

C Calculate derivative of stress dify

      do k=2,nz
```

```
      do i=2,nx
      dify(i,1,k)=(sayn(i,2,k)-sayn(i,1,k))/dy
      dify(i,ny,k)=(sayn(i,ny+1,k)-sayn(i,ny,k))/dy
      end do
      end do

      b(2)=0.0
      a(2)=11.0/12.0
      c(2)=-1.0/24.0

      do k=2,nz
      do i=2,nx
      d(i,2,k)=(sayn(i,3,k)-sayn(i,2,k))/dy
     $ -1.0/24.0*dify(i,1,k)
      end do
      end do

      do j=3,ny-2
      b(j)=-1.0/24.0
      a(j)=11.0/12.0
      c(j)=-1.0/24.0
      do i=2,nx
      do k=2,nz
      d(i,j,k)=(sayn(i,j+1,k)-sayn(i,j,k))/dy
      end do
      end do
      end do

      b(ny-1)=-1.0/24.0
      a(ny-1)=11.0/12.0
      c(ny-1)=0.0

      do i=2,nx
      do k=2,nz
      d(i,ny-1,k)=(sayn(i,ny,k)-sayn(i,ny-1,k))/dy
     $ -1.0/24.0*dify(i,ny,k)
      end do
      end do

      beta(ny)=0.0
      do i=2,nx
      do k=2,nz
      gama(i,ny,k)=0.0
      end do
      end do

      do m=2,ny-1
      j=ny-m+1
      beta(j)=b(j)/(a(j)-c(j)*beta(j+1))
      do i=2,nx
      do k=2,nz
      gama(i,j,k)=(d(i,j,k)+c(j)*gama(i,j+1,k))/(a(j)
     $ -c(j)*beta(j+1))
      end do
      end do
      end do

      do i=2,nx
      do k=2,nz
      u2(i,1,k)=0.0
      end do
      end do

      do j=2,ny-1
      do i=2,nx
      do k=2,nz
      u2(i,j,k)=beta(j)*u2(i,j-1,k)+gama(i,j,k)
      dify(i,j,k)=u2(i,j,k)
      end do
      end do
      end do

      do i=1,nx
      a(i)=0
      b(i)=0
      c(i)=0
      beta(i)=0
      do j=1,ny
      do k=1,nz
      gama(i,j,k)=0.0
      d(i,j,k)=0.0
      end do
       end do
      end do

C Calculate derivative of stress difz

      do i=2,nx
      do j=2,ny
      difz(i,j,1)=(sazn(i,j,2)-sazn(i,j,1))/dz
      difz(i,j,nz)=(sazn(i,j,nz+1)-sazn(i,j,nz))/dz
      end do
      end do

      b(2)=0.0
      a(2)=11.0/12.0
      c(2)=-1.0/24.0

      do i=2,nx
      do j=2,ny
      d(i,j,2)=(sazn(i,j,3)-sazn(i,j,2))/dz-1.0/24.0*difz(i,j,1)
      end do
      end do

      do k=3,nz-2
      b(k)=-1.0/24.0
      a(k)=11.0/12.0
      c(k)=-1.0/24.0
      do j=2,ny
      do i=2,nx
      d(i,j,k)=(sazn(i,j,k+1)-sazn(i,j,k))/dz
      end do
      end do
      end do

      b(nz-1)=-1.0/24.0
      a(nz-1)=11.0/12.0
      c(nz-1)=0.0

      do i=2,nx
      do j=2,ny
      d(i,j,nz-1)=(sazn(i,j,nz)-sazn(i,j,nz-1))/dz
     $ -1.0/24.0*difz(i,j,nz)
      end do
```

```
      end do

      beta(nz)=0.0
      do i=2,nx
      do j=2,ny
      gama(i,j,nz)=0.0
      end do
      end do

      do m=2,nz-1
      k=nz-m+1
      beta(k)=b(k)/(a(k)-c(k)*beta(k+1))
      do j=2,ny
      do i=2,nx
      gama(i,j,k)=(d(i,j,k)+c(k)*gama(i,j,k+1))/(a(k)
     $ -c(k)*beta(k+1))
      end do
      end do
      end do

      do i=2,nx
      do j=2,ny
      u3(i,j,1)=0.0
      end do
      end do

      do i=2,nx
      do j=2,ny
      do k=2,nz-1
      u3(i,j,k)=beta(k)*u3(i,j,k-1)+gama(i,j,k)
      difz(i,j,k)=u3(i,j,k)
      end do
      end do
      end do

      do i=1,nx
      a(i)=0
      b(i)=0
      c(i)=0
      beta(i)=0
      do j=1,ny
      do k=1,nz
      gama(i,j,k)=0.0
      d(i,j,k)=0.0
      end do
      end do
      end do

C Calculate derivative of stress difxyx

      do k=2,nz
      do j=1,ny
      difxyx(2,j,k)=(saxyn(2,j,k)-saxyn(1,j,k))/dx
      difxyx(nx,j,k)=(saxyn(nx,j,k)-saxyn(nx-1,j,k))/dx
      end do
      end do

      b(3)=0.0
      a(3)=11.0/12.0
      c(3)=-1.0/24.0

      do k=2,nz
      do j=1,ny
      d(3,j,k)=(saxyn(3,j,k)-saxyn(2,j,k))/dx
     $ -1.0/24.0*difxyx(2,j,k)
      end do
      end do

      do i=4,nx-2
      b(i)=-1.0/24.0
      a(i)=11.0/12.0
      c(i)=-1.0/24.0
      do j=1,ny
      do k=2,nz
      d(i,j,k)=(saxyn(i,j,k)-saxyn(i-1,j,k))/dx
      end do
      end do
      end do

      b(nx-1)=-1.0/24.0
      a(nx-1)=11.0/12.0
      c(nx-1)=0.0

      do k=2,nz
      do j=1,ny
      d(nx-1,j,k)=(saxyn(nx-1,j,k)-saxyn(nx-2,j,k))/dx
     $ -1.0/24.0*difxyx(nx,j,k)

      end do
      end do

      beta(nx)=0.0
      do k=2,nz
      do j=1,ny
      gama(nx,j,k)=0.0
      end do
      end do

      do m=3,nx-1
      i=nx-m+2
      beta(i)=b(i)/(a(i)-c(i)*beta(i+1))
      do j=1,ny
      do k=2,nz
      gama(i,j,k)=(d(i,j,k)+c(i)*gama(i+1,j,k))/(a(i)
     $ -c(i)*beta(i+1))
      end do
      end do
      end do

      do j=1,ny
      do k=2,nz
      u4(2,j,k)=0.0
      end do
      end do
      do i=3,nx-1
      do j=1,ny
      do k=2,nz
      u4(i,j,k)=beta(i)*u4(i-1,j,k)+gama(i,j,k)
      difxyx(i,j,k)=u4(i,j,k)
      end do
      end do
      end do

      do i=1,nx
```

```
      a(i)=0
      b(i)=0
      c(i)=0
      beta(i)=0
      do j=1,ny
      do k=1,nz
      gama(i,j,k)=0.0
      d(i,j,k)=0.0
      end do
      end do
      end do

C Calculate derivative of stress difxyy

      do k=2,nz
      do i=1,nx
      difxyy(i,2,k)=(saxyn(i,2,k)-saxyn(i,1,k))/dy
      difxyy(i,ny,k)=(saxyn(i,ny,k)-saxyn(i,ny-1,k))/dy
      end do
      end do

      b(3)=0.0
      a(3)=11.0/12.0
      c(3)=-1.0/24.0

      do k=2,nz
      do i=1,nx
      d(i,3,k)=(saxyn(i,3,k)-saxyn(i,2,k))/dy
     $ -1.0/24.0*difxyy(i,2,k)
      end do
      end do

      do j=4,ny-2
      b(j)=-1.0/24.0
      a(j)=11.0/12.0
      c(j)=-1.0/24.0
      do i=1,nx
      do k=2,nz
      d(i,j,k)=(saxyn(i,j,k)-saxyn(i,j-1,k))/dy
      end do
      end do
      end do

      b(ny-1)=-1.0/24.0
      a(ny-1)=11.0/12.0
      c(ny-1)=0.0

      do k=2,nz
      do i=1,nx
      d(i,ny-1,k)=(saxyn(i,ny-1,k)-saxyn(i,ny-2,k))/dy
     $ -1.0/24.0*difxyy(i,ny,k)
      end do
      end do

      beta(ny)=0.0
      do k=2,nz
      do i=1,nx
      gama(i,ny,k)=0.0
      end do
      end do

      do m=3,ny-1
      j=ny-m+2
      beta(j)=b(j)/(a(j)-c(j)*beta(j+1))
      do i=1,nx
      do k=2,nz
      gama(i,j,k)=(d(i,j,k)+c(j)*gama(i,j+1,k))/(a(j)
     $ -c(j)*beta(j+1))
      end do
      end do
      end do

      do i=1,nx
      do k=2,nz
      u5(i,2,k)=0.0
      end do
      end do
      do i=1,nx
      do j=3,ny-1
      do k=2,nz
      u5(i,j,k)=beta(j)*u5(i,j-1,k)+gama(i,j,k)
      difxyy(i,j,k)=u5(i,j,k)
      end do
      end do
      end do

      do i=1,nx
      a(i)=0
      b(i)=0
      c(i)=0
      beta(i)=0
      do j=1,ny
      do k=1,nz
      gama(i,j,k)=0.0
      d(i,j,k)=0.0
      end do
      end do
      end do

C Calculate derivative of stress difxzx

      do k=1,nz
      do j=2,ny
      difxzx(2,j,k)=(saxzn(2,j,k)-saxzn(1,j,k))/dx
      difxzx(nx,j,k)=(saxzn(nx,j,k)-saxzn(nx-1,j,k))/dx
      end do
      end do

      b(3)=0.0
      a(3)=11.0/12.0
      c(3)=-1.0/24.0

      do k=1,nz
      do j=2,ny
      d(3,j,k)=(saxzn(3,j,k)-saxzn(2,j,k))/dx
     $ -1.0/24.0*difxzx(2,j,k)
      end do
      end do

      do i=4,nx-2
      b(i)=-1.0/24.0
      a(i)=11.0/12.0
      c(i)=-1.0/24.0
      do j=2,ny
```

```
      do k=1,nz
      d(i,j,k)=(saxzn(i,j,k)-saxzn(i-1,j,k))/dx
      end do
      end do
      end do

      b(nx-1)=-1.0/24.0
      a(nx-1)=11.0/12.0
      c(nx-1)=0.0

      do k=1,nz
      do j=2,ny
      d(nx-1,j,k)=(saxzn(nx-1,j,k)-saxzn(nx-2,j,k))/dx
     $ -1.0/24.0 *difxzx(nx,j,k)
      end do
      end do

      beta(nx)=0.0
      do k=1,nz
      do j=2,ny
      gama(nx,j,k)=0.0
      end do
      end do

      do m=3,nx-1
      i=nx-m+2
      beta(i)=b(i)/(a(i)-c(i)*beta(i+1))
      do j=2,ny
      do k=1,nz
      gama(i,j,k)=(d(i,j,k)+c(i)*gama(i+1,j,k))/(a(i)
     $ -c(i)*beta(i+1))
      end do
      end do
      end do

      do j=1,ny
      do k=2,nz
      u6(2,j,k)=0.0
      end do
      end do
      do i=3,nx-1
      do j=2,ny
      do k=1,nz
      u6(i,j,k)=beta(i)*u6(i-1,j,k)+gama(i,j,k)
      difxzx(i,j,k)=u6(i,j,k)
      end do
      end do
      end do

      do i=1,nx
      a(i)=0
      b(i)=0
      c(i)=0
      beta(i)=0
      do j=1,ny
      do k=1,nz
      gama(i,j,k)=0.0
      d(i,j,k)=0.0
      end do
      end do
      end do
```

```
C Calculate derivative of stress difxzz

      do i=1,nx
      do j=2,ny
      difxzz(i,j,2)=(saxzn(i,j,2)-saxzn(i,j,1))/dz
      difxzz(i,j,nz)=(saxzn(i,j,nz)-saxzn(i,j,nz-1))/dz
      end do
      end do

      b(3)=0.0
      a(3)=11.0/12.0
      c(3)=-1.0/24.0

      do i=1,nx
      do j=2,ny
      d(i,j,3)=(saxzn(i,j,3)-saxzn(i,j,2))/dz
     $ -1.0/24.0*difxzz(i,j,2)
      end do
      end do

      do k=4,nz-2
      b(k)=-1.0/24.0
      a(k)=11.0/12.0
      c(k)=-1.0/24.0
      do j=2,ny
      do i=1,nx
      d(i,j,k)=(saxzn(i,j,k)-saxzn(i,j,k-1))/dz
      end do
      end do
      end do

      b(nz-1)=-1.0/24.0
      a(nz-1)=11.0/12.0
      c(nz-1)=0.0

      do i=1,nx
      do j=2,ny
      d(i,j,nz-1)=(saxzn(i,j,nz-1)-saxzn(i,j,nz-2))/dz
     $ -1.0/24.0*difxzz(i,j,nz)
      end do
      end do

      beta(nz)=0.0
      do i=1,nx
      do j=2,ny
      gama(i,j,nz)=0.0
      end do
      end do

      do m=3,nz-1
      k=nz-m+2
      beta(k)=b(k)/(a(k)-c(k)*beta(k+1))
     do j=2,ny
      do i=1,nx
      gama(i,j,k)=(d(i,j,k)+c(k)*gama(i,j,k+1))/(a(k)
     $ -c(k)*beta(k+1))
      end do
      end do
      end do

      do i=1,nx
      do j=2,ny
```

```
      u7(i,j,2)=0.0
      end do
      end do
      do i=1,nx
      do j=2,ny
      do k=3,nz-1
      u7(i,j,k)=beta(k)*u7(i,j,k-1)+gama(i,j,k)
      difxzz(i,j,k)=u7(i,j,k)
      end do
      end do
      end do

      do i=1,nx
      a(i)=0
      b(i)=0
      c(i)=0
      beta(i)=0
      do j=1,ny
      do k=1,nz
      gama(i,j,k)=0.0
      d(i,j,k)=0.0
      end do
      end do
      end do

C Calculate derivative of stress difyzy

      do k=1,nz
      do i=2,nx
      difyzy(i,2,k)=(sayzn(i,2,k)-sayzn(i,1,k))/dy
      difyzy(i,ny,k)=(sayzn(i,ny,k)-sayzn(i,ny-1,k))/dy
      end do
      end do

      b(3)=0.0
      a(3)=11.0/12.0
      c(3)=-1.0/24.0

      do k=1,nz
      do i=2,nx
      d(i,3,k)=(sayzn(i,3,k)-sayzn(i,2,k))/dy
     $ -1.0/24.0*difyzy(i,2,k)
      end do
      end do

      do j=4,ny-2
      b(j)=-1.0/24.0
      a(j)=11.0/12.0
      c(j)=-1.0/24.0
      do i=2,nx
      do k=1,nz
      d(i,j,k)=(sayzn(i,j,k)-sayzn(i,j-1,k))/dy
      end do
      end do
      end do

      b(ny-1)=-1.0/24.0
      a(ny-1)=11.0/12.0
      c(ny-1)=0.0


      do k=1,nz
      do i=2,nx
      d(i,ny-1,k)=(sayzn(i,ny-1,k)-sayzn(i,ny-2,k))/dy
     $ -1.0/24.0*difyzy(i,ny,k)
      end do
      end do

      beta(ny)=0
      do k=1,nz
      do i=2,nx
      gama(i,ny,k)=0
      end do
      end do

      do m=3,ny-1
      j=ny-m+2
      beta(j)=b(j)/(a(j)-c(j)*beta(j+1))
      do i=2,nx
      do k=1,nz
      gama(i,j,k)=(d(i,j,k)+c(j)*gama(i,j+1,k))/(a(j)
     $ -c(j)*beta(j+1))
      end do
      end do
      end do

      do i=2,nx
      do k=1,nz
      u8(i,2,k)=0.0
      end do
      end do
      do i=2,nx
      do j=3,ny-1
      do k=1,nz
      u8(i,j,k)=beta(j)*u8(i,j-1,k)+gama(i,j,k)
      difyzy(i,j,k)=u8(i,j,k)
      end do
      end do
      end do

      do i=1,nx
      a(i)=0
      b(i)=0
      c(i)=0
      beta(i)=0
      do j=1,ny
      do k=1,nz
      gama(i,j,k)=0.0
      d(i,j,k)=0.0
      end do
      end do
      end do

C Calculate derivative of stress difyzz

      do i=2,nx
      do j=1,ny
      difyzz(i,j,2)=(sayzn(i,j,2)-sayzn(i,j,1))/dz
      difyzz(i,j,nz)=(sayzn(i,j,nz)-sayzn(i,j,nz-1))/dz
      end do
      end do

      b(3)=0.0
      a(3)=11.0/12.0
```

```
      c(3)=-1.0/24.0

      do i=2,nx
      do j=1,ny
      d(i,j,3)=(sayzn(i,j,3)-sayzn(i,j,2))/dz
     $ -1.0/24.0*difyzz(i,j,2)
      end do
      end do

      do k=4,nz-2
      b(k)=-1.0/24.0
      a(k)=11.0/12.0
      c(k)=-1.0/24.0
      do j=1,ny
      do i=2,nx
      d(i,j,k)=(sayzn(i,j,k)-sayzn(i,j,k-1))/dz
      end do
      end do
      end do

      b(nz-1)=-1.0/24.0
      a(nz-1)=11.0/12.0
      c(nz-1)=0.0

      do i=2,nx
      do j=1,ny
      d(i,j,nz-1)=(sayzn(i,j,nz-1)-sayzn(i,j,nz-2))/dz
     $ -1.0/24.0 *difyzz(i,j,nz)
      end do
      end do

      beta(nz)=0.0
      do i=2,nx
      do j=1,ny
      gama(i,j,nz)=0.0
      end do
      end do

      do m=3,nz-1
      k=nz-m+2
      beta(k)=b(k)/(a(k)-c(k)*beta(k+1))
      do j=1,ny
      do i=2,nx
      gama(i,j,k)=(d(i,j,k)+c(k)*gama(i,j,k+1))/(a(k)
     $ -c(k)*beta(k+1))
      end do
      end do
      end do

      do i=2,nx
      do j=1,ny
      u9(i,j,2)=0.0
      end do
      end do
      do i=2,nx
      do j=1,ny
      do k=3,nz-1
      u9(i,j,k)=beta(k)*u9(i,j,k-1)+gama(i,j,k)
      difyzz(i,j,k)=u9(i,j,k)
      end do
      end do
      end do

      do i=1,nx
      a(i)=0
      b(i)=0
      c(i)=0
      beta(i)=0
      do j=1,ny
      do k=1,nz
      gama(i,j,k)=0.0
      d(i,j,k)=0.0
      end do
      end do
      end do

C Calculate velocity

      call velocity(nx,ny,nz,nz2,dx,dy,dz,dt,TEo,TEold,
     $ saxo,sayo,sazo,saxyo,saxzo,sayzo,
     $ saxn,sayn,sazn,saxyn,saxzn,sayzn,vxo,
     $ vyo,vzo,vxn,vyn,vzn,
     $ uxo,uyo,uzo,uxn,uyn,uzn,difx,dify,
     $ difz,difxyy,difxzz,difxyx,difyzz,difxzx,difyzy)

C Calculate strain

      do k=2,nz
      do j=2,ny
      do i=2,nx
      epxn(i,j,k)=(theta*(vxn(i,j,k)-vxn(i-1,j,k))
     $ +(1.0-theta)*(vxo(i,j,k)-vxo(i-1,j,k)))*dt/dx
     $ +epxo(i,j,k)

      epyn(i,j,k)=(theta*(vyn(i,j,k)-vyn(i,j-1,k))
     $ +(1.0-theta)*(vyo(i,j,k)-vyo(i,j-1,k)))*dt/dy
     $ +epyo(i,j,k)

      epzn(i,j,k)=(theta*(vzn(i,j,k)-vzn(i,j,k-1))
     $ +(1.0-theta)*(vzo(i,j,k)-vzo(i,j,k-1)))*dt/dz
     $ +epzo(i,j,k)
      end do
      end do
      end do

C Calculate Shear strain

      do k=2,nz
      do j=2,ny-1
      do i=2,nx-1
      epxyn(i,j,k)=(theta*(vxn(i,j+1,k)-vxn(i,j,k))
     $ +(1.0-theta)*(vxo(i,j+1,k)-vxo(i,j,k)))*dt/dy
     $ +(theta*(vyn(i+1,j,k)-vyn(i,j,k))
     $ +(1.0-theta)*(vyo(i+1,j,k)-vyo(i,j,k)))*dt/dx
     $ +epxyo(i,j,k)
      end do
      end do
      end do

      do k=2,nz-1
      do j=2,ny
      do i=2,nx-1
      epxzn(i,j,k)=(theta*(vxn(i,j,k+1)-vxn(i,j,k))
     $ +(1.0-theta)*(vxo(i,j,k+1)-vxo(i,j,k)))*dt/dz
```

```
 $ +(theta*(vzn(i+1,j,k)-vzn(i,j,k))
 $ +(1.0-theta)*(vzo(i+1,j,k)-vzo(i,j,k)))*dt/dx
 $ +epxzo(i,j,k)
    end do
    end do
    end do

    do k=2,nz-1
    do j=2,ny-1
    do i=2,nx
    epyzn(i,j,k)=(theta*(vyn(i,j,k+1)-vyn(i,j,k))
$ +(1.0-theta)*(vyo(i,j,k+1)-vyo(i,j,k)))*dt/dz
$ +(theta*(vzn(i,j+1,k)-vzn(i,j,k))
$ +(1.0-theta)*(vzo(i,j+1,k)-vzo(i,j,k)))*dt/dy
$ +epyzo(i,j,k)
    end do
    end do
    end do

C Check convergence

    do k=1,nz+1
    do j=1,ny+1
    do i=1,nx+1
    det1=epxn(i,j,k)-xsaoo(i,j,k)
    det2=epyn(i,j,k)-ysaoo(i,j,k)
    det3=epzn(i,j,k)-zsaoo(i,j,k)
    det4=epxyn(i,j,k)-ssaooxy(i,j,k)
    det5=epxzn(i,j,k)-ssaooxz(i,j,k)
    det6=epyzn(i,j,k)-ssaooyz(i,j,k)
    det=max(abs(det1),abs(det2),abs(det3),abs(det4),
$ abs(det5),abs(det6))

    if( abs(det).gt.detuvmax) detuvmax=abs(det)
    if( abs(det1).gt.det1max) det1max=abs(det1)
    if( abs(det2).gt.det2max) det2max=abs(det2)
    if( abs(det3).gt.det3max) det3max=abs(det3)
    if( abs(det4).gt.det4max) det4max=abs(det4)
    if( abs(det5).gt.det5max) det5max=abs(det5)
    if( abs(det6).gt.det6max) det6max=abs(det6)
    end do
    end do
    end do

    do k=1,nz+1
    do j=1,ny+1
    do i=1,nx+1
    xsaoo(i,j,k)=epxn(i,j,k)
    ysaoo(i,j,k)=epyn(i,j,k)
    zsaoo(i,j,k)=epzn(i,j,k)
    ssaooxy(i,j,k)=epxyn(i,j,k)
    ssaooxz(i,j,k)=epxzn(i,j,k)
    ssaooyz(i,j,k)=epyzn(i,j,k)
    end do
    end do
    end do

    write(*,*) 'detuvmax=', detuvmax

C  End do with detmax

    enddo
```

```
C  End the current time step

C-------------------------------------------------------------
    do k=1,nz+1
    do j=1,ny+1
    do i=1,nx+1
    TEo(i,j,k)=TEold(i,j,k)
    TLo(i,j,k)=TLold(i,j,k)
    epxo(i,j,k)=epxn(i,j,k)
    epyo(i,j,k)=epyn(i,j,k)
    epzo(i,j,k)=epzn(i,j,k)
    epxyo(i,j,k)=epxyn(i,j,k)
    epxzo(i,j,k)=epxzn(i,j,k)
    epyzo(i,j,k)=epyzn(i,j,k)
    saxo(i,j,k)=saxn(i,j,k)
    sayo(i,j,k)=sayn(i,j,k)
    sazo(i,j,k)=sazn(i,j,k)
    saxyo(i,j,k)=saxyn(i,j,k)
    saxzo(i,j,k)=saxzn(i,j,k)
    sayzo(i,j,k)=sayzn(i,j,k)
    vxo(i,j,k)=vxn(i,j,k)
    vyo(i,j,k)=vyn(i,j,k)
    vzo(i,j,k)=vzn(i,j,k)
    uxo(i,j,k)=uxn(i,j,k)
    uyo(i,j,k)=uyn(i,j,k)
    uzo(i,j,k)=uzn(i,j,k)
    end do
    end do
    end do


    if (big.lt.(TEold(11,11,1)-300.0)) then
      big=TEold(11,11,1)-300.0
    end if

    TEm(n)=TEold(11,11,1)
    TLm(n)=TLold(11,11,1)
    u1m(n)=uxn(11,11,2)
    u2m(n)=uyn(11,11,2)
    u3m(n)=uzn(11,11,1)
    v1m(n)=vxn(11,11,2)
    v2m(n)=vyn(11,11,2)
    v3m(n)=vzn(11,11,1)

    icounter=icounter+1
    write(*,*) icounter

C Output
    write(8,1020) t(n),TEm(n),TLm(n)
    write(7,1020) t(n),u1m(n),u2m(n),u3m(n)

C Output intermediate result

    if (n.eq.50) then
C The result at time t=0.25ps
C Electron temp

    open(unit=10,file='ctexz025ps.txt')
    do k=1,nz+1
    write(10,1010) (TEold(i,11,k),i=1,nx+1)
    enddo
```

```
      open(unit=11,file='te025ps.txt')
      do k=1,nz+1
      write(11,1020) TEold(11,11,k)
      enddo
C Lattice temp
      open(unit=12,file='ctlxz025ps.txt')
      do k=1,nz+1
      write(12,1010) (TLold(i,11,k),i=1,nx+1)
      enddo
      open(unit=13,file='tl025ps.txt')
      do k=1,nz+1
      write(13,1020) TLold(11,11,k)
      enddo
      end if

      if (n.eq.100) then
C The result at time t=0.5ps
C Electron temp
      open(unit=14,file='ctexz05ps.txt')
      do k=1,nz+1
      write(14,1010) (TEold(i,11,k),i=1,nx+1)
      enddo
      open(unit=15,file='te05ps.txt')
      do k=1,nz+1
      write(15,1020) TEold(11,11,k)
      enddo
C Lattice temp
      open(unit=16,file='ctlxz05ps.txt')
      do k=1,nz+1
      write(16,1010) (TLold(i,11,k),i=1,nx+1)
      enddo
      open(unit=17,file='tl05ps.txt')
      do k=1,nz+1
      write(17,1020) TLold(11,11,k)
      enddo
      end if

      if (n.eq.200) then
C The result at time t=1ps
C Electron temp
      open(unit=18,file='ctexz1ps.txt')
      do k=1,nz+1
      write(18,1010) (TEold(i,11,k),i=1,nx+1)
      enddo
      open(unit=19,file='te1ps.txt')
      do k=1,nz+1
      write(19,1020) TEold(11,11,k)
      enddo
C Lattice temp
      open(unit=20,file='ctlxz1ps.txt')
      do k=1,nz+1
      write(20,1010) (TLold(i,11,k),i=1,nx+1)
      enddo
      open(unit=21,file='tl1ps.txt')
      do k=1,nz+1
      write(21,1020) TLold(11,11,k)
      enddo
C Stress
      open(unit=22,file='saz1ps.txt')
      do k=1,nz+1
      write(22,1020) sazn(11,11,k)
      enddo
      open(unit=76,file='sax1ps.txt')
      do k=2,nz
      write(76,1020) saxn(11,11,k)
      enddo
      open(unit=77,file='say1ps.txt')
      do k=2,nz
      write(77,1020) sayn(11,11,k)
      enddo
      end if

      if (n.eq.1000) then
C The result at time t=5ps

C Displacement un
      open(unit=23,file='uxnxz5ps.txt')
      do k=2,nz
      write(23,1010) (uxn(i,11,k),i=1,nx)
      enddo
      open(unit=24,file='uznxz5ps.txt')
      do k=1,nz
      write(24,1010) (uzn(i,11,k),i=1,nx)
      enddo
      open(unit=25,file='uynyz5ps.txt')
      do k=2,nz
      write(25,1010) (uyn(11,j,k),j=1,ny)
      enddo
      open(unit=64,file='uxn5ps.txt')
      do k=2,nz
      write(64,1020) uxn(11,11,k)
      enddo
      open(unit=65,file='uyn5ps.txt')
      do k=2,nz
      write(65,1020) uyn(11,11,k)
      enddo
      open(unit=66,file='uzn5ps.txt')
      do k=1,nz
      write(66,1020) uzn(11,11,k)
      enddo
C Stress
      open(unit=26,file='saxxz5ps.txt')
      do k=2,nz
      write(26,1010) (saxn(i,11,k),i=1,nx+1)
      enddo
      open(unit=27,file='sazxz5ps.txt')
      do k=1,nz+1
      write(27,1010) (sazn(i,11,k),i=1,nx+1)
      enddo
      open(unit=28,file='sayyz5ps.txt')
      do k=2,nz
      write(28,1010) (sayn(11,j,k),j=1,ny+1)
      enddo
      open(unit=29,file='saz5ps.txt')
      do k=1,nz+1
      write(29,1020) sazn(11,11,k)
      enddo
      open(unit=78,file='sax5ps.txt')
      do k=2,nz
      write(78,1020) saxn(11,11,k)
      enddo
      open(unit=79,file='say5ps.txt')
      do k=2,nz
      write(79,1020) sayn(11,11,k)
```

```
      enddo
      end if

      if (n.eq.2000) then
C The result at time t=10ps

      open(unit=30,file='ctexz10ps.txt')
      do k=1,nz+1
      write(30,1010) (TEold(i,11,k),i=1,nx+1)
      enddo
      open(unit=31,file='te10ps.txt')
      do k=1,nz+1
      write(31,1020) TEold(11,11,k)
      enddo
C Lattice temp
      open(unit=32,file='ctlxz10ps.txt')
      do k=1,nz+1
      write(32,1010) (TLold(i,11,k),i=1,nx+1)
      enddo
      open(unit=63,file='tl10ps.txt')
      do k=1,nz+1
      write(63,1020) TLold(11,11,k)
      enddo
C Displacement un
      open(unit=33,file='uxnxz10ps.txt')
      do k=2,nz
      write(33,1010) (uxn(i,11,k),i=1,nx)
      enddo
      open(unit=34,file='uznxz10ps.txt')
      do k=1,nz
      write(34,1010) (uzn(i,11,k),i=1,nx)
      enddo
      open(unit=35,file='uynyz10ps.txt')
      do k=2,nz
      write(35,1010) (uyn(11,j,k),j=1,ny)
      enddo
      open(unit=67,file='uxn10ps.txt')
      do k=2,nz
      write(67,1020) uxn(11,11,k)
      enddo
      open(unit=68,file='uyn10ps.txt')
      do k=2,nz
      write(68,1020) uyn(11,11,k)
      enddo
      open(unit=69,file='uzn10ps.txt')
      do k=1,nz
      write(69,1020) uzn(11,11,k)
      enddo
C Stress
      open(unit=36,file='saxxz10ps.txt')
      do k=2,nz
      write(36,1010) (saxn(i,11,k),i=1,nx+1)
      enddo
      open(unit=37,file='sazxz10ps.txt')
      do k=1,nz+1
      write(37,1010) (sazn(i,11,k),i=1,nx+1)
      enddo
      open(unit=38,file='sayyz10ps.txt')
      do k=2,nz
      write(38,1010) (sayn(11,j,k),j=1,ny+1)
      enddo
      open(unit=39,file='saz10ps.txt')
      do k=1,nz+1
      write(39,1020) sazn(11,11,k)
      enddo
      open(unit=80,file='sax10ps.txt')
      do k=2,nz
      write(80,1020) saxn(11,11,k)
      enddo
      open(unit=81,file='say10ps.txt')
      do k=2,nz
      write(81,1020) sayn(11,11,k)
      enddo
      end if
      if (n.eq.3000) then
C The result at time t=15ps
C Displacement un
      open(unit=40,file='uxnxz15ps.txt')
      do k=2,nz
      write(40,1010) (uxn(i,11,k),i=1,nx)
      enddo
      open(unit=41,file='uznxz15ps.txt')
      do k=1,nz
      write(41,1010) (uzn(i,11,k),i=1,nx)
      enddo
      open(unit=42,file='uynyz15ps.txt')
      do k=2,nz
      write(42,1010) (uyn(11,j,k),j=1,ny)
      enddo
      open(unit=70,file='uxn15ps.txt')
      do k=2,nz
      write(70,1020) uxn(11,11,k)
      enddo
      open(unit=71,file='uyn15ps.txt')
      do k=2,nz
      write(71,1020) uyn(11,11,k)
      enddo
      open(unit=72,file='uzn15ps.txt')
      do k=1,nz
      write(72,1020) uzn(11,11,k)
      enddo
C Stress
      open(unit=43,file='saxxz15ps.txt')
      do k=2,nz
      write(43,1010) (saxn(i,11,k),i=1,nx+1)
      enddo
      open(unit=44,file='sazxz15ps.txt')
      do k=1,nz+1
      write(44,1010) (sazn(i,11,k),i=1,nx+1)
      enddo
      open(unit=45,file='sayyz15ps.txt')
      do k=2,nz
      write(45,1010) (sayn(11,j,k),j=1,ny+1)
      enddo
      open(unit=46,file='saz15ps.txt')
      do k=1,nz+1
      write(46,1020) sazn(11,11,k)
      enddo
      open(unit=82,file='sax15ps.txt')
      do k=2,nz
      write(82,1020) saxn(11,11,k)
      enddo
      open(unit=83,file='say15ps.txt')
      do k=2,nz
```

```
      write(83,1020) sayn(11,11,k)
      enddo
      end if
      if (n.eq.3400) then
C The result at time t=17ps
      open(unit=58,file='saz17ps.txt')
      do k=1,nz+1
      write(58,1020) sazn(11,11,k)
      enddo

      end if
      if (n.eq.4000) then
C The result at time t=20ps

      open(unit=47,file='ctexz20ps.txt')
      do k=1,nz+1
      write(47,1010) (TEold(i,11,k),i=1,nx+1)
      enddo
      open(unit=48,file='te20ps.txt')
      do k=1,nz+1
      write(48,1020) TEold(11,11,k)
      enddo
C Lattice temp
      open(unit=49,file='ctlxz20ps.txt')
      do k=1,nz+1
      write(49,1010) (TLold(i,11,k),i=1,nx+1)
      enddo
      open(unit=50,file='tl20ps.txt')
      do k=1,nz+1
      write(50,1020) TLold(11,11,k)
      enddo
C Displacement un
      open(unit=51,file='uxnxz20ps.txt')
      do k=2,nz
      write(51,1010) (uxn(i,11,k),i=1,nx)
      enddo
      open(unit=52,file='uznxz20ps.txt')
      do k=1,nz
      write(52,1010) (uzn(i,11,k),i=1,nx)
      enddo
      open(unit=53,file='uynyz20ps.txt')
      do k=2,nz
      write(53,1010) (uyn(11,j,k),j=1,ny)
      enddo
      open(unit=73,file='uxn20ps.txt')
      do k=2,nz
      write(73,1020) uxn(11,11,k)
      enddo
      open(unit=74,file='uyn20ps.txt')
      do k=2,nz
      write(74,1020) uyn(11,11,k)
      enddo
      open(unit=75,file='uzn20ps.txt')
      do k=1,nz
      write(75,1020) uzn(11,11,k)
      enddo
C Stress
      open(unit=54,file='saxxz20ps.txt')
      do k=2,nz
      write(54,1010) (saxn(i,11,k),i=1,nx+1)
      enddo
      open(unit=55,file='sazxz20ps.txt')
      do k=1,nz+1
      write(55,1010) (sazn(i,11,k),i=1,nx+1)
      enddo
      open(unit=56,file='sayyz20ps.txt')
      do k=2,nz
      write(56,1010) (sayn(11,j,k),j=1,ny+1)
      enddo
      open(unit=57,file='saz20ps.txt')
      do k=1,nz+1
      write(57,1020) sazn(11,11,k)
      enddo
      open(unit=84,file='sax20ps.txt')
      do k=2,nz
      write(84,1020) saxn(11,11,k)
      enddo
      open(unit=85,file='say20ps.txt')
      do k=2,nz
      write(85,1020) sayn(11,11,k)
      enddo
      end if

C Complete the whole period
 1    end do

      print *, big

      open(unit=59,file='Te10(x,y=0).dat')
      do k=1,nz+1
      write(59,1010) (z(k)*1.0D+6), TEold(11,11,k)
      enddo

      open(unit=60,file='Tl10(x,y=0).dat')
      do k=1,nz+1
      write(60,1010) (z(k)*1.0D+6), TLold(11,11,k)
      enddo

      open(unit=61,file='Tem224.dat')
      do n=1,nt
      write(61,1020) (t(n)*1.0D+12),((TEm(n)-300.0)/big)
      enddo

      open(unit=62,file='um224.dat')
      do n=1,nt
      write(62,1020) (t(n)*1.0D+12),(u3m(n)*1.0D+9)
      enddo

      open(unit=6,file='sigmaz10(x,y=0).dat')
      print *, "zonezse1"
      do k=1,nz+1
      print *, (z(k)*1.0D+6), (sazn(11,11,k)*1.0D-9)
      enddo


 1010          format(401e15.6)
 1020          format(e15.6,3e15.6)
      end

C End main program

C Subroutines

C Calculate temperature
```

```
      subroutine temp(nx,ny,nz,nz2,
     $ dx,dy,dz,x,y,z,t,dt,TLo,TLold,TEo,TEold,
     $ epxn,epyn,epzn,epxo,epyo,epzo)

      implicit double precision (a-h,l,o-z)
      dimension x(51),y(51),z(221)
      dimension TEo(41,41,101),TEold(41,41,101),
     $  TLo(41,41,101),TLold(41,41,101),
     $  TEnew(41,41,101),TLnew(41,41,101),
     $  epxn(41,41,101),epyn(41,41,101),epzn(41,41,101),
     $  epxo(41,41,101),epyo(41,41,101),epzo(41,41,101),
     $  dTE(41,41,101),dTL(41,41,101)

      integer iteration,flagE,flagL

C data

C Lame constant
      clemta1=199.0d+9
      clemta2=83.3d+9
C Shear modulus
      cmiu1=27.0d+9
      cmiu2=115.0d+9
C Thermal expansion coefficient
      alpha1=14.2d-6
      alpha2=4.9d-6
C Electron heat capacity
      ce01=2.1d+4
      ce02=5.8d+4
C Lattic heat capacity
      cl1=2.5d+6
      cl2=3.3d+6
C Electron - lattic coupling factor
      g1=2.6d+16
      g2=42.0d+16
C Electron thermal conducitivity
      cke01=315.0
      cke02=94.0
C Laser fluence
      flu=1000.0
C Laser pulse duration
      tp=0.1d-12
C Optical penetration depth
      delta=15.3d-9
C Surface reflectivity
      sur=0.93
C Spatial profile parameters
      zs=1.0d-6

      iteration=0

      rx=dt/(4.0*dx*dx)
      ry=dt/(4.0*dy*dy)
      rz=dt/(4.0*dz*dz)
      deterror=1.0d-3

C------------------------Iteration starts-------------------------
C flagE and flagL indicate whether TE and TL are
                    precise enough
C keep on iterating as long as flagE or flagL equals to 1

2     do j=2,ny
      do i=2,nx
      clemta=clemta1
      cmiu=cmiu1
      alpha=alpha1
      ce0=ce01
      cl=cl1
      g=g1
      cke0=cke01
      d0=g*dt/(2.0*cl)
      ee=(3.0*clemta+2.0*cmiu)*alpha*300.0/cl
      do k=2,nz2-1

C Heat source
      aa=-z(k)/delta-((x(i)-10.0*dx)*(x(i)-10.0*dx)
     $   +(y(j)-10.0*dy)*(y(j)-10.0*dy))/(zs*zs)
     $   -2.77*(t-2.0*tp)*(t-2.0*tp)/(tp*tp)

      q=0.94*flu*(1.0-sur)*exp(aa)/(tp*delta)

      a0=ce0*(TEo(i,j,k)+TEold(i,j,k))/(2.0*300.0)
      b1=cke0*(TEold(i+1,j,k)/TLold(i+1,j,k)
     $ +TEold(i,j,k)/TLold(i,j,k))*rx
      b2=cke0*(TEold(i,j,k)/TLold(i,j,k)
     $ +TEold(i-1,j,k)/TLold(i-1,j,k))*rx
      b3=cke0*(TEold(i,j+1,k)/TLold(i,j+1,k)
     $ +TEold(i,j,k)/TLold(i,j,k))*ry
      b4=cke0*(TEold(i,j,k)/TLold(i,j,k)
     $ +TEold(i,j-1,k)/TLold(i,j-1,k))*ry
      b5=cke0*(TEold(i,j,k+1)/TLold(i,j,k+1)
     $ +TEold(i,j,k)/TLold(i,j,k))*rz
      b6=cke0*(TEold(i,j,k)/TLold(i,j,k)
     $ +TEold(i,j,k-1)/TLold(i,j,k-1))*rz

      c1=cke0*(TEo(i+1,j,k)/TLo(i+1,j,k)
     $ +TEo(i,j,k)/TLo(i,j,k))*rx
      c2=cke0*(TEo(i,j,k)/TLo(i,j,k)
     $ +TEo(i-1,j,k)/TLo(i-1,j,k))*rx
      c3=cke0*(TEo(i,j+1,k)/TLo(i,j+1,k)
     $  +TEo(i,j,k)/TLo(i,j,k))*ry
      c4=cke0*(TEo(i,j,k)/TLo(i,j,k)
     $  +TEo(i,j-1,k)/TLo(i,j-1,k))*ry
      c5=cke0*(TEo(i,j,k+1)/TLo(i,j,k+1)
     $  +TEo(i,j,k)/TLo(i,j,k))*rz
      c6=cke0*(TEo(i,j,k)/TLo(i,j,k)
     $  +TEo(i,j,k-1)/TLo(i,j,k-1))*rz

      dd=a0+b1+b2+b3+b4+b5+b6+g*dt/(2.0*(1.0+d0))
      TEnew(i,j,k)=(b1*TEold(i+1,j,k)+b2*TEold(i-1,j,k)
     $  +b3*TEold(i,j+1,k)+b4*TEold(i,j-1,k)
     $  +b5*TEold(i,j,k+1)+b6*TEold(i,j,k-1)
     $  -g*dt*(TEo(i,j,k)-TLo(i,j,k))/(2.0*(1.0+d0))
     $  +g*dt*TLo(i,j,k)/(2.0*(1.0+d0))+a0*TEo(i,j,k)
     $  -g*dt*ee*((epxn(i,j,k)+epyn(i,j,k)+epzn(i,j,k))
     $  -(epxo(i,j,k)+epyo(i,j,k)+epzo(i,j,k)))
     $  /(2.0*(1.0+d0))
     $  +c1*(TEo(i+1,j,k)-TEo(i,j,k))
     $   -c2*(TEo(i,j,k)-TEo(i-1,j,k))
     $   +c3*(TEo(i,j+1,k)-TEo(i,j,k))
     $   -c4*(TEo(i,j,k)-TEo(i,j-1,k))
     $  +c5*(TEo(i,j,k+1)-TEo(i,j,k))
     $   -c6*(TEo(i,j,k)-TEo(i,j,k-1))
```

```
$   +q*dt)/dd

     TLnew(i,j,k)=d0*TEnew(i,j,k)/(1.0+d0)
$   +d0*(TEo(i,j,k)-TLo(i,j,k))/(1.0+d0)
$        +TLo(i,j,k)/(1.0+d0)
$        -ee/(1.0+d0)
$        *((epxn(i,j,k)+epyn(i,j,k)+epzn(i,j,k))
$        -(epxo(i,j,k)
$        +epyo(i,j,k)+epzo(i,j,k)))
     end do
     clemta=clemta2
     cmiu=cmiu2
     alpha=alpha2
     ce0=ce02
     cl=cl2
     g=g2
     cke0=cke02
     d0=g*dt/(2.0*cl)
     ee=(3.0*clemta+2.0*cmiu)*alpha*300.0/cl
     do k=nz2+1,nz
     aa=-z(k)/delta-((x(i)-10.0*dx)*(x(i)-10.0*dx)
$     +(y(j)-10.0*dy)*(y(j)-10.0*dy))/(zs*zs)
$    -2.77*(t-2.0*tp)*(t-2.0*tp)/(tp*tp)

     q=0.94*flu*(1.0-sur)*exp(aa)/(tp*delta)

     a0=ce0*(TEo(i,j,k)+TEold(i,j,k))/(2.0*300.0)
     b1=cke0*(TEold(i+1,j,k)/TLold(i+1,j,k)
$   +TEold(i,j,k)/TLold(i,j,k))*rx
     b2=cke0*(TEold(i,j,k)/TLold(i,j,k)
$   +TEold(i-1,j,k)/TLold(i-1,j,k))*rx
     b3=cke0*(TEold(i,j+1,k)/TLold(i,j+1,k)
$   +TEold(i,j,k)/TLold(i,j,k))*ry
     b4=cke0*(TEold(i,j,k)/TLold(i,j,k)
$   +TEold(i,j-1,k)/TLold(i,j-1,k))*ry
     b5=cke0*(TEold(i,j,k+1)/TLold(i,j,k+1)
$   +TEold(i,j,k)/TLold(i,j,k))*rz
     b6=cke0*(TEold(i,j,k)/TLold(i,j,k)
$   +TEold(i,j,k-1)/TLold(i,j,k-1))*rz

     c1=cke0*(TEo(i+1,j,k)/TLo(i+1,j,k)
$   +TEo(i,j,k)/TLo(i,j,k))*rx
     c2=cke0*(TEo(i,j,k)/TLo(i,j,k)
$   +TEo(i-1,j,k)/TLo(i-1,j,k))*rx
     c3=cke0*(TEo(i,j+1,k)/TLo(i,j+1,k)
$   +TEo(i,j,k)/TLo(i,j,k))*ry
     c4=cke0*(TEo(i,j,k)/TLo(i,j,k)
$    +TEo(i,j-1,k)/TLo(i,j-1,k))*ry
     c5=cke0*(TEo(i,j,k+1)/TLo(i,j,k+1)
$    +TEo(i,j,k)/TLo(i,j,k))*rz
     c6=cke0*(TEo(i,j,k)/TLo(i,j,k)
$   +TEo(i,j,k-1)/TLo(i,j,k-1))*rz

     dd=a0+b1+b2+b3+b4+b5+b6+g*dt/(2.0*(1.0+d0))
     TEnew(i,j,k)=(b1*TEold(i+1,j,k)+b2*TEold(i-1,j,k)
$   +b3*TEold(i,j+1,k)+b4*TEold(i,j-1,k)
$   +b5*TEold(i,j,k+1)+b6*TEold(i,j,k-1)
$   -g*dt*(TEo(i,j,k)-TLo(i,j,k))/(2.0*(1.0+d0))
$   +g*dt*TLo(i,j,k)/(2.0*(1.0+d0))+a0*TEo(i,j,k)
$   -g*dt*ee*((epxn(i,j,k)+epyn(i,j,k)+epzn(i,j,k))
$   -(epxo(i,j,k)+epyo(i,j,k)+epzo(i,j,k)))
$   /(2.0*(1.0+d0))
$   +c1*(TEo(i+1,j,k)-TEo(i,j,k))
$   -c2*(TEo(i,j,k)-TEo(i-1,j,k))
$   +c3*(TEo(i,j+1,k)-TEo(i,j,k))
$   -c4*(TEo(i,j,k)-TEo(i,j-1,k))
$   +c5*(TEo(i,j,k+1)-TEo(i,j,k))
$    -c6*(TEo(i,j,k)-TEo(i,j,k-1))
$   +q*dt)/dd

     TLnew(i,j,k)=d0*TEnew(i,j,k)/(1.0+d0)
$    +d0*(TEo(i,j,k)-TLo(i,j,k))/(1.0+d0)
$    +TLo(i,j,k)/(1.0+d0)
$     -ee/(1.0+d0)
$     *((epxn(i,j,k)+epyn(i,j,k)+epzn(i,j,k))
$     -(epxo(i,j,k)
$     +epyo(i,j,k)+epzo(i,j,k)))
     end do
     k=nz2
C    Stenfan-Boltzmann constant
     sigma=5.669d-8
     b1=cke01*(TEold(i,j,k)/(TLold(i,j,k)))
     b2=cke02*(TEold(i,j,k+1)/(TLold(i,j,k+1)))
     TEnew(i,j,k)=TEold(i,j,k-1)-sigma*dz/b1*
$          (TEold(i,j,k)**4-TEold(i,j,k+1)**4)
     TEnew(i,j,k+1)=TEold(i,j,k+2)-
                    b1/b2*(TEold(i,j,k)-TEold(i,j,k-1))
     TLnew(i,j,k)=TLold(i,j,k-1)-sigma*dz/cke01*
$          (TLold(i,j,k)**4-TLold(i,j,k+1)**4)
     TLnew(i,j,k+1)=TLold(i,j,k+2)-cke01/cke02*
$           (TLold(i,j,k)-TLold(i,j,k-1))
     end do
     end do
C  Boundary Conditions
     do k=2,nz
     do j=2,ny
     TEnew(1,j,k)=TEnew(2,j,k)
     TEnew(nx+1,j,k)=TEnew(nx,j,k)
     TLnew(1,j,k)=TLnew(2,j,k)
     TLnew(nx+1,j,k)=TLnew(nx,j,k)
     end do
     end do
C
     do k=2,nz
     do i=2,nx
     TEnew(i,1,k)=TEnew(i,2,k)
     TEnew(i,ny+1,k)=TEnew(i,ny,k)
     TLnew(i,1,k)=TLnew(i,2,k)
     TLnew(i,ny+1,k)=TLnew(i,ny,k)
     end do
     end do
C
     do j=2,ny
     do i=2,nx
     TEnew(i,j,1)=TEnew(i,j,2)
     TEnew(i,j,nz+1)=TEnew(i,j,nz)
     TLnew(i,j,1)=TLnew(i,j,2)
     TLnew(i,j,nz+1)=TLnew(i,j,nz)
     end do
     end do

C  Test for convergence
     detmax=0.0
     do i=2,nx
```

```
      do j=2,ny
      do k=2,nz
      det1=abs(TEnew(i,j,k)-TEold(i,j,k))
      if (det1.gt.detmax) detmax=det1
      det2=abs(TLnew(i,j,k)-TLold(i,j,k))
      if (det2.gt.detmax) detmax=det2
      enddo
      enddo
      enddo

      if (detmax.le.deterror) goto 3
      do i=1,nx+1
      do j=1,ny+1
      do k=1,nz+1
      TEold(i,j,k)=TEnew(i,j,k)
      TLold(i,j,k)=TLnew(i,j,k)
      enddo
      enddo
      enddo
      iteration=iteration+1
      goto 2

C Update all the TEold, TLold with TEnew and TLnew

3     do j=1,ny+1
      do i=1,nx+1
      do k=1,nz+1
      TEold(i,j,k)=TEnew(i,j,k)
      TLold(i,j,k)=TLnew(i,j,k)
      enddo
      enddo
      enddo

      write (*,*) "iteration=", iteration
C-----------------------------Iterations Done----------------

      END
C  End of subroutine temp()
C  Calculate velocity

 Subroutine
velocity(nx,ny,nz,nz2,dx,dy,dz,dt,TEo,TEold,
$ saxo,sayo,sazo,saxyo,saxzo,sayzo,
$ saxn,sayn,sazn,saxyn,saxzn,sayzn,
$ vxo,vyo,vzo,vxn,vyn,vzn,uxo,uyo,uzo,
$ uxn,uyn,uzn,difx,dify,
$ difz,difxyy,difxzz,difxyx,difyzz,difxzx,difyzy)

      implicit double precision (a-h,l,o-z)

      dimension TEo(41,41,101),TEold(41,41,101),
$ saxo(41,41,101),sayo(41,41,101),sazo(41,41,101),
$ saxyo(41,41,101),saxzo(41,41,101),sayzo(41,41,101),
$ saxn(41,41,101),sayn(41,41,101),sazn(41,41,101),
$ saxyn(41,41,101),saxzn(41,41,101),sayzn(41,41,101),
$ vxo(41,41,101),vyo(41,41,101),vzo(41,41,101),
$ vxn(41,41,101),vyn(41,41,101),vzn(41,41,101),
$ uxo(41,41,101),uyo(41,41,101),uzo(41,41,101),
$ uxn(41,41,101),uyn(41,41,101),uzn(41,41,101),
$ difx(41,41,101),dify(41,41,101),difz(41,41,101),
$ difxyy(41,41,101),
$ difxzz(41,41,101),difxyx(41,41,101),
$ difyzz(41,41,101),
$ difxzx(41,41,101),difyzy(41,41,101)

C Density
      lou1=1.93d+4
      lou2=7190.0
C  Electron - blast coefficient
      tri1=70.0
      tri2=193.3

      theta=0.5

      do j=2,ny
      do i=1,nx
      lou=lou1
      tri=tri1
      do k=2,nz2

      vxn(i,j,k)=(difx(i,j,k)
$ +difxyy(i,j,k)+difxzz(i,j,k)
$ +tri*theta*(TEold(i+1,j,k)
$ *TEold(i+1,j,k)-TEold(i,j,k)*TEold(i,j,k))/dx
$  +tri*(1.0-theta)*(TEo(i+1,j,k)
$  *TEo(i+1,j,k)-TEo(i,j,k)*TEo(i,j,k))
$  /dx)*dt/lou+vxo(i,j,k)

      uxn(i,j,k)=(theta*vxn(i,j,k)
$  +(1.0-theta)*vxo(i,j,k))*dt+uxo(i,j,k)
      end do
      lou=lou2
      tri=tri2
      do k=nz2+2,nz
      vxn(i,j,k)=(difx(i,j,k)
$  +difxyy(i,j,k)+difxzz(i,j,k)
$  +tri*theta*(TEold(i+1,j,k)
$  *TEold(i+1,j,k)-TEold(i,j,k)*TEold(i,j,k))/dx
$  +tri*(1.0-theta)*(TEo(i+1,j,k)
$  *TEo(i+1,j,k)-TEo(i,j,k)*TEo(i,j,k))
$  /dx)*dt/lou+vxo(i,j,k)

      uxn(i,j,k)=(theta*vxn(i,j,k)
$  +(1.0-theta)*vxo(i,j,k))*dt+uxo(i,j,k)
      end do
      k=nz2+1
      vxn(i,j,k)= vxn(i,j,k-1)
      uxn(i,j,k)=uxn(i,j,k-1)
      end do
      end do

      do i=2,nx
      do j=1,ny

      lou=lou1
      tri=tri1
      do k=2,nz2-1
      vyn(i,j,k)=(difxyx(i,j,k)
$  +dify(i,j,k)+difyzz(i,j,k)
$  +tri*theta*(TEold(i,j+1,k)
$  *TEold(i,j+1,k)-TEold(i,j,k)*TEold(i,j,k))/(dy)
$  +tri*(1.0-theta)*(TEo(i,j+1,k)
$   *TEo(i,j+1,k)-TEo(i,j,k)
$ *TEo(i,j,k)) /(dy))*dt/lou+vyo(i,j,k)
```

```
      uyn(i,j,k)=(theta*vyn(i,j,k)
     $   +(1.0-theta)*vyo(i,j,k))*dt+uyo(i,j,k)
      end do
      lou=lou2
      tri=tri2
      do k=nz2+1,nz
      vyn(i,j,k)=(difxyx(i,j,k)
     $  +dify(i,j,k)+difyzz(i,j,k)
     $  +tri*theta*(TEold(i,j+1,k)
     $  *TEold(i,j+1,k)-TEold(i,j,k)*TEold(i,j,k))/(dy)
     $  +tri*(1.0-theta)*(TEo(i,j+1,k)
     $  *TEo(i,j+1,k)-TEo(i,j,k)*TEo(i,j,k))
     $  /(dy))*dt/lou+vyo(i,j,k)

      uyn(i,j,k)=(theta*vyn(i,j,k)
     $  +(1.0-theta)*vyo(i,j,k))*dt+uyo(i,j,k)
      end do
      k=nz2+1
      vyn(i,j,k)= vyn(i,j,k-1)
      uyn(i,j,k)= uyn(i,j,k-1)
      end do
      end do

      do i=2,nx
      do j=2,ny
      lou=lou1
      tri=tri1
      do k=1,nz2

      vzn(i,j,k)=(difxzx(i,j,k)
     $  +difyzy(i,j,k)+difz(i,j,k)
     $  +tri*theta*(TEold(i,j,k+1)
     $  *TEold(i,j,k+1)-TEold(i,j,k)
     $  *TEold(i,j,k))/(dz)
     $  +tri*(1.0-theta)*(TEo(i,j,k+1)
     $  *TEo(i,j,k+1)-TEo(i,j,k)*TEo(i,j,k))
     $  /(dz))*dt/lou+vzo(i,j,k)

      uzn(i,j,k)=(theta*vzn(i,j,k)
     $   +(1.0-theta)*vzo(i,j,k))*dt+uzo(i,j,k)

      end do
      lou=lou2
      tri=tri2
      do k=nz2+1,nz
      vzn(i,j,k)=(difxzx(i,j,k)
     $  +difyzy(i,j,k)+difz(i,j,k)
     $  +tri*theta*(TEold(i,j,k+1)
     $  *TEold(i,j,k+1)-TEold(i,j,k)*TEold(i,j,k))/(dz)
     $  +tri*(1.0-theta)*(TEo(i,j,k+1)
     $  *TEo(i,j,k+1)-TEo(i,j,k)
     $  *TEo(i,j,k))/(dz))*dt/lou+vzo(i,j,k)

      uzn(i,j,k)=(theta*vzn(i,j,k)
     $   +(1.0-theta)*vzo(i,j,k))*dt+uzo(i,j,k)

      end do
      end do
      end do

      return
      end
```

REFERENCES

[1] D.Y. Tzou, J.K. Chen, and J.E. Beraun, "Hot–electron blast induced by ultrashort-pulsed lasers in layered media," *International Journal of Heat and Mass Transfer,* vol. 45, pp. 3369-3382, (2002).

[2] A. Mandelis and S.B. Peralta, "Thermal wave based materials characterization and nondestructive evaluation of high-temperature superconductors: A critical review, in: R. Kossowsky (Ed.)," *Physics and Materials Science of High Temperature Superconductors II,* Kluwer Academic Publishers, Boston, MA, pp. 413-440, (1992).

[3] J. Opsal, "The application of thermal wave technology to thickness and grain size of aluminum films," in Metallization: *Performance and Reliability Issues for VLSI and ULSI, SPIE,* vol. 1596, pp. 120-131, (1991).

[4] J.A. Knapp, P. Borgesen, and R.A. Zuhr, "Beam-solid interactions: Physical phenomena," *Mater. Res. Soc. Symp. Proc,* vol. 157. (1990).

[5] D.J. Elliot and B.P. Piwczyk, "Single and multiple pulse ablations of polymetic and high density materials with excimer laser radiation at 193 nm and 248 nm," *Mater. Res. Soc. Symp. Proc.* Vol. 129, pp. 627-636, (1989).

[6] C.P. Grigoropoulos, "Heat transfer in laser processing of thin films, in: C.L. Tien (Ed.)," *Annual Review of Heat Transfer, v*ol. V, Hemisphere, New York, pp. 77-130, (1994).

[7] J. Narayan, V.P. Gosbole, and G.W. White, "Laser method for synthesis and processing of continuous diamond films on nondiamond substrates," *Science,* vol. 252, pp. 416-418, (1991).

[8] S. Zhang, P. Wang, and W. Dai, "A finite difference method for studying thermal deformation in 3D double-layered micro-structures exposed to ultrashort-pulsed lasers," *The Open Applied Mathematics Journal,* vol. 2, pp. 104-125, (2008).

[9] J.K. Chen and J.E. Beraun, "Thermomechanical response of metal films heated by ultrashort-pulsed lasers," *Journal of Thermal Stresses,* vol.25, pp. 539-558, (2002).

[10] J.K. Chen, J.E. Beraun, and C.L. Tham, "Investigation of thermal response caused by pulse laser heating," *Numerical Heat Transfer,* Part A, vol. 44, pp. 705-722, (2003).

[11] J.K. Chen, J.E. Beraun, and C.L. Tham, "Comparision of one-dimensional and two-dimensional axsymmetric pproaches to the thermomechanical response caused by ultrashort laser heating," *J. Opt. A: Pure Appl. Opt,* vol. 4, pp. 650-661, (2004).

[12] H. Wang, W. Dai, R Nassar and R. Melnik, "A finite difference method for studying thermal deformation in a thin film exposed to ultrashort-pulsed lasers," *International Journal of Heat and Mass Transfer,* vol. 49, pp. 2712-2723, (2006).

[13] H. Wang, W. Dai, R Nassar and R. Melnik, "A finite difference method for studying thermal deformation in a double-layered thin film exposed to ultrashort-pulsed lasers," *International Journal of Thermal Sciences,* vol. 46, pp. 1179-1196, (2006).

[14] H. Wang, W. Dai and L. G. Hewavitharana, "A finite difference method for studying thermal deformation in a double-layered thin film with imperfect interfacial contact exposed to ultrashort-pulsed lasers," *International Journal of Thermal Sciences,* vol. 47, pp. 7-24, (2007).

[15] X. Du, W. Dai, and P. Wang, "A finite difference method for studying thermal deformation in a 3D micro-sphere exposed to ultrashort-pulsedlasers," *Numerical Heat Transfer,* Part A, vol. 53, pp. 457-484, (2007).

[16] S. Zhang, W. Dai, H. Wang and R.VN Melnik, "A finite difference method for studying thermal deformation in a 3D thin film exposed to ultrashort pulsed lasers," *International Journal of Heat and Mass Transfer,* vol. 53, pp. 457-484, (2007).

[17] X. Qi and C.S. Suh, "Generalized thermo-elastodynamics for semiconductor material subject to ultrafast laser heating, Part I: Model Description and Validation," *International Journal of Heat and Mass Transfer,* vol. 53, pp. 41-47, (2010).

[18] X. Qi and C.S. Suh, "Generalized thermo-elastodynamics for semiconductor material subject to ultrafast laser heating, Part II: Near-field response and damage evalution," *International Journal of Heat and Mass Transfer,* vol. 53, pp. 744-752, (2010).

[19] W.B. Lor and H.S. Chu, "Propagation of thermal waves from a surface or an interface between dissimilar material," *Numerical Heat Transfer,* Part A, vol. 36, pp. 681-697, (1999).

[20] W.B. Lor and H.S. Chu, "Effect of interface thermal resistance on heat transfer in a composite medium using the thermal wave model," *International Journal of Heat and Mass Transfer,* vol 43, pp. 653-663, (2000).

[21] E.T. Swartz and R.O. Pohl, "Thermal boundary resistance", *Reviews of Modern Physics,* vol. 61, pp. 605-668, (1989).

[22] R.C. Cammarata, "Surface and interface stress effects in thin films," *Progress in Surface Science,* vol. 46, pp. 1-38, (1994).

[23] P. Hossenini-Tehrani and M.R. Eslami, "Stress and temperature distribution at layer interface excited by pulsed laser heating," *Journal of Strain Analysis,* vol. 10, pp.395-402, (2004).

[24] V.L. Levitas, B.F. Henson, L.B. Smilowitz, and B.W. Asay, "Solid-solid phase transformation via internal stress-induced virtual melting, significantly below the melting temperature, application to HMX energetic crystal," *Journal of Physical Chemistry,* vol. 110, pp.10105-10119, (2006).

[25] E. Suhir and M. Vujosevic, "Interfacial stresses in a bi-material assembly with a compliant bonding layer," *Journal of Physics D: Applied Physics,* vol. 41, pp.115504-115515, (2008).

[26] Y. Jannot, A. Degiovanni, and G. Payet, "Thernal conductivity measurement of insulating materials with a three layers device," *International Journal of Heat and Mass Transfer,* vol. 52, pp.1105-1111, (2009).

[27] G. Vidalain, L. Gosselin, and M. Lacroix, "An enhanced thermal conduction model for the prediction of convection dominated solid-liquid phase change," *International Journal of Heat and Mass Transfer,* vol. 52, pp.1753-1760, (2009).

[28] R.H.W. Hoppe and S.I. Petrova, "Multi-scale method for the crack problem in microstructual materials," *Journal of Computational Methods in Applied Mathematics,* vol. 1, pp. 69-86, (2010).

[29] S.P. Timoshenko and J.N. Goodier, *Theory of Elasticity,* 3rd ed., McGraw Hill, New York, (1970).

[30] M.H. Sadd, *Elasticity: Theory, Applications, and Numeric,* Elsevier, New York, (2005).

[31] T. Niu and W. Dai, "A hyperbolic two-step model based finite difference scheme for studying thermal deformation a 3D thin film exposed to ultrashort pulsed lasers," *Numerical Heat Transfer,* vol. 53, pp. 1294-1320, (2008).

[32] H. Wang, *A Finite Difference Method for Studying Thermal Deformation in Two-Dimensional Micro Scale Metal Thin Films Exposed to Ultrashort-Pulsed Lasers,* Ph. D. Dissertation, Louisiana Tech University, LA, (2007).

[33] S. Zhang, *A Finite Difference Method for Studying Thermal Deformation in 3D Thin Films Exposed to Ultrashort-Pulsed Lasers,* Ph. D. Dissertation, Louisiana Tech University, LA, (2008).

[34] I. Kaba, *A Numerical Method to Solve the Two-Step Parabolic Heat Transport Equations in a Microsphere Subjected to an Ultrafast Laser Pulse,* Ph.D. Dissertation, Louisiana Tech University, LA, (2004).

[35] I. Kaba and W. Dai, "A stable three-level finite difference scheme for solving the parabolic two-step model in a 3D micro-sphere heated by ultrashort-pulsed lasers," *Journal of Computational and Applied Mathematics,* vol. 181, pp. 125-147, (2005).

[36] D.Y. Tzou, *Macro-To Micro Heat Transfer: The Lagging Behavior*, Taylor & Francis, Washington, DC, (1997).

[37] B.R. Barron, *A FE-FD Hybrid Scheme for Solving Parabolic Two-Step Micro Heat Transport Equation in Irregular Shaped Three Dimensional Double-Layered Thin Films Exposed to Ulrashort-Pulse Lasers,* Ph.D. Dissertation, Louisiana Tech University, LA, (2005).

[38] B.R. Barron and W. Dai, "A hybrid FE-FD scheme for solving parabolic two-step micro heat transport equations in an irregularly shaped three-dimensional double-layered thin film," *Numerical Heat Transfer, Part B,* vol. 49, pp. 437-465, (2006).

[39] T.Q. Qiu, *Energy Dissipation and Transport During High-Power and Short-Pulse Laser-Metal Interactions,* Ph.D. Dissertation, University of California, Berkely, CA, (1993).

[40] R. Barron, *Cryogenic Systems, second edition*, Oxford Science Publications, New York, NY, (1985).

[41] M.I. Kaganov, I.M. Lifshitz, and M.V. Tanatarov, "Relaxation between electrons and crystalline lattices," *Soviet Physics JETP,* vol. 4, pp. 173-178, (1957).

[42] T.Q. Qiu and C.L. Tien, "Short-pulse laser heating on metals," *International Journal of Heat and Mass Transfer,* vol. 35, pp. 719-726, (1992).

[43] S.D. Brorson and J.G. Fujimoto, and E.P. Ippen, "Femtosecond electron heat transfer dynamics in thin gold film," *Physical Review Letter,* vol. 59, pp. 1962-1965, (1987).

[44] J.K. Chen and J.E. Beraun, "A generalized smoothed particle hydromechanics method for nonlinear dynamic problems," *Computational Methods in Applied Mechanical Enginering,* vol. 190, pp. 225-239, (2000).

[45] D.Y. Tzou, J.K. Chen and J.E. Beraun, "Hot–electron blast induced by ultrashort pulsed lasers in layered media," *International Journal of Heat and Mass Transfer,* vol. 45, pp. 3369-3382, (2002).

[46] J.K. Chen, J.E. Beraun and C.L. Tham, "Comparison of one-dimensional and two-dimensional axisymmetric approaches to the thermomechanical response caused by ultrashort laser heating," *Journal of Optics A: Pure Applied Optics,* vol. 4, pp. 650-661, (2002).

[47] T.Q. Qiu and C.L. Tien, "Short-Pulse Laser Heating on Metals," *International Journal of Heat and Mass Transfer,* vol. 35, pp. 719-726, (1992).

[48] H. Reismann and P.S. Pawlik, *Elasticity, Theory and Applications,* Wiley, New York, (1980).

[49] W. Dai and R. Nassar, "A finite difference scheme for solving a three-dimensional heat transport equation in a thin film with micro-scale thickness," *International Journal for Numerical Methods in Engineering*, vol.50, pp. 1665-1680, (2001).

[50] W. Dai and R. Nassar, "A finite difference method for solving 3-D heat transport equations in a double-layered thin film with microscale thickness and nonlinear interfacial conditions," *Numerical Heat Transfer, Part A*, vol.39, pp. 21-33, (2001).

[51] A.A. Joshi and A. Majumdar, "Transient ballistic and diffusive phonon heat transport in thin films," *Journal of Applied Physics*, vol.74, pp. 31-39, (1993).

[52] S.D. Brorson, J.G. Fujimoto, and E.P. Ippen, "Femtosecond electron heat transfer dynamics in thin gold film," *Physical Review Letter,* vol. 59, pp. 1962-1965, (1987).

[53] A.B. Bruno and H.W. Jerome, *Theory of Thermal Stresses,* New Education Edition, Dover Publications, (1997).

[54] E.T. Swartz and R.O. Pohl, "Thermal boundary resistance," *Reviews of Modern Physics,* vol. 61, pp. 605-668, (1989).

[55] T.Q. Qiu and C.L. Tien, "Short-femtosecond laser heating of multi-layer metals I analysis," *International Journal of Heat and Mass Transfer,* vol. 37, pp. 2789-2797, (1994).

[56] W. Dai, Q. Li, R. Nassar, and L. Shen, "An unconditionally stable three level finite difference scheme for solving parabolic two-step micro heat transport equations in a three-dimensional double-layered thin film," *International Journal for Numerical Methods in Engineering*, vol. 59, pp. 493-509, (2004).

[57] T.D. Nguyen, "Intrinsic stress and micro structural evolution in sputtered nanometer single and multilayered films," *Materials Research Society Symposia Proceedings*, vol. 343, pp. 579-584, (1994).

[58] K.O. Schweitz, "Interface stress in Au/Ni multilayers" *Journal of Applied Physics*, vol.88, pp. 1401-1406, (2000).

[59] V.I. Levitas, B.F. Henson, L.B. Smilowitz and B.W. Asay, "Solid-solid phase transformation via internal stress-induced virtual melting, significantly below the melting temperature. Application to HMX energetic crystal," *Journal of Physics & Chemistry*, vol. 110, pp. 10105-10119, (2006).

[60] T.Q. Qiu, T. Juhasz, C. Suarez and W.E. Bron, C.L. Tien, "Femtosecond laser heating of multi-layer metals II experiments," *International Journal of Heat and Mass Transfer,* vol. 37, pp. 2789-2808, (1994).

[61] A. N. Smith, J.L. Hosterler and P.M. Norris, "Nonequilibrium heating in metal films: An analytical and numerical analysis," *Numerical Heat Transfer, Part A,* vol. 35, pp. 345 – 357, (1999).

[62] G.W.C. Kaye, *Tables of Physical and Chemical Constants and Some Mathematical Functions, 14th ed,* Longman, London, UK, (1973).